SYNTHESIS AND PROPERTY INVESTIGATION OF METAL-BASED NANOMATERIALS FOR BIOTECHNOLOGICAL APPLICATIONS

A thesis presented to the faculty of the Graduate School of Western Carolina University in partial fulfillment of the requirements for the degree of Master of Science in Chemistry.

By

Nalin Dammika Darsanasiri

Director: Dr. Channa R. De Silva,
Assistant Professor, Inorganic Chemistry,
Department of Chemistry & Physics

Committee members: Dr. David D. Evanoff, Chemistry
Dr. Indrani Bose, Biology

April 2014

ACKNOWLEDGEMENTS

I would like to thank the Department of Chemistry and Physics, Department of Biology at Western Carolina University (WCU), Cullowhee, NC, 28723, USA for providing me the opportunity to complete my M.S degree thesis work. I am thankful to my TRAC members Assistant Professor Channa R. De Silva, Assistant Professor David D. Evanoff, and Associate Professor Indrani Bose, for their continuous involvement in the project. I realize that it would not be possible to accomplish this project without the efforts of my TRAC committee. I would like to extend my deepest gratitude to my research advisor, Assistant Professor Channa R. De Silva for his encouragement and spontaneous willingness to answer my numerous questions. I would like to thank our collaborators Professor Romanowski and Mr. Christian Gainer, Department of Biomedical Engineering, Bio5 Institute, University of Arizona, Tucson, AZ, 85719, USA. My sincere thanks goes to Professor David Butcher, Associate Dean of the College of Arts and Sciences at WCU and Associate Professor Cynthia A. Atterholt, Head of the Department of Chemistry and Physics at WCU for their regular support and guidance which helped me to accomplish my M.S. degree successfully and on time. I would like to respectfully thank all the faculty members in the Department of Chemistry and Physics at WCU and thank my friends and family members for their kind cooperation throughout my studies at Western Carolina University.

TABLE OF CONTENTS

LIST OF TABLES

Table Page

CHAPTER 3:

LIST OF FIGURES

LIST OF ABBREVIATIONS

btfa = 4,4,4-trifluoro-1-pheny-1,3-butanedione
dmph = dimethyl phenanthroline
DMF = N,N-dmethyl formamide
PEG = poly (ethylene glycol)
PVP = poly (vinylpyrrolidine)
XRD = X-ray powder diffraction
TEM = transmission electron microscopy
SEM = scanning electron microscopy
FT-IR = Fourier transmission infrared
EDX = energy dispersive X-ray mapping studies
MIC = Minimum inhibitory concentration
TSA = Tryptic soy agar
OD = Optical density
UV = Ultraviolet
NPs = Nanoparticles
ROS = Reactive oxygen species
EtOH = Ethanol
a.u = arbitrary units
rpm = revolution per minute

ABSTRACT

SYNTHESIS AND PROPERTY INVESTIGATION OF METAL-BASED NANOMATERIALS FOR BIOTECHNOLOGICAL APPLICATIONS

Nalin Dammika Darsanasiri

Western Carolina University (April 2014)

Director: Dr Channa R. De Silva

Luminescent lanthanide-based materials have drawn recent interest due to their applications in *in vitro* cellular imaging. Sensitive biological analysis requires optical labels with high water dispersibility & stability and excellent luminescent properties. Most literature reported lanthanide complexes with high luminescence intensity are hydrophobic and unstable, limiting their biological applications. This project was designed to incorporate a highly luminescent lanthanide β-diketonate complex in a silica nanoparticle. $Eu(btfa)_3dmph$ complex was synthesized, which exhibits red luminescence at 614 nm with a narrow (15 nm) full with half-maximum (btfa=4,4,4-trifluoro-1-phenyl-1,3-butanedione, dmph=4,7-dimethyl,1,10-phenanthroline). A synthetic procedure was optimized to incorporate the Eu-complex in a silica-based nanoparticle with an average particle diameter of 36 nm. Eu-complex based silica nanoparticles exhibit high stability and water-dispersibility with a luminescence quantum yield of 10 %. The nanoparticles showed antimicrobial activity against clinically important *E.coli, S.aureus* and *S.epidermidis*. Synthesis, materials characterization, and antimicrobial studies of the complex and the nanoparticles was discussed in the first part of this thesis.

Nanotechnology is emerging as a new interdisciplinary field combining biology, chemistry, physics, and material science. Recent advances promise developments in the

synthesis, modification and practical applications of polymer-coated manganese (Mn)-based zinc oxide (ZnO) nanoparticles (NPs). The size distribution, shape, and surface modification of metal-based ZnO nanoparticles are the key factors determining their specific physical properties. Due to the strong antibacterial properties and low toxicity towards mammalian cells, ZnO NPs have been successfully used in a wide range of applications including wound dressing, protective clothing, antibacterial surfaces, food preservation, and cosmetics as biocidal and disinfecting agents. In this study, cotton textiles with antimicrobial activity were developed by incorporating polymer-coated Mn-doped ZnO nanoparticles. Antimicrobial potential of synthesized Mn-doped zinc oxide (ZnO) nanoparticles against two bacteria strains (*Escherichia coli* as Gram-negative bacteria, *Staphylococcus aureus* as Gram-positive bacteria) in liquid and solid phases was studied in this work. Polymer-coated Mn-doped ZnO nanoparticles were prepared by the modified co-precipitation method. Characterization of the nanoparticles was carried out using Ultra-violet visible spectroscopy, scanning electron microscopy (SEM), transmission electron microscopy (TEM) and X-ray powder diffraction (XRD). The average particle size of the nanoparticles was found to be less than 15 nm. The antibacterial activity of the nanoparticles was evaluated using minimum inhibitory concentration (MIC) and agar diffusion method. Disk diffusion studies revealed that the nanoparticles have excellent antimicrobial activity against *E.coli* and *S.aureus* bacterial species. Therefore, it was concluded that the polymer-coated Mn-doped ZnO nanoparticles were excellent antibacterial agents with potential clinical applications.

CHAPTER 1

INTRODUCTION

1.1 BACKGROUND

1.1.1 Lanthanide-based silica nanomaterials

A bright photoluminescent europium complex was first reported by Weissman in 1942.[01] Ever since, lanthanide-based materials have shown great potential for their use in luminescent applications. Successful use of highly luminescent rare-earth doped nanoparticles, combining the various properties of doping ions and the nanoparticle matrix, has ensured the expanded use of nanoparticles. Replacement of organic dyes with inorganic materials, such as lanthanide compound is an interesting strategy for synthesizing efficient luminescent multifunctional nanoparticles, because of their impressive optical properties. As they are characterized by high photostability, long luminescence lifetimes, narrow emission bands, and a broad absorption band, lanthanide ions are indeed very well suited for luminescence applications without emission intermittency.[02, 03] The emission from lanthanide ions has been utilized extensively in biological systems.[04] One important application is the labeling of biologically-relevant molecules for detection of cellular functions. The photoluminescence (PL) properties of trivalent lanthanide ions are interested because of their broad applications in chemical and biological sensors, medical diagnostics, cellular imaging and thin film devices and biomedical imaging.[04, 05] Lanthanide ions exhibit spectrally narrow emission bands due to intra-atomic electronic transitions within the *f* electronic energy levels.[06] Recently, lanthanide complexes with tunable

wavelengths have been developed with emission wavelengths ranging from 520 nm to 680 nm with lifetimes ranging from 50 to 500 μs.[07] The long lifetimes provide a means to detect the biomolecules with high sensitivity.

Several lanthanide complexes have been used for *in vitro* luminescence assays. Among the various classes of lanthanide chelators, β-diketonates are the most widely studied lanthanide complexes. Lanthanide β-diketonate complexes are attractive candidates for luminescent applications because the ligands are commercially available, inexpensive, and provide materials with high quantum yields. Lanthanide β-diketonates have been used in *in vitro* luminescence assays. Although there has been recent success in utilizing this class of materials in biomedical imaging applications, they suffer from several drawbacks. The disadvantages of lanthanide β-diketonates for the use in biomedical imaging applications include stability, toxicity and poor water solubility of the complexes.

The photobleaching and quenching of organic dye molecules and the toxicity of quantum dots have seriously limited their applications in biological imaging including *in vivo* studies. One alternative is to use highly luminescent europium complexes dispersed in silica particles for bio-medical imaging experiments.[08] Few research groups have been reported in the literature explaining the preparation of such lanthanide complexes with potential imaging capabilities.[09, 10] However, the biocompatibility and luminescence efficiency of these materials must be improved for future *in vivo* imaging applications.[11, 12] Wang and co-workers recently reported the synthesis of two photon lanthanide chromophores containing silica nanoparticles prepared by a solution

microemulsion process for the bio-imaging of cancer cells.[13] They presented a one-step alternative route to stabilize these lanthanide complexes in aqueous solution by embedding them in silica nanoparticles. The lanthanide complexes were grafted onto silica nanoparticles. [13]

Some lanthanide complexes have antimicrobial activity. Several research groups have synthesized lanthanide-based nanoparticles that are suitable as antimicrobial agents. The antimicrobial activity of the ligands and their complexes as inhibiting agents has been screened *in vitro* against two kinds of pathogenic bacteria *Salmonella paratyphi* and *Bacillus cirroflagellosus* as well as the pathogenic fungi *Aspergillus niger* and *Candida albicans.*[14] There are several antimicrobial susceptibility tests used to determine the antimicrobial activity of materials such as agar diffusion and minimum inhibitory concentration. Minimum inhibitory concentrations (MICs) are defined as the lowest concentration of an antimicrobial agent that will inhibit the visible growth of a microorganism after overnight incubation. The Alamar Blue bioassay has been utilized over the past 50 years to assess cell viability, minimum inhibitory concentration and cytotoxicity in a range of biological and environmental systems and in a number of cell types including bacteria, yeast, fungi, protozoa and cultured mammalian and piscine cells. [15] The antibacterial activity of the ligand, metal salts, and the corresponding complexes have been assayed simultaneously against some clinical important bacteria (*S. aureus, E. coli* and *Pseudomonas aeruginosa)* and fungi. [16]

1.1.2 Surface functionalization of Mn-doped ZnO nanoparticles and their attachment to cotton fabric

Clothing and textile materials are good media for growth of microorganisms such as bacteria and fungi. According to recent reports, microorganisms can survive on fabric materials for more than 90 days in a hospital environment.[17] Such a high survival rate of pathogens on medically used textiles may contribute to transmissions of diseases in hospitals. As a means of reducing bacterial population in healthcare settings and possibly to cut pathogenic infections caused by the textile materials, utilization of antimicrobial textiles in healthcare facilities is considered to be a potential solution. Textile products have progressed to a point where they can provide a complete barrier to microbiological agents. Today, expectations go beyond the barrier and the world now seeks antimicrobial-finished fabric that goes a step further and prevents transmission or propagation of microorganisms.

Nanotechnology research in textiles is being practiced rather intensively aiming at upgrading both present functions and performance of textile materials. For example, fabric manufactured with fibers containing nanosized fillers or nanoparticles (Ag, TiO_2 and ZnO) will enhance the performance of the fabrics to a greater extent.[18]

Semiconductor materials of the periodic table, groups II–VI semiconductors have attracted great interest due to their unique properties and potential applications.[19] ZnO is a semiconductor with a wide band gap (3.3 eV), high excitation binding energy, abundant in nature, and environmentally friendly. These characteristics make this material attractive for many applications such as solar cells, optical coatings, photocatalysts,

antibacterial agents, electrical devices, active medium in UV semiconductor lasers and in gas sensors.[20]

Recently, there has been much attention focused on modifying ZnO by doping with transition metals such as Ag, Cu, Co, Ti.[21] Various techniques have been used to synthesize ZnO and transition metal-doped ZnO nanoparticles which can be categorized into either chemical or physical methods. More recently, synthesis of Mn-doped ZnO nanoparticles was reported by a wet chemical method.[22] The synthesized Mn-doped ZnO was applied as a photocatalyst to photodegradation under visible light irradiation.

Control of colloidal properties and stability of the dispersion of nanoparticles (ZnO, TiO_2, Ag, etc) is important. Aggregation, which can occur during the formation of nanoparticles, may affect the particle size. Agglomeration of nanosized ZnO may occur because of the following reason. Formation of the bonds of Zn-O-Zn among nanoparticles due to the existence of water molecules resulting in hard agglomerates, which impede the particle size of ZnO nanoparticles.[23] Therefore, removal of the water moiety in precursors is a key process for reducing hard agglomerates. Various methods have been employed to remove the water in precursors. Among them, polymer coating is an effective way for modifying the particles surface and it also prevents the agglomeration of ZnO nanoparticles.[24] Studies of the capping of ZnO nanoparticles by polyvinyl pyrrolidone (PVP) and polyethylene glycol (PEG) have been previously performed.[24] Recently, polymer coated ZnO nanoparticles have been attached onto cotton textile.

1.2 INTRODUCTION TO RESEARCH

1.2.1 Lanthanide-based silica nanomaterials [$Eu(btfa)_3dmph$ doped silica nanoparticles]

The β-diketonate complexes in this research were easily synthesized using the general reaction using europium (III) chloride (Figure 2.1). However, there were some potential pitfalls in that the coordinated water could cause luminescent quenching due to some of the vibrational states of O-H matching the excited states of the luminescent lanthanide. To avoid these potential quenching effects, another neutral ligand (dmph) was used to replace the coordinated water molecules. The dmph ligand has two nitrogen atoms with lone pairs of electrons. These types of ligands were neutral and would be referred to as an N-donor ligand. Coordinated H_2O ligands were substituted by this dmph to form the $Eu(\beta\text{-diketonate})_3dmph$ complex.

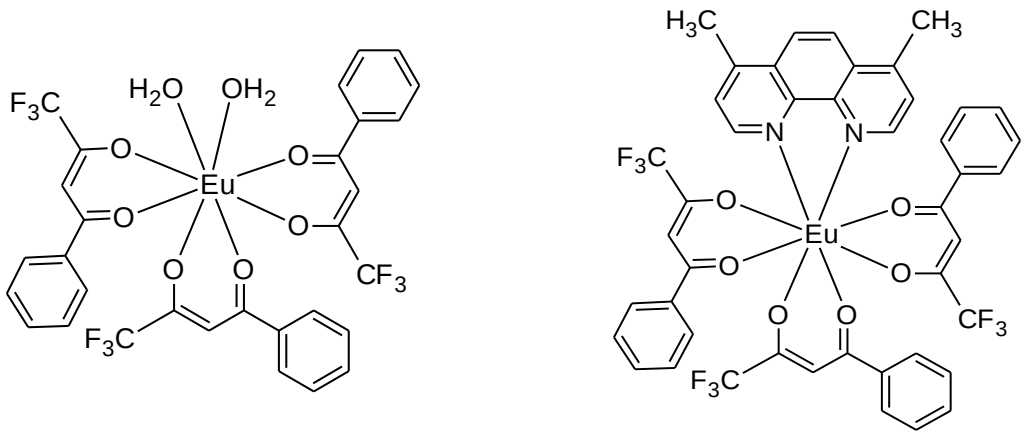

(a) (b)

Figure 1.1. Chemical structure of (a) $Eu(\beta\text{-diketonate})_3(H_2O)_2$ and (b) $Eu(\beta\text{-diketonate})_3(dmph)$ complex.

Normally $Eu(btfa)_3dmph$ complexes were not water soluble. Therefore europium-based complexes cannot be used as cellular-based imaging agents. Even though this class of compounds show impressive luminescence characteristics, they were not biocompatible. One approach was to incorporate europium complexes in a silica nanoparticle. Lanthanide coated silica based nanoparticles have been synthesized in the literature resulting larger particles with no luminescence due to vibrational quenching.[25]

This research project was designed to synthesize water dispersible and highly luminescent lanthanide nanoparticles for potential biomedical application. In this project, mainly focused on developing a silica-based nanoparticle incorporating the europium-complex within the nanoparticle. The Stöber method was modified for the preparation of $Eu(btfa)_3dmph$ incorporated silica nanoparticles and optimized a preparative procedure to incorporate the europium complex in a silica-based [$Eu(btfa)_3dmph$] nanoparticle.[26] Eu-β-diketonate complexes coordinated to an N-donor substituted phenanthroline type ligand have not yet been incorporated in a silica-based nanoparticle to the best of our knowledge. Both btfa and dmph ligands were capable of absorbing light for an efficient ligand-to-metal energy transfer. This was guaranteed a high photoluminescence while the silica matrix provides the dispersibility of the materials in aqueous buffers for biological applications.

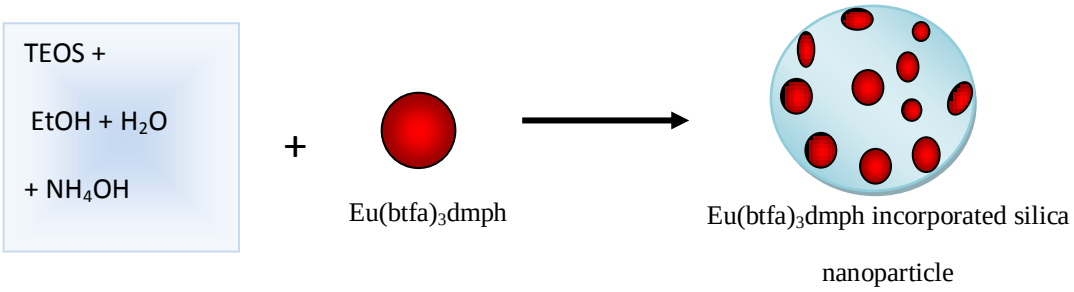

Figure 1.2. Incorporation of Eu(btfa)$_3$dmph complex in silica nanoparticles.

The silica coated nanoparticles were characterized using different analytical techniques. The antimicrobial activity of the synthetic lanthanide complexes was evaluated against some medically important bacteria (*Staphylococcus aureus, Escherichia coli* and *Staphylococcus epidermidis)* and fungi (*Candida sp, Aspergilles sp*). Antimicrobial activity of Eu(btfa)$_3$dmph and Eu(btfa)$_3$dmph incorporated silica nanoparticles have not been reported. Lanthanide-based materials have potential applications in *in vitro* and *in vivo* imaging. Thus it was important to evaluate their antimicrobial activity against pathogenic microorganisms. Antimicrobial activity was determined using international standards testing methods such as agar diffusion test, minimum inhibitory concentration and viable cell counting methods. The minimum inhibitory concentration was determined by using Almar Blue assay.[27, 28]

1.2.2 Surface functionalization of Mn-doped ZnO nanoparticles and attached onto cotton fabric

According to the published data, ZnO nanoparticles have been proven to possess antifungal and antibacterial activity against clinically important bacteria.[29] The suggested

mechanism for the antibacterial activity of ZnO is based mainly on catalysis of formation of reactive oxygen species (ROS) from water and oxygen that disrupt the integrity of the bacterial membrane.[28] Doping of metal oxide and/or transition metals (like Mn) increases the surface defects. In addition, it affects the optical and electronic properties and can presumably shift the optical absorption towards the lower wavelength side.[29] Prediction can be made from the results that Mn-doping change the band gap of ZnO nanoparticles and increased the antimicrobial activity of Mn-doped ZnO nanoparticles. However, polymer-coated Mn-doped ZnO nanoparticles attached onto cotton fabric and antimicrobial activities of functionalized cotton fabric have not yet been reported. Also, the antimicrobial activity of polymer-coated Mn-doped ZnO nanoparticles has not been evaluated.

In this study, Mn-doped ZnO nanoparticles were synthesized and functionalized using polyvinylpyrrolidone (PVP) (Figure 1.3) and polyethylene glycol (PEG) (Figure 1.4). The functionalized nanoparticles can be used as an antibacterial and antifungal agent for cotton textile. Different percentage of Mn-doped ZnO (5%, 7.5% and 10%) nanoparticles were synthesized. Antimicrobial activity of surfactant coated Mn-doped ZnO nanoparticles were determined according to ISO (International Organization for Standardization) standard antimicrobial testing methods with comparing polymer-uncoated Mn-doped ZnO nanoparticles. These polymer-coated Mn-doped ZnO nanoparticles were attached onto cotton fabric. Hypothesis was made that polymer-coated Mn-doped ZnO nanoparticles would tightly bind to the cotton textile.

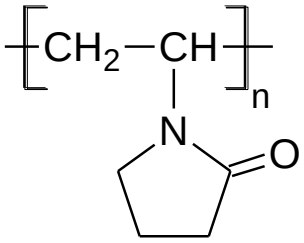

Figure 1.3. Chemical structure of polyvinylpyrrolidone (PVP)

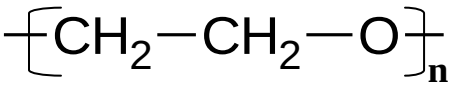

Figure 1.4. Chemical structure of polyethylene glycol (PEG) [30]

CHAPTER 2

EXPERIMENTAL

2.1 MATERIALS

All the chemicals, reagents and culture media were purchased from Aldrich and Fisher Scientific USA and used without further purification. Nanopure water with a resistivity of 18.2 MΩ was obtained from a Barnstead NANOpure Diamond system with a 0.2 μm hollow fiber filter.

2.2 LANTHANIDE-BASED SILICA NANOMATERIALS [$Eu(btfa)_3dmph$ DOPED SILICA NANOPARTICLES]

2.2.1 Synthesis of $Eu(btfa)_3(H_2O)_2$

In a round bottom flask with a magnetic stirrer, $EuCl_3 \cdot 6H_2O$ (0.336 g, 0.91 mmol) was dissolved in argon-purged nanopure water and heated at 40 °C for 15 min. NaOH (0.12 g, 3 mmol) and 4,4,4-trifluoro-1-phenyl-1,3-butanedione (btfa) (0.6 g, 3 mmol) were added into a scintillation vial containing argon-purged nanopure water (10 mL) and stirred until a clear solution was obtained. NaOH/btfa mixture was added drop-wise into the round bottom flask containing $EuCl_3 \cdot 6H_2O$ solution under stirring. The reaction mixture was heated at 60 °C for 30 min. Then the reaction mixture was stirred at room temperature for additional 3 h (Figure 2.1). The mixture was centrifuged at 4000 rpm for 10 min, washed with nanopure water, and centrifuged again for 10 min. Supernatant was poured off and the pellet was air dried. (Pale yellow solid was obtained)

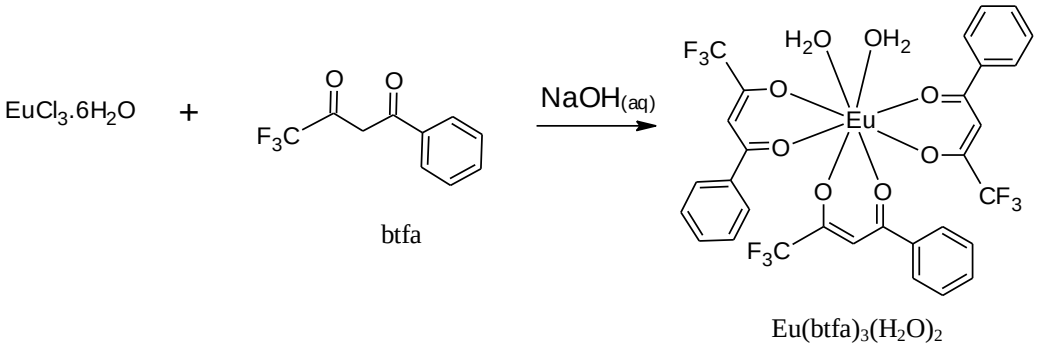

Figure 2.1. Synthesis of $Eu(btfa)_3(H_2O)_2$ complex.

2.2.2 Synthesis of $Eu(btfa)_3$dmph complex

To a solution of $Eu(btfa)_3(H_2O)_2$ (83.3 mg, 0.1 mmol) in acetone (15 mL) was added dmph (22.6 mg, 0.1 mmol) in acetone (15 mL). The resulting clear mixture was stirred at 60 °C for 30 min and then at room temperature for 12 h (Figure 2.2). The mixture was filtered and the filtrate was allowed to evaporate at room temperature to afford analytically pure product as pale yellow solid crystals.

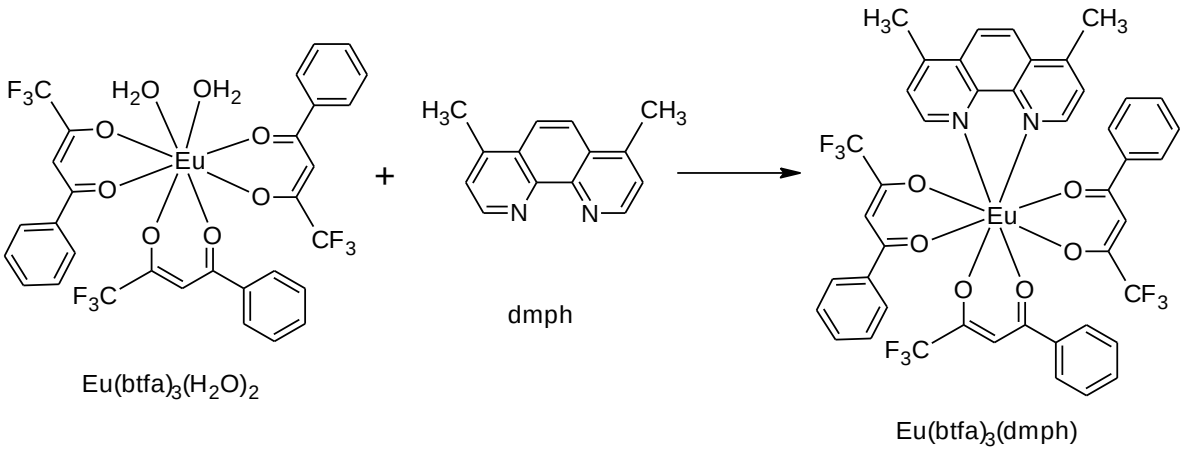

Figure 2.2. Synthesis of $Eu(btfa)_3$(dmph) complex.

2.2.3 Synthesis of $Eu(btfa)_3dmph$ incorporated silica nanoparticles

Silica nanoparticles were synthesized by using the Stöber method.[23] Small size of $Eu(btfa)_3dmph$ incorporated silica nanoparticles were synthesized by changing the reaction conditions and reactant compositions. $Eu(btfa)_3dmph$ complex [(20 mg, 0.0336 mmol), (30 mg, 0.050 mmol) or (40 mg, 0.067 mmol)] was added into ethanol (50 mL) and the mixture was stirred at 30 °C for 30 min. Tetraethylorthosilicate (TEOS) (0.0133 mol, 3 mL), 28% NH_4OH (1 mL) and nanopure water (2 mL) were added into the $Eu(btfa)_3dmph$/ethanol mixture. The reaction mixture was stirred for 18 h at 55 °C (Figure 2.3). The reaction mixture was centrifuged at 4000 rpm for 20 min. The pellets were washed with ethanol to remove un-reacted chemicals and centrifuged at 4000 rpm for 20 min.

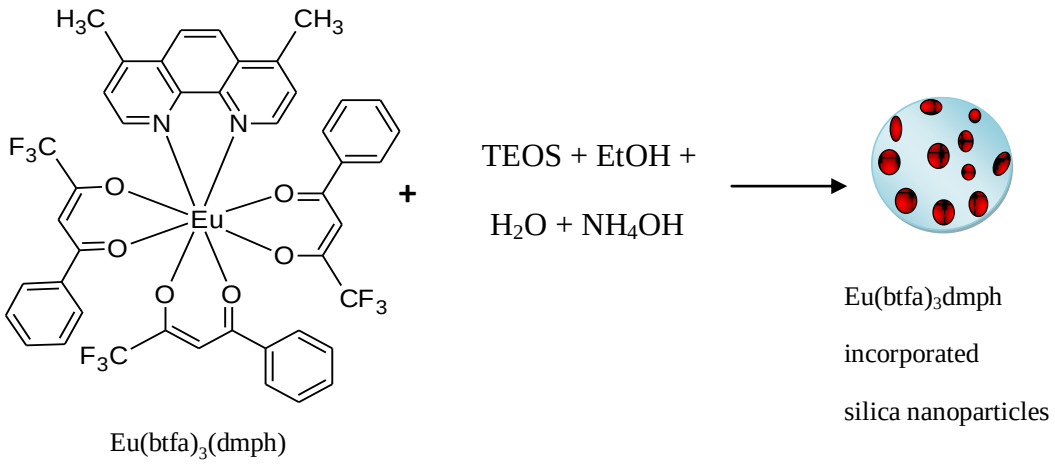

Figure 2.3. $Eu(btfa)_3(dmph)$ incorporated silica nanoparticles.

2.2.4 Synthesis of silica nanoparticles

Tetraethylorthosilicate (TEOS) (0.0133 mol, 3 mL), 28% NH_4OH (1 mL) and nanopure water (2 mL) were added into the ethanol solution (50 mL). The reaction mixture was stirred for 18 h at 55 °C. The reaction mixture was centrifuged at 4000 rpm for 20 min. The pellets were washed with ethanol to remove un-reacted chemicals and again centrifuged at 4000 rpm for 20 min.

2.3 SURFACTANT COATED Mn-DOPED ZnO NANOPARTICLES

2.3.1 Synthesis of poly (ethylene glycol)-coated Mn-doped ZnO nanoparticles

0.225 M of $ZnSO_4 \cdot 7H_2O$ aqueous solution (0.98 g, 0.0034 mol) in H_2O (15 mL), 0.012 M of $MnSO_4 \cdot H_2O$ aqueous solution (0.03 g, 0.00018 mol) in H_2O (15 mL), 0.725 M KOH (0.6 g, 0.0011 mol) in H_2O (15 mL) were prepared. Poly(ethylene glycol) (PEG) aqueous solution (1 g) in H_2O (15 mL) was prepared and heated to 65 °C. The aqueous solution of $ZnSO_4 \cdot 7H_2O$ and $MnSO_4 \cdot H_2O$ was added drop wise into the PEG solution under vigorous stirring. KOH solution (15 mL) was added drop wise to the reaction mixture within 10 min. The resulted reaction mixture was heated and stirred at 65 °C for 2 h. The mixture was cooled to room temperature and was aged for two days. The product was isolated by centrifugation at 4000 rpm for 15 min and it was washed with de-ionized water. The undoped ZnO nanoparticles were prepared using an identical preparative method. PEG-coated 7.5% and 10% Mn-doped ZnO nanoparticles were synthesized by using $MnSO_4 \cdot H_2O$ (0.045 g, 0.00027 mol) and (0.06 g, 0.00036 mol), respectively and using identical preparative method.

2.3.2 Synthesis of poly vinylpyrrolidine-coated Mn-doped ZnO nanoparticles

Poly vinylpyrrolidine (PVP) aqueous solution (1 g) in H_2O (15 mL) was prepared and heated to 65 °C. PVP-coated Mn-doped ZnO nanoparticles were synthesized adopting an otherwise identical preparative and purification procedure as for PEG-coated Mn-doped ZnO nanoparticles.

2.3.3 Coating of cotton textile with nanoparticles

Cotton woven textile samples were washed in a water bath at 60 °C for 30 min and dried in an oven at 60 °C overnight. The clean textiles were cut into 3 cm × 3 cm squares. The cotton samples were added into the aqueous solution of surface functionalized 5% Mn-doped ZnO nanoparticles (1 g/mL in H_2O) and stirred at 90 °C for 30 min. The wet samples were left overnight to evaporate the solvent at room temperature. The modified cotton textile samples were cut into 2 cm x 2 cm sized pieces and used for antimicrobial activity studies.

2.4 MATERIAL CHARACTERIZATION

2.4.1 UV-visible Absorption spectroscopy

UV-visible spectra were recorded on an Agilent 8453 UV-visible spectrometer. Samples were prepared by dispersing 2 mg of the nanoparticle samples in 2 mL of solvent (water or dichloromethane). Nanoparticle samples were sonicated for 10 minutes at room temperature before collecting the spectra. The absorption spectra were collected from 200 nm to 700 nm using quartz cuvettes.

2.4.2 Luminescence Spectroscopy

Photoluminescence spectra were collected using a Perkin Elmer LS-55 fluorescence spectrometer with a 5 nm slit width using quartz cuvettes. The excitation wavelength was 350 nm. The emission spectra were collected from 200 nm to 700 nm using a scan speed of 200 nm/minute. Photoluminescence quantum yields were calculated using cresyl violet perchlorate in methanol as the standard. Quantum yield of cresyl violet perchlorate is 0.54.[27] The relative quantum yields were calculated using equation 1, where *Abs, A* and *n* denote the absorbance at λ max, integrated area of the emission band of interest, and the refractive index of the solvent, respectively. Subscripts *R* and *S* refer to the reference and the sample, respectively

$$\phi_S = \phi_R \frac{(Abs_R)}{(Abs_S)} \frac{(A_S)}{(A_R)} \frac{(n^2_S)}{(n^2_R)} \qquad (1)$$

2.4.3 X-ray Powder Diffraction Studies

Solid nanoparticle samples (ZnO and Mn-doped ZnO nanoparticles) were dried in an oven at 100 ^{0}C for 24 h. The nanoparticle powders were ground and placed on the XRD well plate. X-ray powder diffraction spectra were collected using a desktop X-ray diffractometer "MiniFlex$^+$", with a Co-Kα (λ = 1.78899 A˚) radiation and a scan speed of 0.5° min^{-1}. Diffraction data were collected from 2θ = 3˚ to 2θ = 80˚. The X-ray generator was set at a power of 30 kV with a current of 15 mA. X-ray diffraction data were analyzed using Materials Data Jade 7 software.

2.4.4 Scanning Electron Microscopy (SEM) Studies

Scanning electron microscopy analysis (SEM) was performed on $Eu(btfa)_3dmph$ incorporated silica nanoparticles and Mn-doped ZnO nanoparticles using STEM-Hitachi HD2000 microscope with operating voltage of 200 kV**.** Samples were prepared by making a dispersion of nanoparticles (1 mg/mL) in water and drop casting them (200 μL) onto a carbon coated copper grid (300 mesh). Samples were dried at room temperature for 4 h.

Scanning electron microscopy analysis (SEM) was performed on PVP-coated Mn-doped ZnO nanoparticles attached cotton textile using variable pressure electron microscopy (SU6600 microscope) with operating voltage of 20 kV and pressure at 30 Pa.

2.4.5 Transmission Electron Microscopy (TEM) Studies

Size and the shape of the Mn-doped ZnO nanoparticles were determined using a TEM-H9500 microscope with an operating voltage of 300 kV. Samples were prepared by making a dispersion of nanoparticles (1 mg nanoparticles / 1mL H_2O) and drop casting them (200 μL) onto a carbon coated copper grid (300 mesh). Samples were dried at room temperature for 4 h.

2.4.6 Antimicrobial activity test

The antimicrobial activity of the $Eu(btfa)_3dmph$, $Eu(btfa)_3dmph$ incorporated silica nanoparticles and Mn-doped ZnO nanoparticles was evaluated against *S.aureus*, *S.epidermidis* and *E.coli* by using ISO standard antimicrobial testing methods

(quantitatively and qualitatively). These methods include agar diffusion method, shake flask test and minimum inhibitory concentration (MIC) method.[28] Agar diffusion method is a qualitatively test to determine antimicrobial activity of diffusible antimicrobial agents. [14, 15]

2.4.6.1 Preparation of Tryptic Soy Agar (TSA) plates

Tryptic soy agar is a general purpose medium, providing enough nutrients to allow for a wide variety of microorganisms to grow. It is used for a wide range of applications including culture storage, enumeration (counting), isolation of pure cultures or simply general culture. Tryptic soy agar powder (40 g) was suspended in a sterilized flask. Deionized water (1 L) was added to that flask and mixed well. The culture solution was autoclaved at 121 °C for 30 min using a Amsco renaissance 3021 gravity sterilizer. After cooling 45 °C, the liquid culture was dispensed into sterilized petri dishes (100 mm x 15 mm).

2.4.6.2 Preparation of Tryptic Soy Broth (TSB)

Tryptic soy broth is a general purpose liquid enrichment medium used in qualitative procedures for the sterility test and for the enrichment and cultivation of aerobic microorganisms. In clinical microbiology, it may be used for the suspension, enrichment and cultivation of strains isolated on other media. Tryptic Soy Broth powder (17 g) was mixed with deionized water (500 mL) in a 1 L flask and mixed gently. The culture solution was autoclaved at 121 °C for 30 min using a Amsco renaissance 3021 gravity sterilizer After cooling to 45 °C, the liquid culture was stored in a refrigerator.

2.4.6.3 Preparation of bacterial solutions for agar diffusion test and MIC test

S.aureus, S.epidermidis and *E.coli* bacterial suspensions were prepared by taking a single colony from the original bacterial culture plate with a loop and inoculating into a sterile tryptic soy broth (20 mL) in a 25 mL separate culture tube under aseptic conditions. The culture tubes were then incubated in a shaking incubator at 37 °C at 110 rpm for 30 min. Bacterial concentration was determined by measuring the optical density (OD) at 600 nm. Normally, the OD value of 0.3 corresponded to a bacteria concentration of 1 x 10^8 CFU/mL. [15]

2.4.6.4 Agar diffusion test for $Eu(btfa)_3dmph$ incorporated silica nanoparticles

Agar diffusion test was performed *in vitro* against several gram positive and gram negative bacteria species. Bacterial solutions of *S.aureus, S.epidermidis and E.coli* (100 µL) were inoculated on to TSA plates separately and evenly spread under aseptic conditions. 10 mm diameter of filter papers presoaked in $Eu(btfa)_3dmph$ complex and $Eu(btfa)_3(H_2O)_2$ complex dispersed in N,N-dimethyl formamide solution (0.25 M) were placed on the plates. The control sample solutions (DMF, $EuCl_3 \cdot H_2O$, dmph and btfa) were also placed on the plates. The inoculated agar plates were incubated at 37 °C for 24 h. The antibacterial activity of $Eu(btfa)_3dmph$ and $Eu(btfa)_3(H_2O)_2$ were demonstrated by the zone of inhibition in comparison to the control samples. Inhibition zone was measured by using 1 mm ruler. A similar procedure was followed for $Eu(btfa)_3dmph$ incorporated silica nanoparticles.

2.4.6.5 Agar diffusion test for surface functionalized Mn-doped ZnO nanoparticles

Bacterial solutions of *S.aureus, S.epidermidis and E.coli* (100 µL) were inoculated on to TSA plates separately and evenly spread under aseptic conditions. 8 mm diameter of wells was made on culture plate using micropipette tip. The bottom of wells were sealed by adding (50 µL) plane agar. All the nanoparticle samples were exposed to UV light for 30 min (SYLVANIA 350 Black light Hg 15 W). The wells were filled with nanoparticles (1 g) (ZnO, Mn-doped ZnO nanoparticles and polymer coated Mn-doped ZnO nanoparticles). The nanoparticles were allowed to diffuse into the agar followed by incubating the plates at 37 °C for 48 h. The inhibition zones of the wells were measured by using inhibition zone scale.

2.4.6.6 Agar diffusion test for surface functionalized Mn-doped ZnO nanoparticles incorporated cotton textile

Mn-doped ZnO nanoparticle incorporated cotton textile (2 cm x 2 cm) possessing antimicrobial activities and unmodified cotton textile were placed in separate positions on two TSA plates under aseptic conditions. Another thin layer of TSA (10 mL) was poured onto the textile samples so that textile materials were sandwiched between the TSA layers. The bacterial solutions of *Staphylococcus epidermidis, Staphylococcus aureus* and *Escherichia coli* (100 µL) were inoculated on to TSA plates and evenly spread. The inoculated agar plates were incubated at 37 °C for 24-48 h in an incubator. Bacterial inhibition was evaluated by measuring the zone of inhibition.

2.4.6.7 Minimum inhibitory concentration

For the minimum inhibitory test, undoped and Mn-doped ZnO nanoparticles were dispersed in autoclaved water (20 mg/mL) in glass vials and the samples were placed in sonicator for 30 min. All the nanoparticle samples were exposed to UV light for 1 h. TSA broth (50 µL) was added to the wells in a 96 well plate. Two-fold dilutions of the nanoparticles were carried out across row by transferring 50 µL from the first well to the second well. The transfer was successively repeated until well number 10. Finally, bacterial solution (25 µL) was inoculated in all wells, with the exception of well number 11 and 12. The wells 11 and 12 were control. The Alamar blue dye solution (25 µL) was added into all wells except number 12. Well 12 was considered as the negative control. The well plate was incubated at 37 °C for 24-48 h in an incubator. The minimum inhibitory concentration that substantially inhibited the growth of the organism was visually determined at the point where there no change in the original blue color of the well was observed. In blue color wells, there were no viable bacteria cells. In pink color wells, there were viable bacteria cells.

2.4.6.8 Shake flask test for textile materials

This method of evaluation involves testing bacterial suspensions directly inoculated onto modified and unmodified cotton textile samples. *S.aureus, S.epidermidis* and *E.coli* bacterial suspensions were prepared by taking a single colony from each original bacterial culture plate with a loop and inoculating into a sterile tryptic soy broth (20 mL) in a 25 mL separate culture tube under aseptic conditions. The culture tubes were then incubated in a shaking incubator at 37 °C at 110 rpm for 1 h and measured the

OD value at 600 nm. After incubating, 100 µL of the bacteria suspension was transferred to a sterile culture tubes that contained tryptic soy broth (20 mL) with modified and unmodified cotton textile (2 x 2 cm) samples separately. The samples were shaken for 5 min. The culture tubes were incubated in a shaking incubator at 37 ℃ and 110 rpm. The optical density of the culture tubes were measured at 600 nm for every 30 min until 7 h.

2.4.7 Antifungal activity test for polymer coated Mn-doped ZnO nanoparticles incorporated cotton textile

Antifungal activity was tested by parallel streak method. Modified and unmodified cotton textile samples were placed on the Yeast Extract-Peptone-Dextrose (YPD) culture plates and a thin YPD gel layer (10 mL) was poured on the textile samples. The parallel streaks were drawn on the top gel layer using a loop that contained fungal colonies of *Cryptococcus*. The plates were incubated at 30 ℃ for 48 h in an incubator.

CHAPTER 3

RESULTS AND DISCUSSION

Our research was planned to prepare two different types of nanoparticles with improved water soluble, low particle size, and low cytotoxicity for biological applications. Results and discussion of this project were focused on europium chelator-based silica nanomaterials and polymer coated Mn-doped ZnO nanoparticles.

3.1 LANTHANIDE-BASED SILICA NANOMATERIALS [$Eu(btfa)_3dmph$ INCORPARATED SILICA NANOPARTICLES]

3.1.1 UV-visible absorption and Luminescence Studies

The UV-vis absorption spectra of $Eu(btfa)_3dmph$ complex, $Eu(btfa)_3(H_2O)_2$ complex and $Eu(btfa)_3dmph$ complex incorporated silica nanoparticles are shown in Figure 3.1a and Figure 3.1b. The $Eu(btfa)_3dmph$ complex has absorption band maxima at 235 nm, 270 nm and 325 nm. The $Eu(btfa)_3(H_2O)_2$ complex also exhibits absorption bands at 260 nm and 325 nm. The btfa ligand absorbs energy at 260 and 325 nm. Dmph ligand has a maximum absorption band at 270 nm. The complex absorbs energy through the ligand system.

Absorption studies were carried of the silica nanoparticles and the $Eu(btfa)_3dmph$ complex incorporated silica nanoparticles. The absorption spectrum of silica nanoparticles exhibits a peak at 210 nm.[26] This is specific for Si-O-Si bonds and it confirms the presence of silica nanoparticles as shown in Figure 3.1b. The optical absorption of $Eu(btfa)_3dmph$ incorporated silica nanoparticles exhibit peaks at 230 nm,

275 nm and 325 nm as shown in Figure 3.1b. Peaks observed in Figure 3.1b confirm the presence of the Eu complex within the silica nanoparticles.

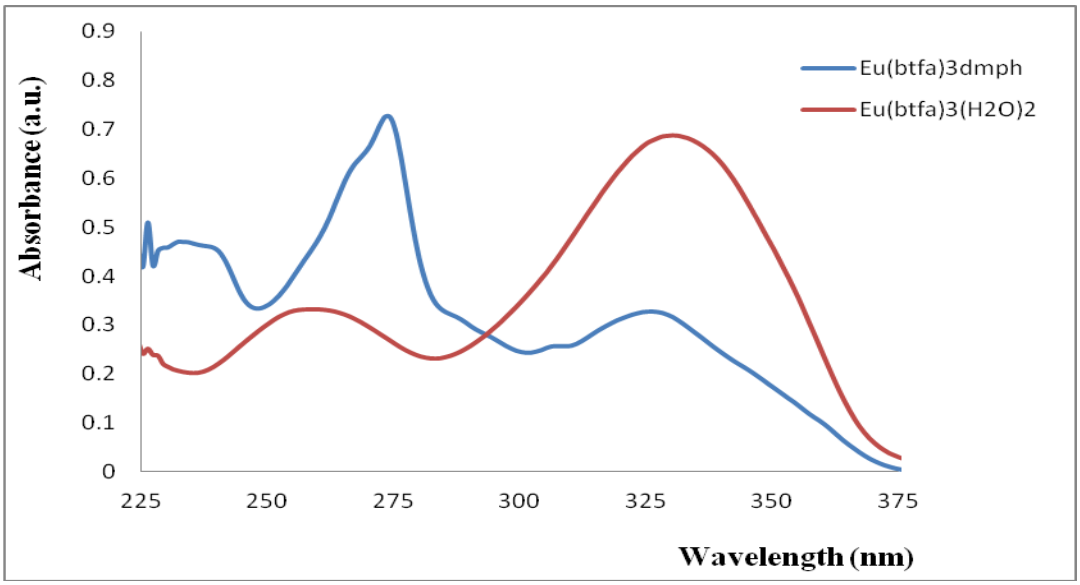

Figure 3.1a. Absorption spectra of $Eu(btfa)_3dmph$ and $Eu(btfa)_3(H_2O)_2$ complexes.

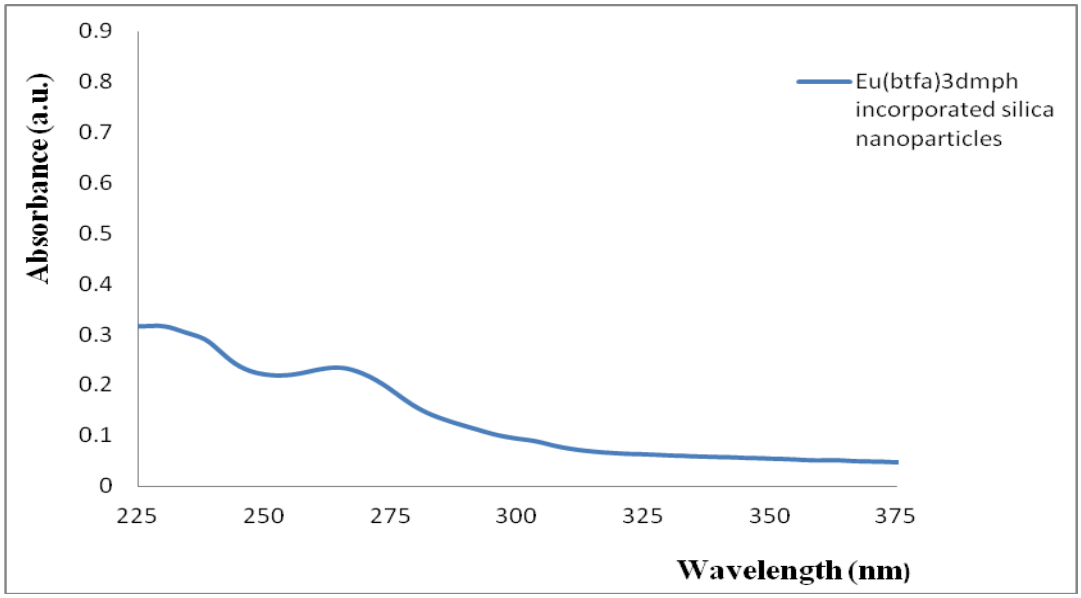

Figure 3.1b. Absorption spectrum of $Eu(btfa)_3dmph$ complex incorporated silica nanoparticles.

The $Eu(btfa)_3dmph$ complex produced a bright red emission as shown in Figure 3.2 (a). The emission spectra were taken using 350 nm excitation at 1×10^{-6} M concentration of $Eu(btfa)_3dmph$ complex in methylene chloride (Figure 3.3a). Both $Eu(btfa)_3dmph$ complex and $Eu(btfa)_3dmph$ complex incorporated silica nanoparticles have the $^5D_0$ to $^7F_1$ (595 nm), $^5D_0$ to $^7F_2$ (614 nm) peaks that are characteristic of Eu^{3+} emission. The $Eu(btfa)_3dmph$ complex has a higher luminescence intensity than that of the $Eu(btfa)_3(H_2O)_2$ complex due to possible vibrational quenching in the presence of coordinated H_2O ligands. The $Eu(btfa)_3dmph$ complex incorporated silica nanoparticles exhibit emission at 614 nm upon 350 nm excitation as shown in Figure 3.3 (b). The energy is transferred from the excited singlet state of the antenna to the triplet state of the ligands followed by an internal energy transfer from the triplet ligand level to the europium ion-based excited states resulting europium-centered luminescence. The most well-known emission line for europium is from the $^5D_0$ state to the $^7F_2$ ground state.[7-8] The picture in Figure 3.2 (b) shows red luminescence of the $Eu(btfa)_3dmph$ complex incorporated silica nanoparticles upon UV excitation.

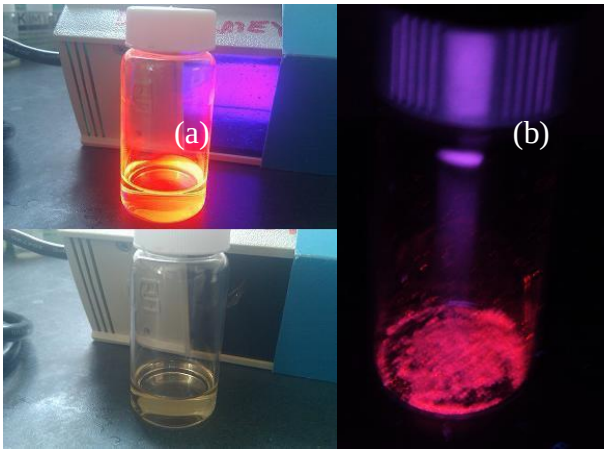

Figure 3.2. (a) $Eu(btfa)_3dmph$ in methylene chloride solution under visible light (bottom) and UV excitation (top), (b) $Eu(btfa)_3dmph$ complex incorporated silica nanoparticles under UV excitation.

The luminescence lifetimes of the $Eu(btfa)_3dmph$ complex were measured upon 355 and 465 nm excitation as a dry powder and in methylene chloride solution. 355 nm radiation was used as the ligand excitation whereas 465 nm can be used for direct excitation of the europium ions via *f* to *f** electronic transitions.

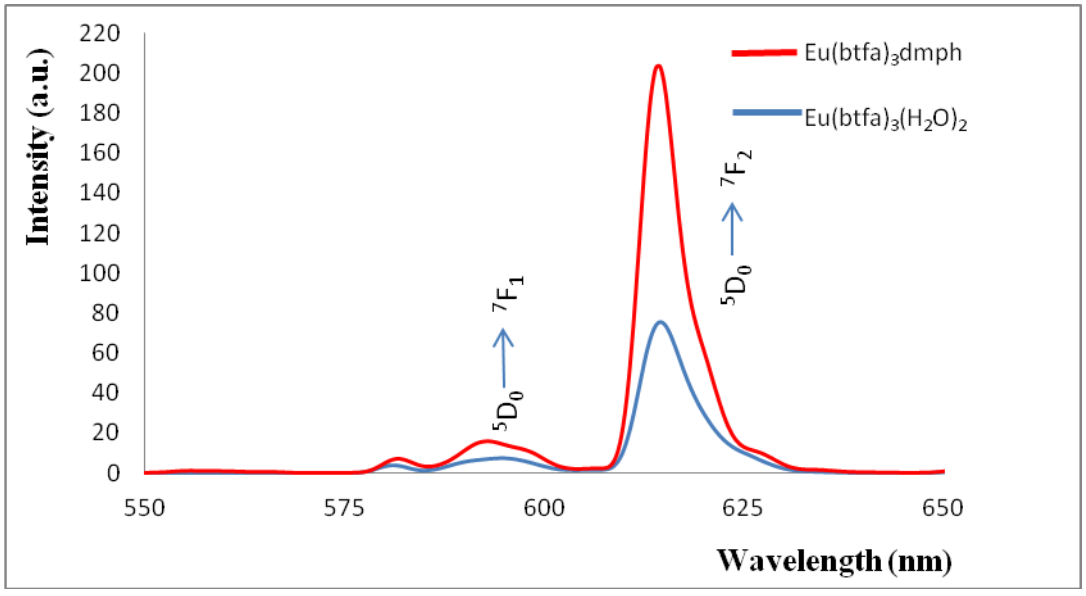

Figure 3.3a. Luminescence spectra of $Eu(btfa)_3(H_2O)_2$ and $Eu(btfa)_3dmph$ complexes,

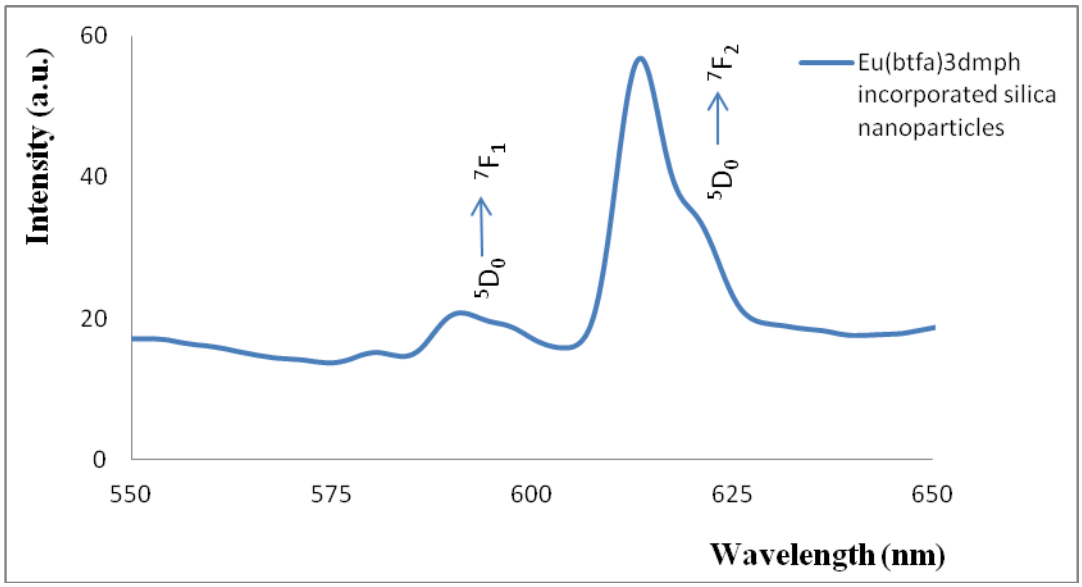

Figure 3.3b. $Eu(btfa)_3dmph$ complexes incorporated silica nanoparticles dispersed in water (excitation wavelength = 350 nm).

The luminescence lifetimes of the $Eu(btfa)_3dmph$ complex are 0.593 ms and 0.572 ms for the dry powder upon 355 nm and 465 nm excitation, respectively. The luminescence lifetime values are 0.813 ms and 0.811 ms for the chelator dissolved in methylene chloride upon 355 nm and 465 nm excitation, respectively. It was compared to the $Eu(btfa)_3(H_2O)_2$ complex under the same conditions. The luminescence lifetimes of the $Eu(btfa)_3(H_2O)_2$ complex are 0.384 ms and 0.771 ms for the dry powder upon 355 nm and 465 nm excitation, respectively. The values for the same complex dissolved in methylene chloride are 0.470 ms and 0.474 ms upon 355 and 465 nm excitation, respectively.

The long luminescence lifetime of the complexes promises their applications in live cells with higher levels of background rejection. The quantum yield of 30 mg

Eu(btfa)$_3$dmph complex incorporated silica nanoparticles was 3.1% and 40 mg Eu(btfa)$_3$dmph incorporated silica nanoparticles was 11.58 %.

3.1.2 Scanning Electron Microscope (SEM) Studies

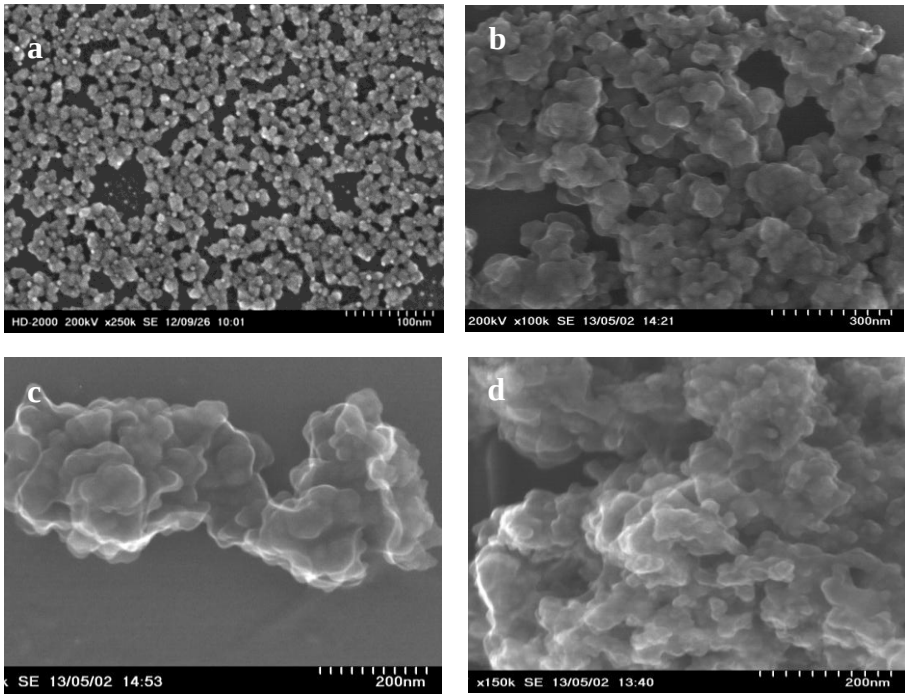

Figure 3.4. SEM image of (a) silica nanoparticles, (b) 20 mg of Eu(btfa)$_3$dmph incorporated silica nanoparticles, (c) 30 mg of Eu(btfa)$_3$dmph incorporated silica nanoparticles and (d) 40 mg of Eu(btfa)$_3$dmph incorporated silica nanoparticles prepared by using modified Stöber method.

For SEM studies, samples were examined using high resolution HD 2000 Hitachi STEM instrument. Figure 3.4 represents the scanning electron micrographs of silica nanoparticles and Eu(btfa)$_3$dmph incorporated silica nanoparticles. The average diameter of silica nanoparticles was 12 nm (Figure 3.4a). The average size of 20 mg

$Eu(btfa)_3dmph$ incorporated silica nanoparticles was 45 nm (Figure 3.4b). The particle size range of 30 mg and 40 mg of $Eu(btfa)_3dmph$ incorporated silica nanoparticle was 40 nm (Figure 3.4c and 3.4d). $Eu(btfa)_3dmph$ incorporated silica nanoparticles were well dispersed in water up to all the doping levels of the complex studied in this work. Clear solutions were obtained in all the dispersions.

3.1.3 Antimicrobial studies

3.1.3.1 Agar diffusion test

The antibacterial activity was evaluated by using agar diffusion test. The antibacterial activity of the corresponding complexes [$Eu(btfa)_3dmph$ incorporated silica nanoparticles, $Eu(btfa)_3dmph$ and $Eu(btfa)_3(H_2O)_2$ complexes] and the individual ligands were tested simultaneously against *S. aures S. epidermidis* and *E.coli* bacteria species. The antimicrobial activities of the complexes and the ligands are shown in Figure 3.5 using *S. aureus*. Inhibition zone of btfa and dmph was 6 mm and 20 mm, respectively. According to Figure 3.5(c) and 3.5(d), the ligand btfa was less antimicrobial active than dmph against *S. aureus*. Compared to the btfa ligand, the $Eu(btfa)_3dmph$ complex (Figure 3.5a) shows higher inhibition zone (28 mm) against bacterial growth.

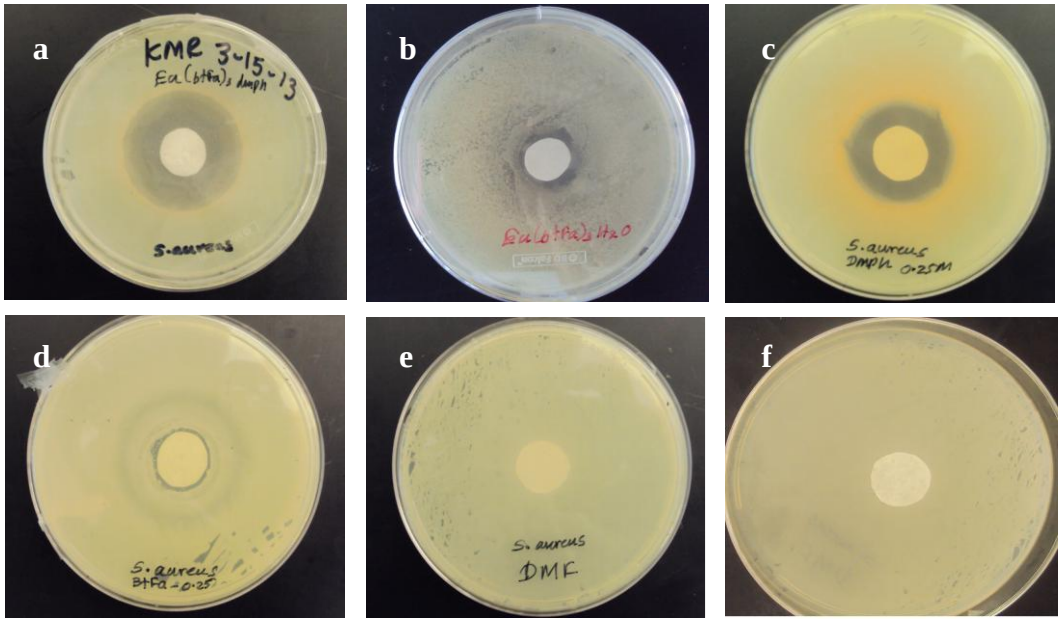

Figure 3.5. Antibacterial activity of (a) 0.25 M $Eu(btfa)_3$dmph, (b) 0.25 M $Eu(btfa)_3(H_2O)_2$, (c) 0.25 M dmph, (d) 0.25 M btfa, (e) N,N-dmethyl formamide and (f) 0.25 M $EuCl_3 \cdot 6H_2O$ against *S. aureus*.

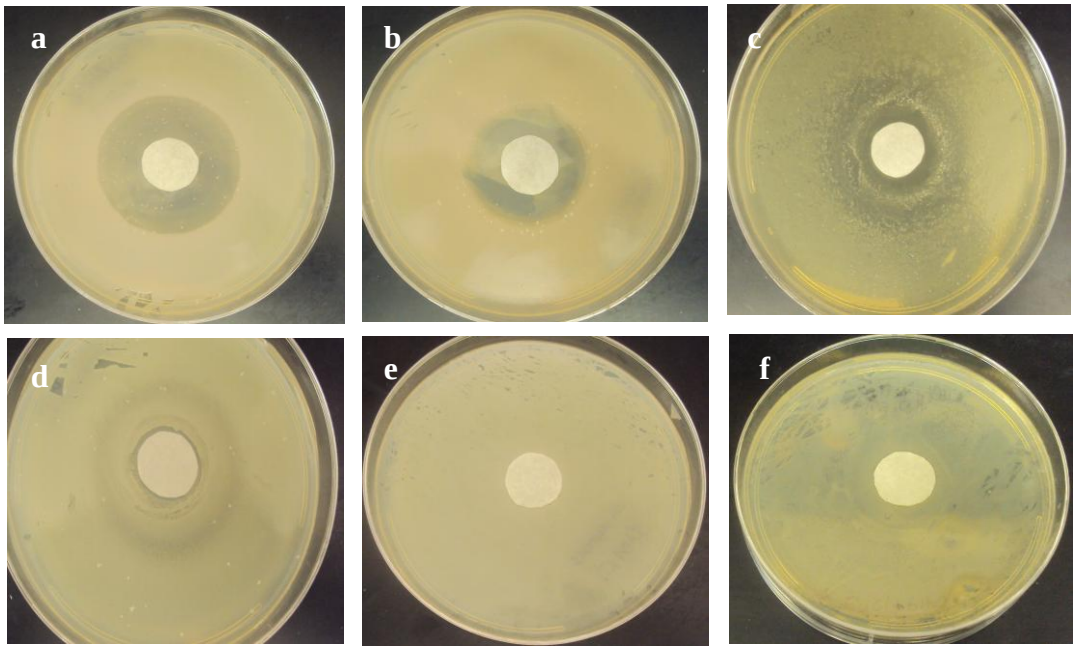

Figure 3.6. Antibacterial activity of (a) 0.25 M $Eu(btfa)_3$dmph, (b) 0.25 M $Eu(btfa)_3(H_2O)_2$, (c) 0.25 M Dmph, (d) 0.25 M Btfa, (e) N,N-Dimethyl Formamide, and (f) 0.25 M $EuCl_3 \cdot 6H_2O$ against *S. epidermidis*.

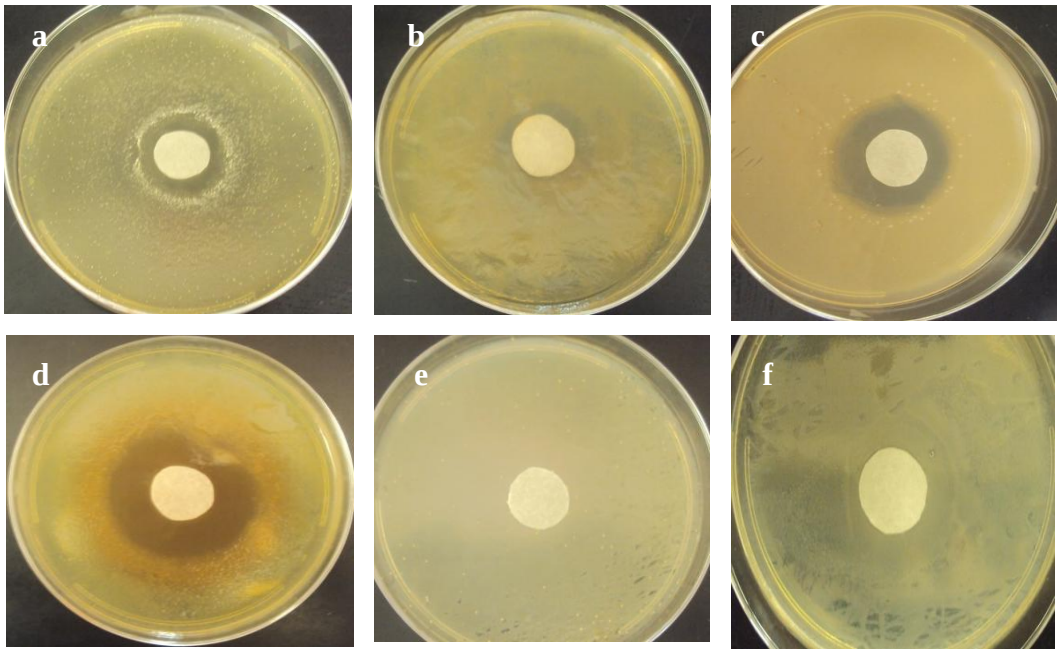

Figure 3.7. Antibacterial activity of (a) 0.25 M $Eu(btfa)_3dmph$, (b) 0.25 M $Eu(btfa)_3(H_2O)_2$, (c) 0.25 M Dmph, (d) 0.25 M Btfa, (e) N,N-Dimethyl Formamide, and (f) 0.25 M $EuCl_3 \cdot 6H_2O$ against *E.coli*.

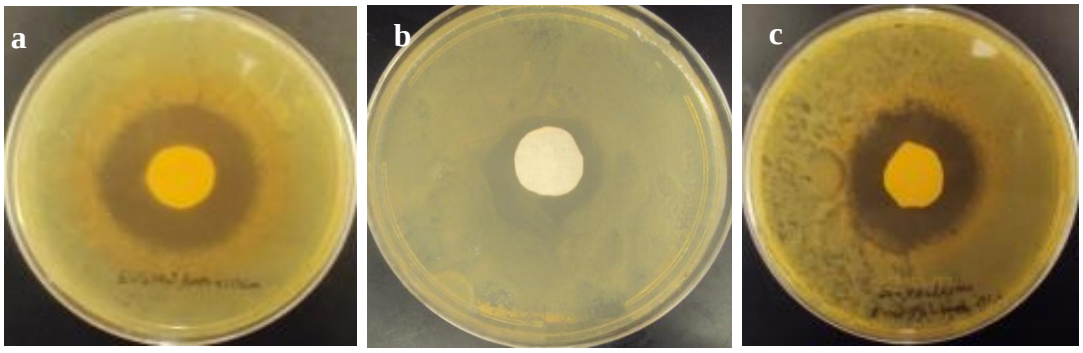

Figure 3.8. Antibacterial activity of $Eu(btfa)_3dmph$ incorporated silica nanoparticles (5 mg/mL in water) against plate (a) *S.aureus* (b) *E.coli* and (c) *S.epidermidis.*

Table 3.1. Inhibition zone values of three bacterial species.

Compounds	Inhibition zone (mm)		
	S.aureus	*S.epidermidis*	*E.coli*
$Eu(btfa)_3dmph$	28	25	26
$Eu(btfa)_3(H_2O)_2$	18	16	17
Dmph-ligand	20	17	25
Btfa-ligand	6	4	28
DMF- solvent	0	0	0
$EuCl_3 \cdot 6H_2O$	0	0	0
$Eu(btfa)_3dmph$ incorporated silica nanoparticles	26	25	18

Compared with gram-positive bacteria, gram-negative bacteria are more resistant against antibiotics, despite their thinner peptidoglycan layer, because of their additional, relatively impermeable lipid membrane. But according to Table 3.1, btfa ligand has a higher inhibition zone against gram-negative *E.coli*.

The complexes of $Eu(btfa)_3dmph$ and $Eu(btfa)_3(H_2O)_2$ show moderate antimicrobial activity against bacteria as compared to $EuCl_3 \cdot 6H_2O$. This is due to the synergistic effect that increases the lipophilicity of the complexes. Chelation decreases the polarity of the metal ion, which further leads to the enhancement of complex's lipophilicity.[14,16] Since the microorganism cell is surrounded by a lipid membrane which favors the passage of lipid soluble materials, increased lipophilicities allow the penetration of complex into and through the membrane and deactivate the active enzyme sites of the microorganisms. Also dmph ligand can intercalate DNA or RNA bases. That may enhance the antimicrobial activity of $Eu(btfa)_3dmph$ complex. [31]

3.1.3.2 Minimum inhibitory concentration (MIC) studies

Alamar Blue has been used extensively in biomedical research to assess the relative susceptibilities of a number of pathogens to anti-microbial compounds.[32] There have been numerous publications that describe the successful use of Alamar Blue in drug screening for bacterial pathogens. In this work, Alamar Blue was used to determine the minimum inhibitory concentration of europium complexes and the nanomaterials. This method is laborious, time consuming, require considerable amount of media. [32] The minimum inhibitory concentration can be visualized by naked eye (color change from blue to pink).

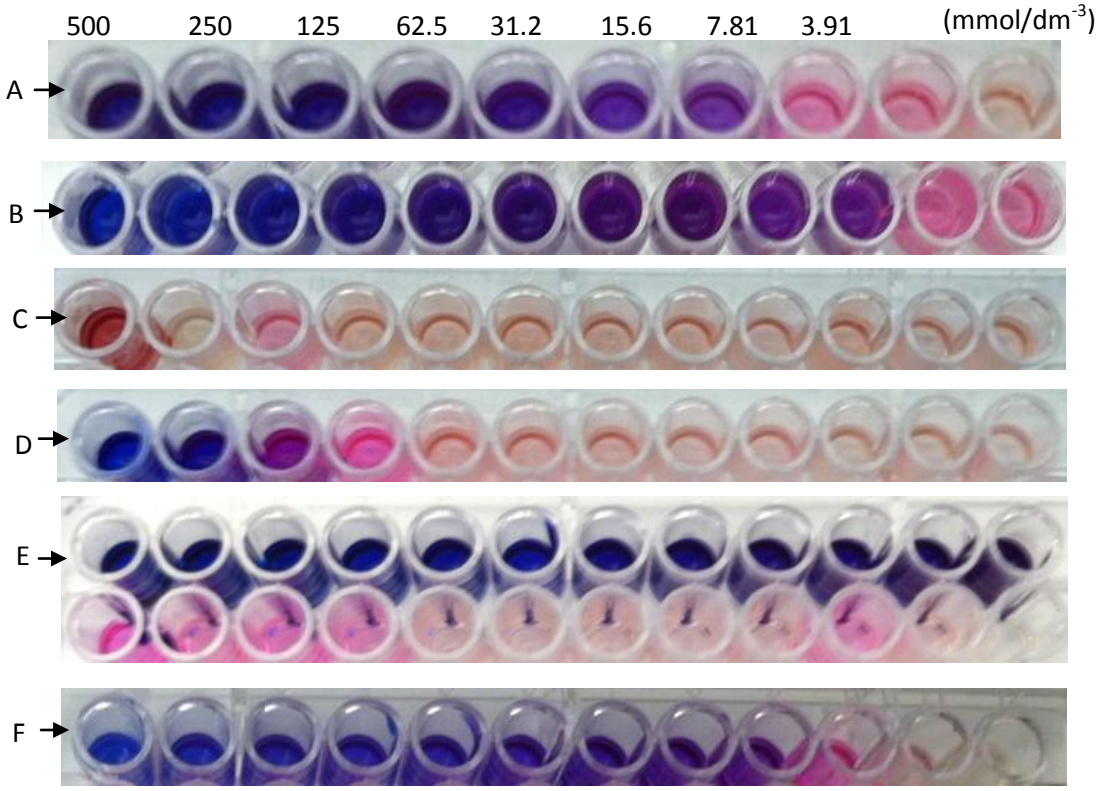

Figure 3.9. Alamar Blue assay used to determine the MIC of (A) 0.1 M btfa, (B) 0.1 M dmph, (C) 0.1 M $EuCl_3 \cdot 6H_2O$, (D) M N,N-Dimethyl Formamide, (E) 0.1 M $Eu(btfa)_3$dmph complex and (F) 0.1 M $Eu(btfa)_3(H_2O)_2$ complex against *S. aureus.*

Alamar Blue monitors the reducing environment of the living cells. The active ingredient of Almar Blue is resazurin. The structures of Alamar Blue (Resazurin) and Resorufin are shown in Figure 3.10. The dye acts as an intermediate electron acceptor in the electron transport chain without interference of the normal transfer of electrons. [33-34] As the indicator dye accepts electrons from metabolically active bacteria cells, it changes from the oxidized (blue state) to the reduced (pink state). Figure 3.9 shows the color changes of Alamar Blue dye from blue to pink. When there are viable bacteria cells in the well, Alamar Blue became pink color. According to Figure 3.9, $Eu(btfa)_3dmph$ has higher antimicrobial activity than $Eu(btfa)_3(H_2O)_2$. This may be due to the relatively higher lipophilicity of the $Eu(btfa)_3$ dmph ligand compared to its aqua analogue. Furthermore dmph ligand may involve in intercalating with DNA or RNA bases of the microorganisms. The minimum inhibitory concentration values of the complexes and the starting materials are shown in Table 3.2.

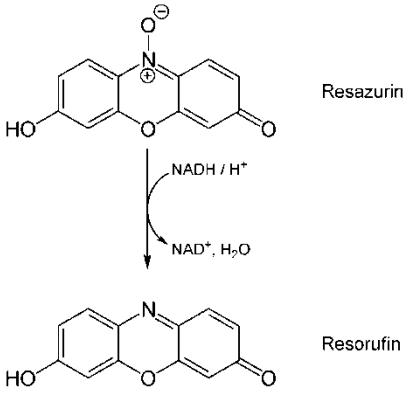

Figure 3.10. The structure of Resazurin and Resorufin.[34]

Table 3.2. Minimum inhibitory concentration against *S. aureus.*

Sample	Minimum Inhibition Concentration ($mol\ dm^{-3}$)
$Eu(btfa)_3dmph$	5.9×10^{-5}
dmph	5.14×10^{-4}
$Eu(btfa)_3(H_2O)_2$	11.3×10^{-4}
$EuCl_3 \cdot 6H_2O$	No MIC
btfa	13.0×10^{-4}
DMF (Solvent)	9.98×10^{-3}

3.2 SURFACE FUNCTIONALIZATION OF Mn-DOPED ZnO NANOPARTICLES AND NANOPARTICLE-INCORPORATED COTTON FABRIC

3.2.1 X-Ray Powder Diffraction Studies

X-Ray powder diffraction (XRD) pattern of the surface functionalized ZnO, ZnO coated with PEG and PVP, Mn-doped ZnO and undoped ZnO nanoparticles are shown in Figures 3.11 – 3.19. XRD peaks of Mn-doped ZnO nanoparticles observed at 2θ values are 32, 34, 36, 48, 57, 63, 68. The literature reported XRD pattern of ZnO nanoparticles is shown in Figure 3.20.[35] The XRD peaks for (100), (002), (101), (102), (110), (103) and (112) planes indicates the formation of phase pure Wurtzite structure of ZnO.[36] The XRD pattern of Mn-doped ZnO and surface functionalized Mn-doped ZnO nanoparticles show

only the peaks corresponding to Wurtzite crystal structure of ZnO. Therefore Mn(III) doping did not alter the basic crystal structure of ZnO.

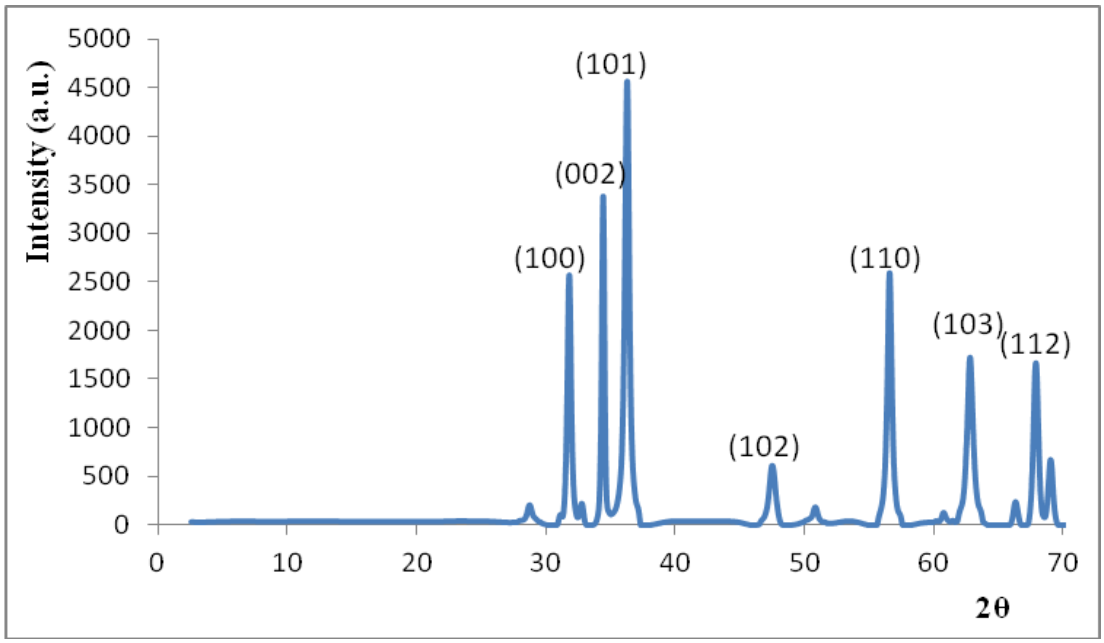

Figure 3.11. XRD pattern of 5% Mn-doped ZnO nanoparticles.

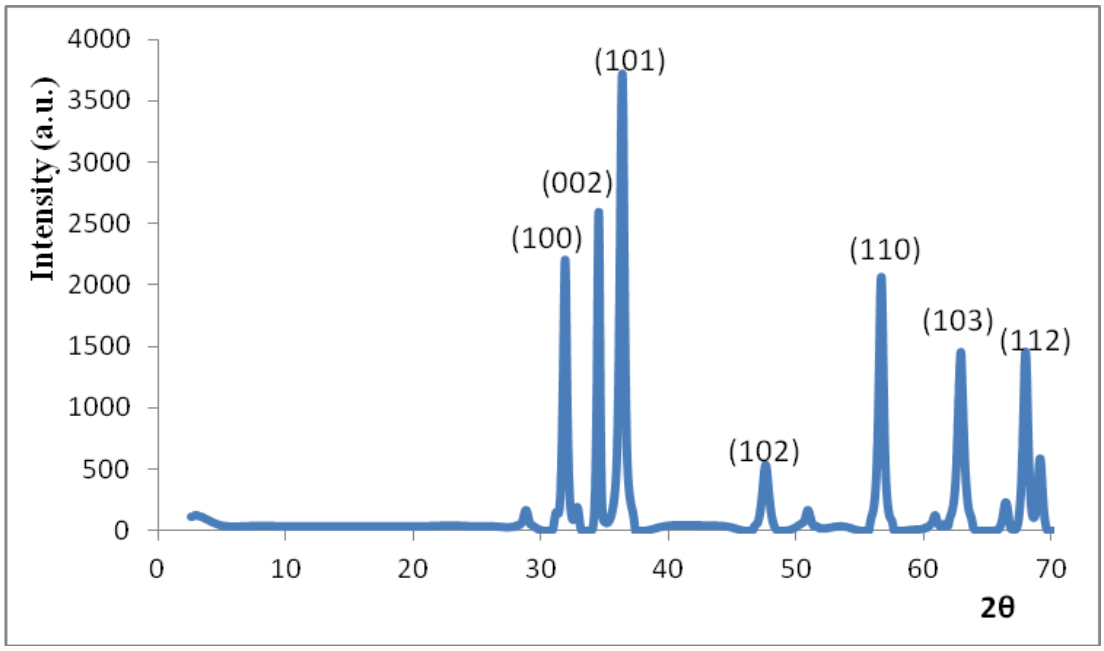

Figure 3.12. XRD pattern of PEG-coated ZnO nanoparticles.

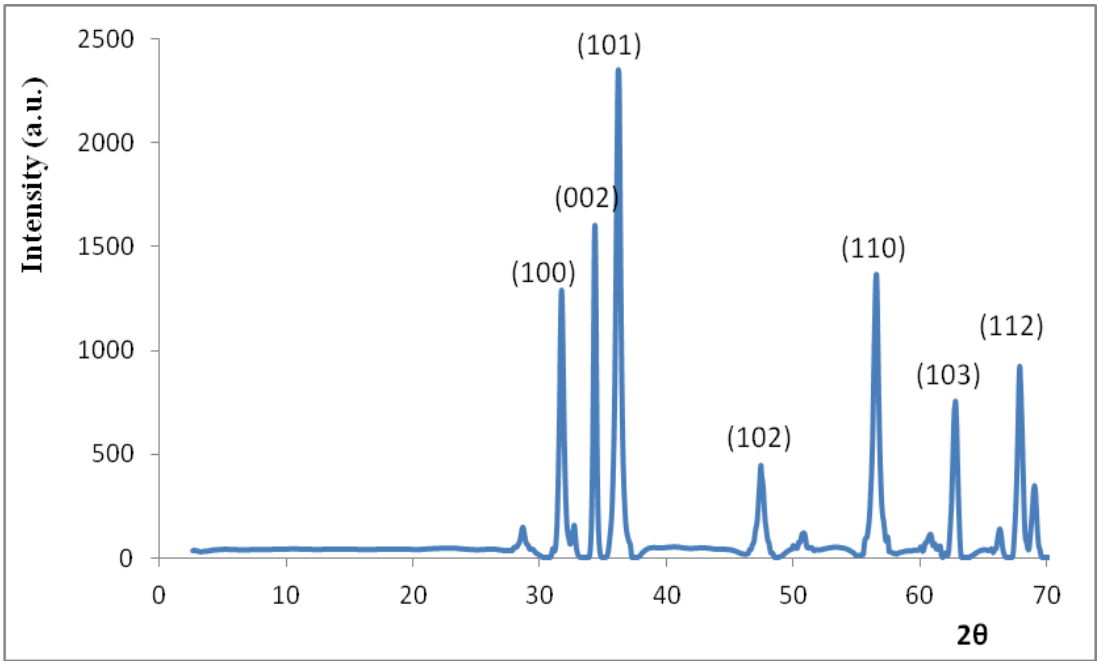

Figure 3.13. XRD pattern of PEG-coated 5% Mn-doped ZnO nanoparticles.

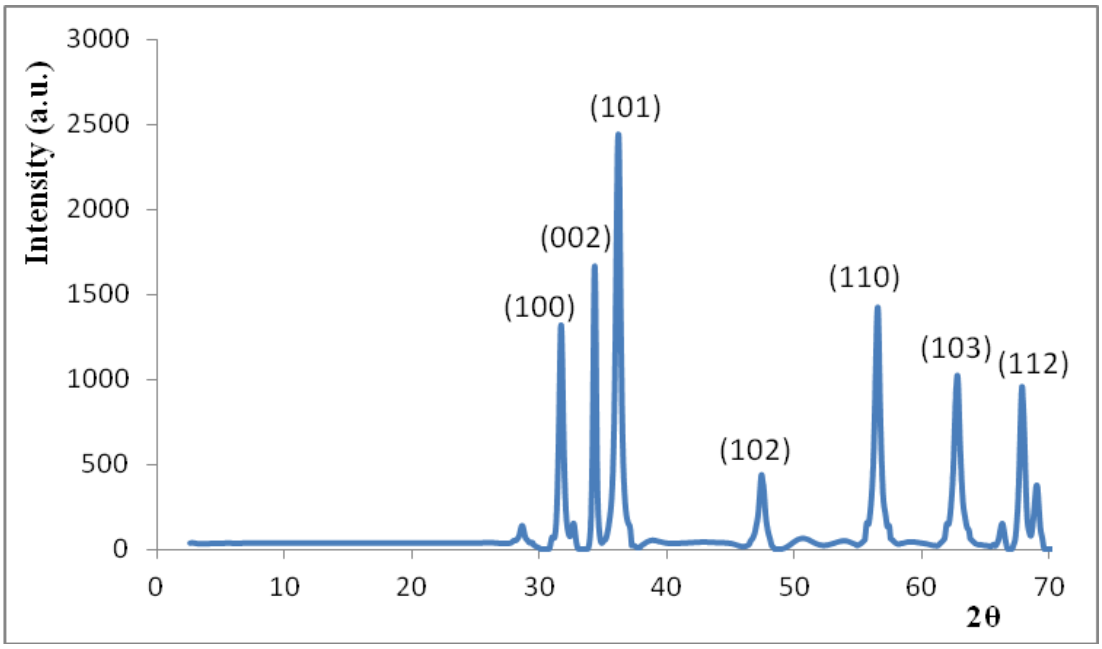

Figure 3.14. XRD pattern of PEG-coated 7.5% Mn-doped ZnO nanoparticles.

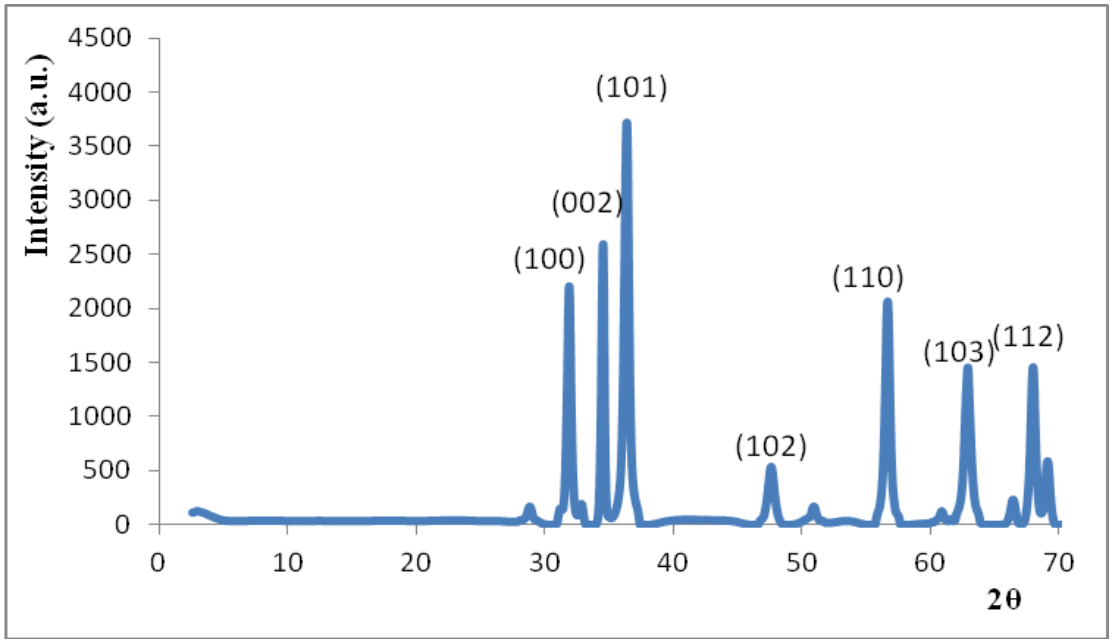

Figure 3.15 . XRD pattern of PEG-coated 10% Mn-doped ZnO nanoparticles.

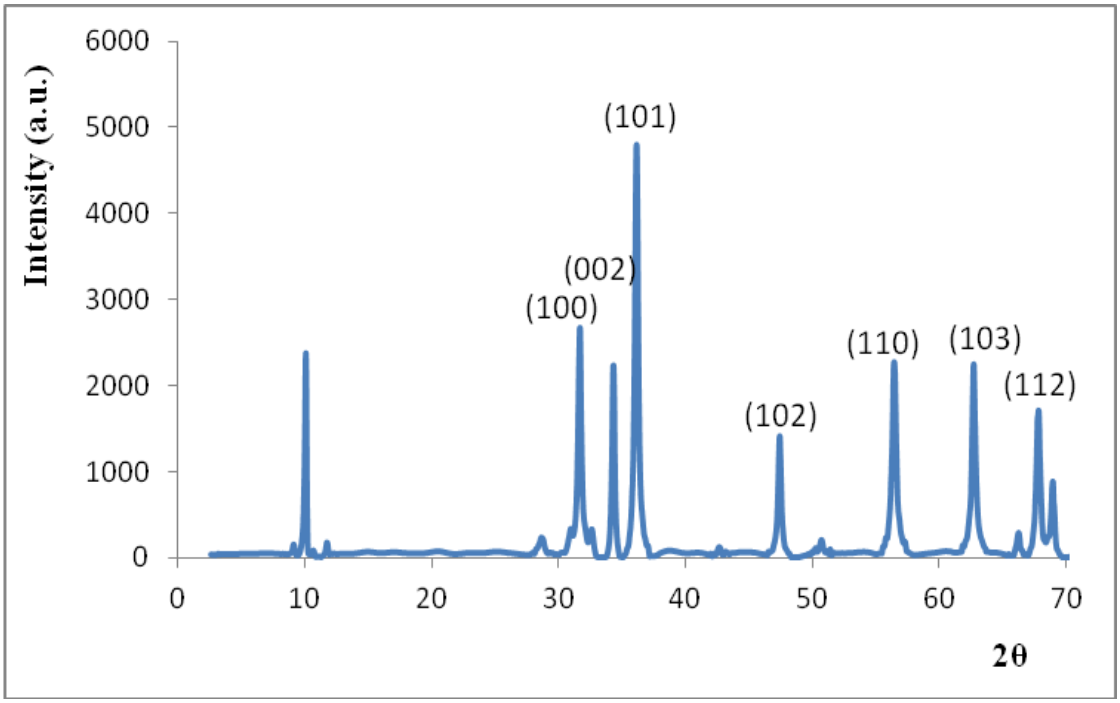

Figure 3.16. XRD pattern of PVP-coated ZnO nanoparticles.

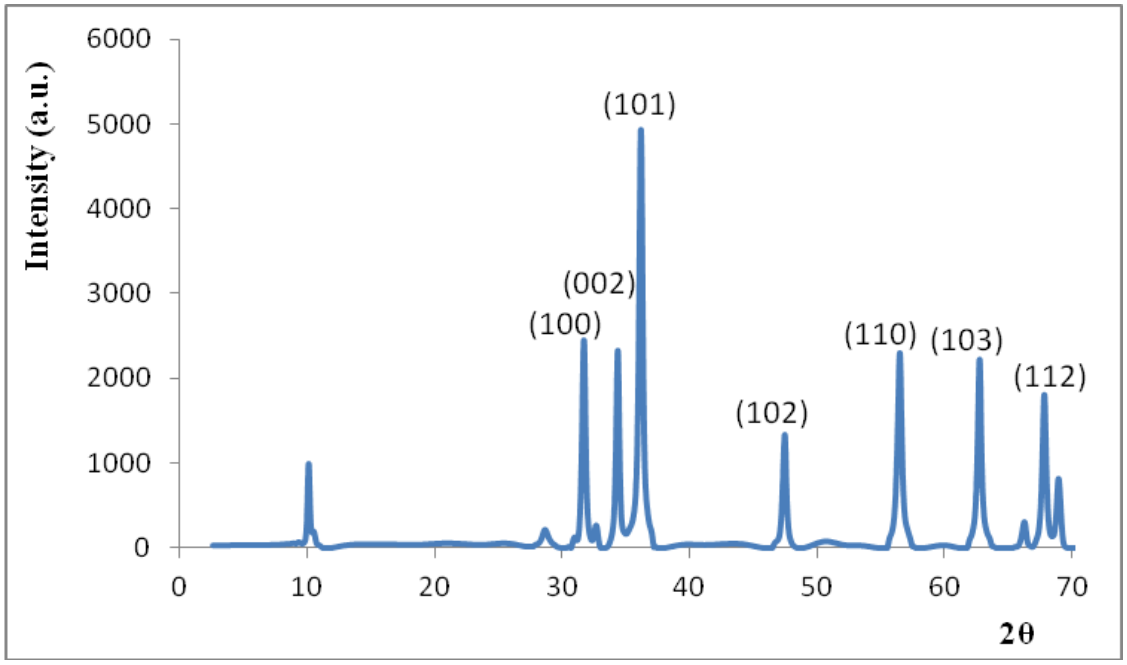

Figure 3.17. XRD pattern of PVP-coated 5% Mn-doped ZnO nanoparticles.

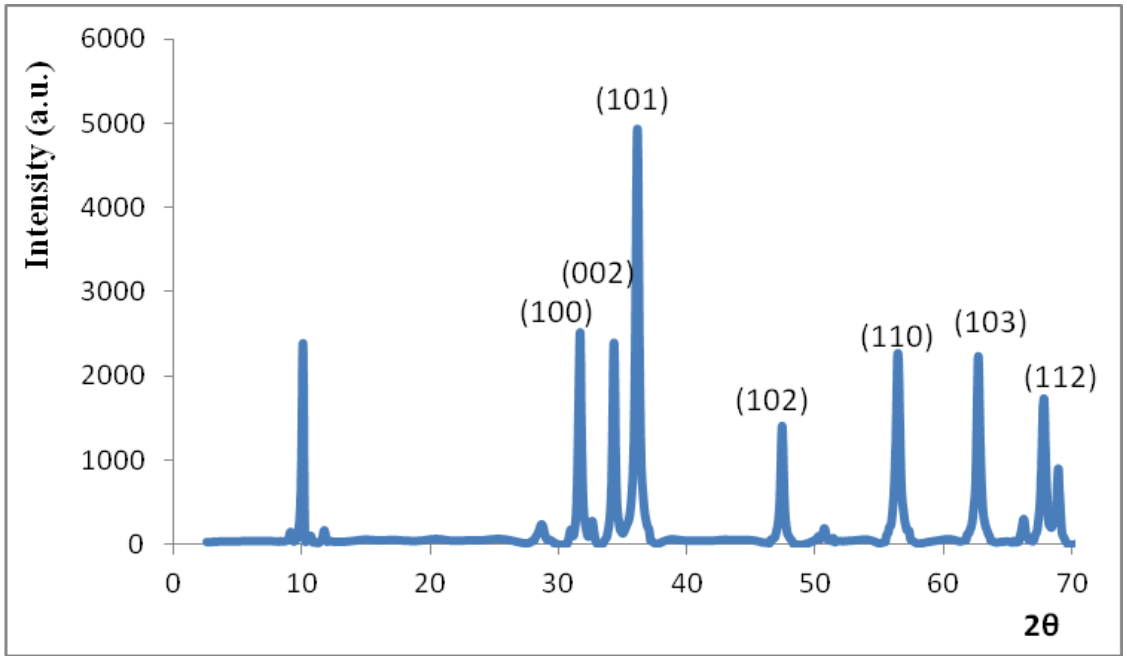

Figure 3.18. XRD pattern of PVP-coated 7.5% Mn-doped ZnO nanoparticles.

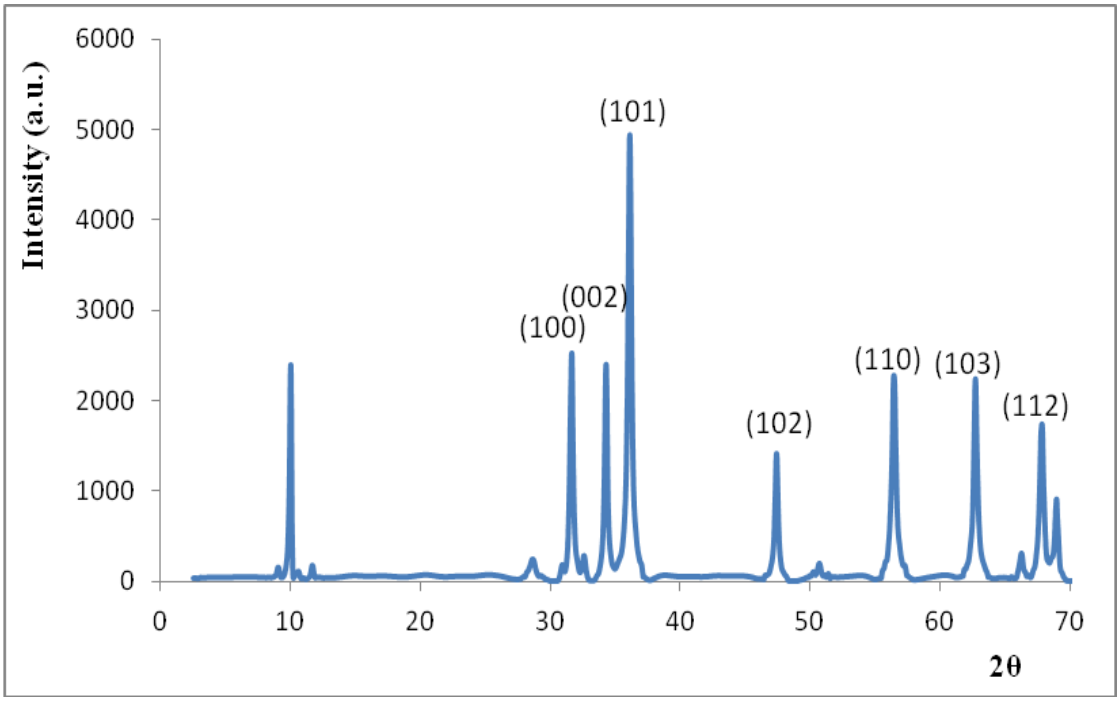

Figure 3.19. XRD pattern of PVP-coated 10% Mn-doped ZnO nanoparticles.

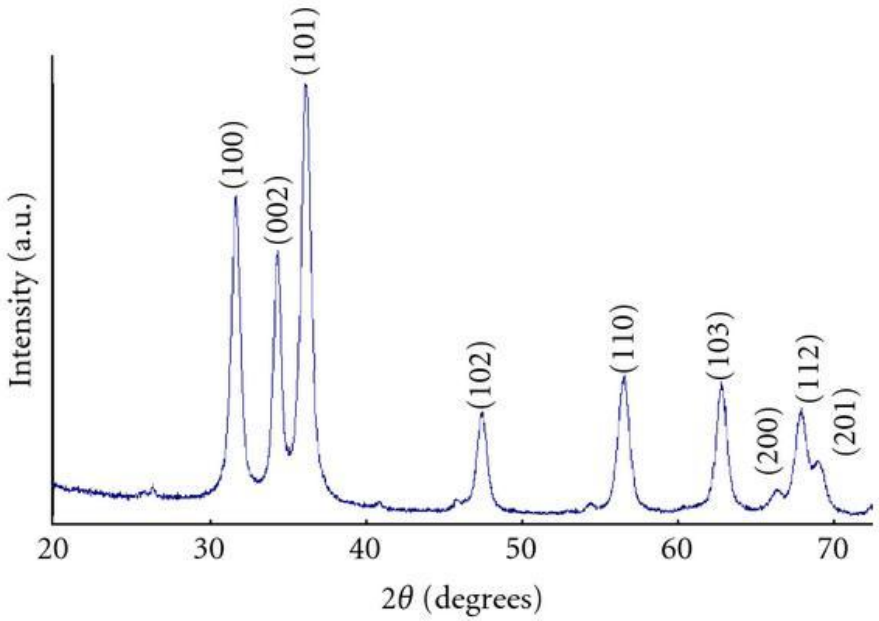

Figure 3.20. Literature reported XRD pattern of ZnO nanoparticles. [35]

Table 3.3. Calculated crystallite size of ZnO nanoparticles using Scherrer equation

Sample name	Crystallite size (nm)
ZnO	41
PEG-coated ZnO	25
PVP-coated ZnO	13
5% Mn-doped ZnO	39
PEG-coated 5% Mn-doped ZnO	26
PVP-coated 5% Mn-doped ZnO	11
7.5% Mn-doped ZnO	38
PEG-coated 7.5% Mn-doped ZnO	23
PVP-coated 7.5% Mn-doped ZnO	16
10% Mn-doped ZnO	41
PEG-coated 10% Mn-doped ZnO	28
PVP-coated 10% Mn-doped ZnO	16

The average crystallite size (D) was estimated using the Scherrer formula. The crystallite size of the surface functionalization of ZnO and Mn-doped ZnO nanoparticles is shown in Table 3.3. Compared to the polymer-uncoated Mn-doped ZnO nanoparticles, the polymer-coated Mn-doped ZnO nanoparticles show lower crystallite size. The results

(Table 3.3) show that the presence of PVP and PEG leads to the formation of slightly smaller Mn-doped ZnO nanoparticles.

3.2.2 Transmission Electron Microscope (TEM) and Scanning Electron Microscope Studies (SEM)

The particle size of the Mn substituted ZnO nanoparticles was determined using TEM and SEM images. Average crystallite size of the nanoparticles was calculated using XRD data and Scherrer's formula. The TEM micrograph of 5% Mn-doped ZnO nanoparticles is shown in Figure 3.21A. It was observed that without PEG and PVP 5% Mn-doped ZnO nanoparticles are agglomerated. The lattice figure of 5% Mn-doped ZnO nanoparticle is shown in Figure 3.21B. The lattice fringes confirm the crystallanity of the Mn-doped ZnO nanoparticles with a lattice spacing of 2.447 Å.

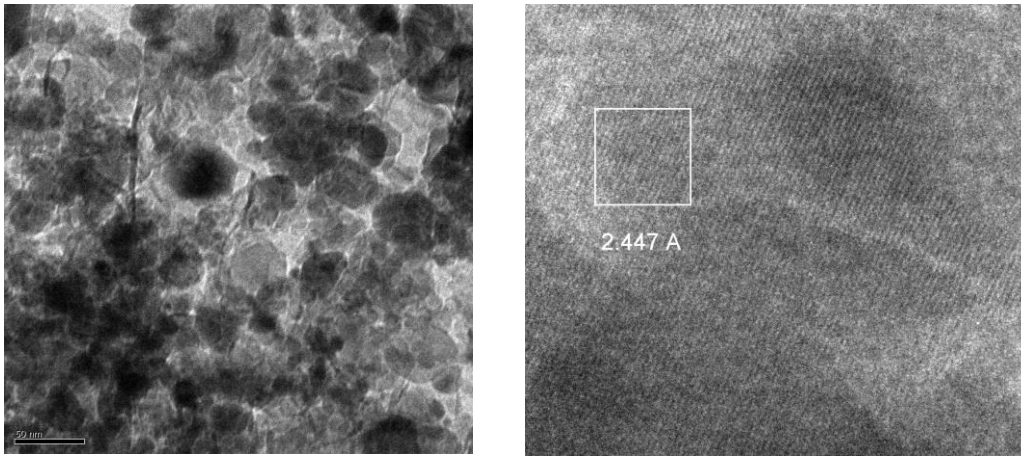

A B

Figure 3.21. Transmission electron microscope images of (A) 5% Mn-doped ZnO nanoparticles, and (B) the lattice structure of 5% Mn-doped ZnO nanoparticles.

TEM images of PEG-coated 5% Mn-doped ZnO nanoparticles and PVP-coated 5% Mn-doped ZnO nanoparticles are shown in Figure 3.22A and Figure 3.22B, respectively. The size of the polymer coated Mn-doped ZnO nanoparticles was determined using TEM images. According to the TEM images, PEG-coated and PVP-coated 5% Mn-doped ZnO nanoparticles have an average particle diameter of 16 nm and 8 nm respectively. The SEM image of 5% Mn-doped ZnO nanoparticle is shown in Figure 3.23. The average particle size of 5% Mn-doped ZnO nanoparticle was 34 nm. Particle size distribution was calculated based on the TEM/SEM images of PEG-coated, PVP-coated 5% Mn-doped ZnO nanoparticles and polymer-uncoated 5% Mn-doped ZnO nanoparticles as shown in Figure 3.24a, 3.24b and 3.24c respectively. Forty three percentages of PEG-coated 5% Mn-doped ZnO nanoparticles have a diameter of 15 nm. Forty nine percentages of PVP-coated 5% Mn-doped ZnO nanoparticles have a diameter of 8 nm. Thirty three percentage of polymer uncoated 5% Mn-doped ZnO nanoparticles have a diameter of 40 nm.

According to the TEM images, PEG- and PVP-coated 5% Mn-doped ZnO nanoparticles have an average particle diameter between 5 -15 nm. From the TEM results, it is also seen that PEG and PVP does affect the size of nanoparticles. This was because the particles are less aggregated in the presence of PEG and PVP, therefore the polymer-coated 5% Mn-doped ZnO nanoparticles sizes were smaller than the size of uncoated 5%Mn-doped ZnO nanoparticles. Also, polymer-coated 5% Mn-doped ZnO nanoparticles were evenly distributed compared to the uncoated nanoparticles, as shown in Figure 3.23.

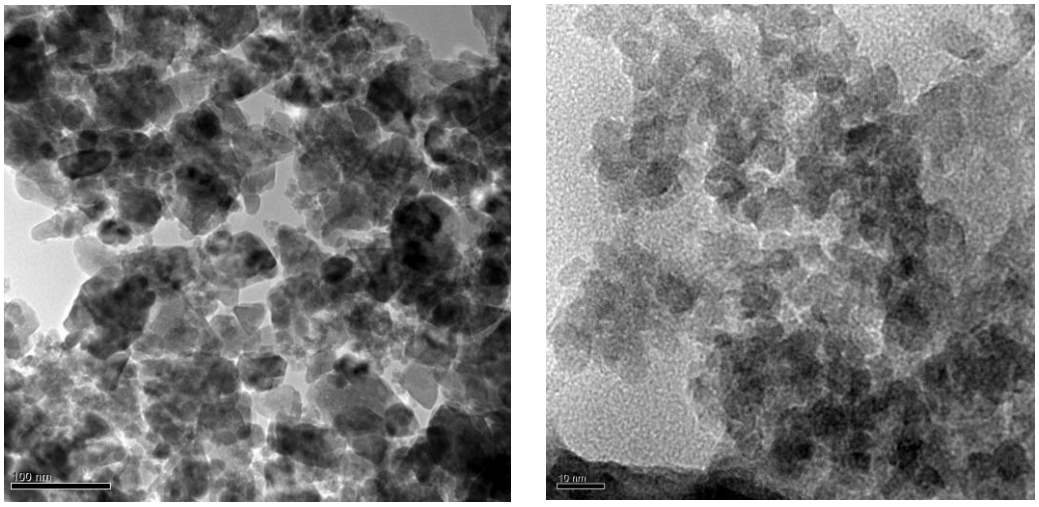

A B

Figure 3.22. Transmission electron microscope images of (A) PEG-coated 5% Mn-doped ZnO nanoparticles, and (B) PVP-coated 5% Mn-doped ZnO nanoparticles.

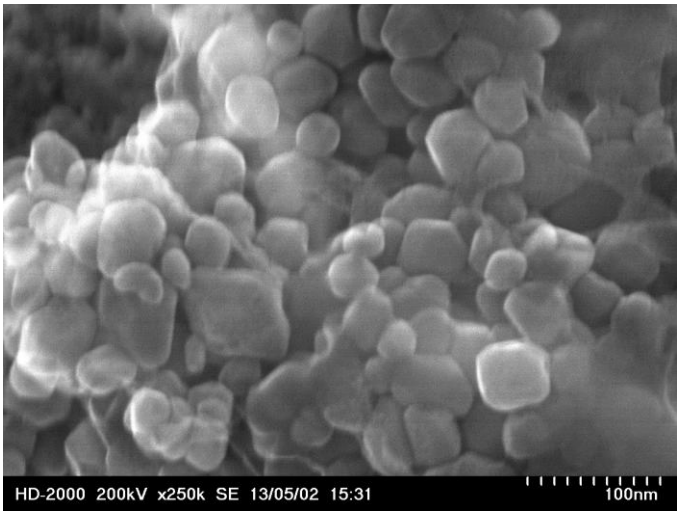

Figure 3.23. Scanning electron microscope (SEM) image of 5% Mn-doped ZnO nanoparticles.

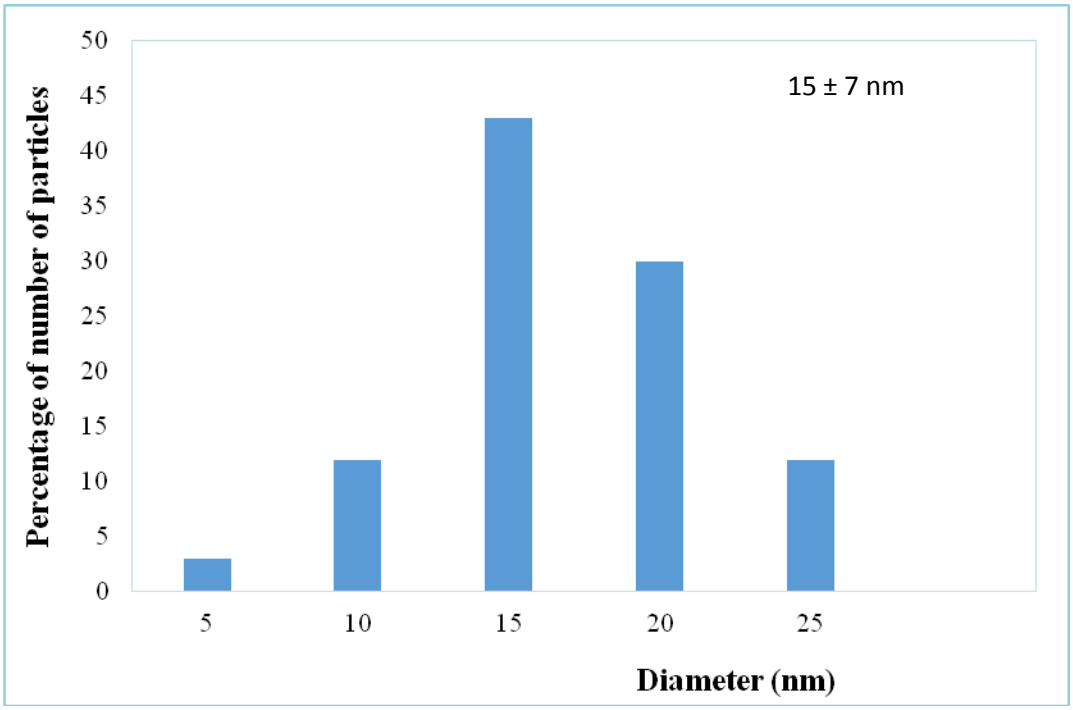

Figure 3.24a. Particles size distribution of PEG-coated 5% Mn-doped ZnO nanoparticles calculated from the TEM image.

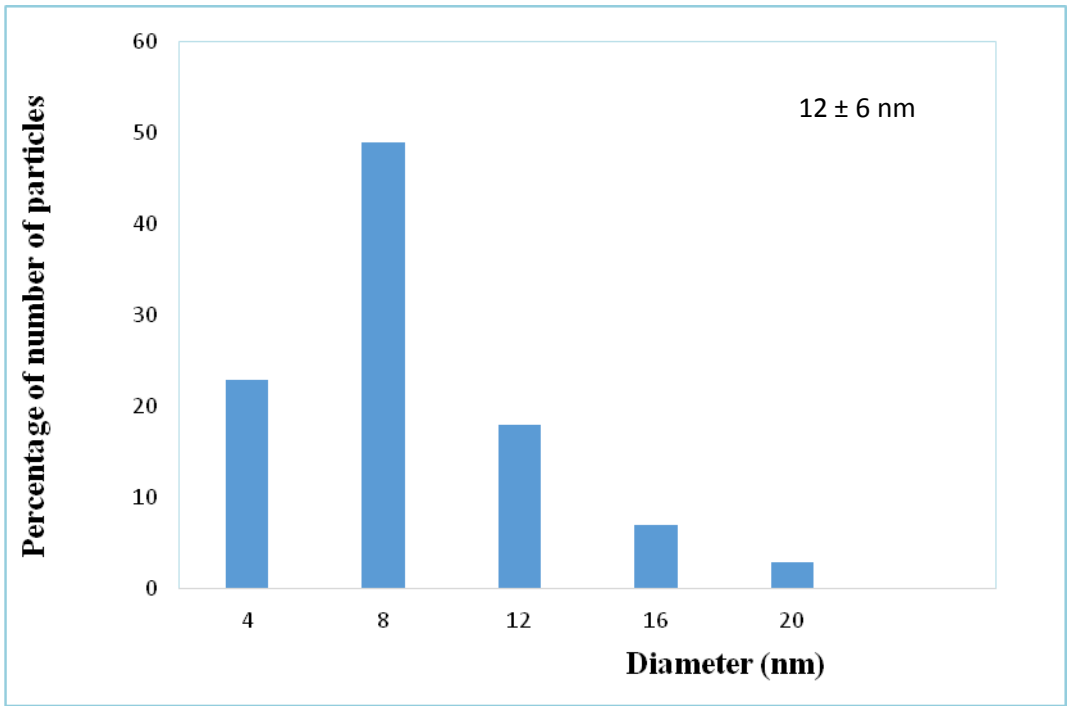

Figure 3.24b. Particles size distribution of PVP-coated 5% Mn-doped ZnO nanoparticles calculated from the TEM image.

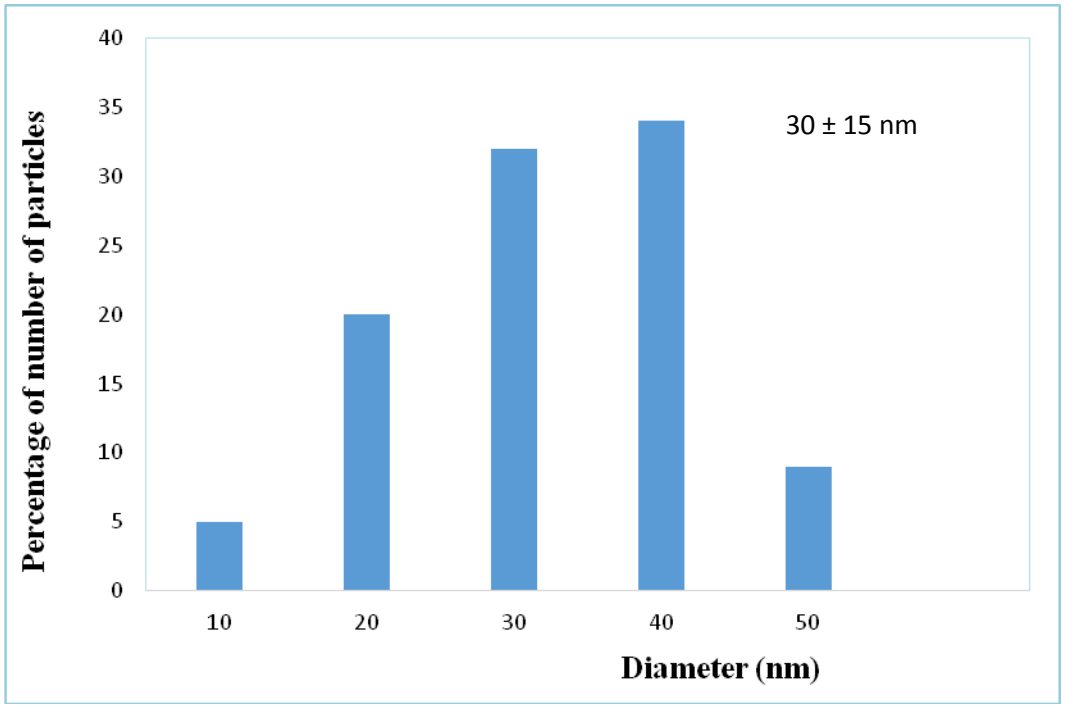

Figure 3.24c. Particles size distribution of 5% Mn-doped ZnO nanoparticles calculated from the SEM image.

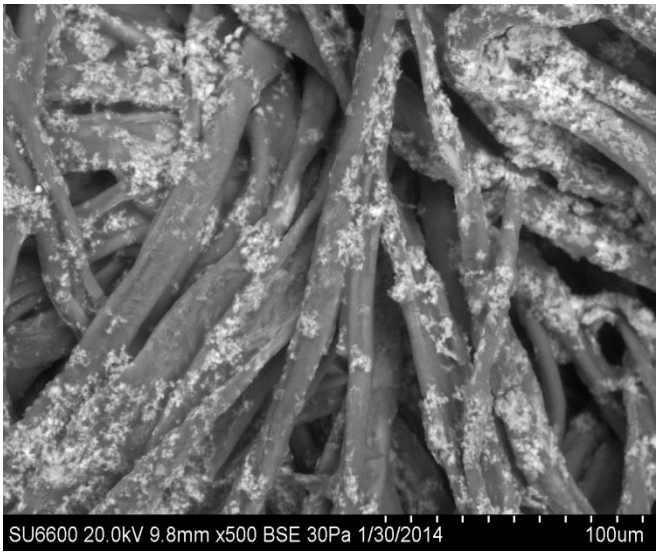

Figure 3.25. Scanning electron microscope (SEM) image of PVP-coated 5% Mn-doped ZnO nanoparticles incorporated cotton textile.

The surfaces of the treated cotton fabrics were observed by SEM microscopy. In Figure 3.25, SEM micrograph shows the PVP-coated 5% Mn-doped ZnO nanoparticles on cotton fabric samples. Physical appearance of modified cotton textile shows that, PVP-coated 5% Mn-doped ZnO nanoparticles tightly bind to the cotton textile compared to the undoped and PEG-coated nanoparticles. This is based on the removal of the nanoparticles with each washing cycle. The PVP-coated Mn-doped ZnO nanoparticles cover a significant area of the fibers present in cotton textile as shown in Figure 3.25.

Energy Dispersive X-Ray Mapping Studies (EDX) can be used to find the chemical composition of materials down to a spot size of a few microns, and to create elemental composition maps. The surface topography of PVP-coated 5% Mn-doped ZnO nanoparticles attached cotton fabrics was investigated using EDX technique. Na, S, Zn and Mn elements are present in cotton textile as shown in the EDX spectra in Figure 3.26 (a) and Figure3.26 (b). The cotton fabrics loaded with PVP-coated 5% Mn-

doped ZnO nanoparticles are direct indication that nanoparticles are directly attached to the cotton fabrics surfaces. The EDX elemental maps (Figure 3.27) endorses the elemental composition of PVP-coated 5% Mn-doped ZnO nanoparticles on cotton textile.

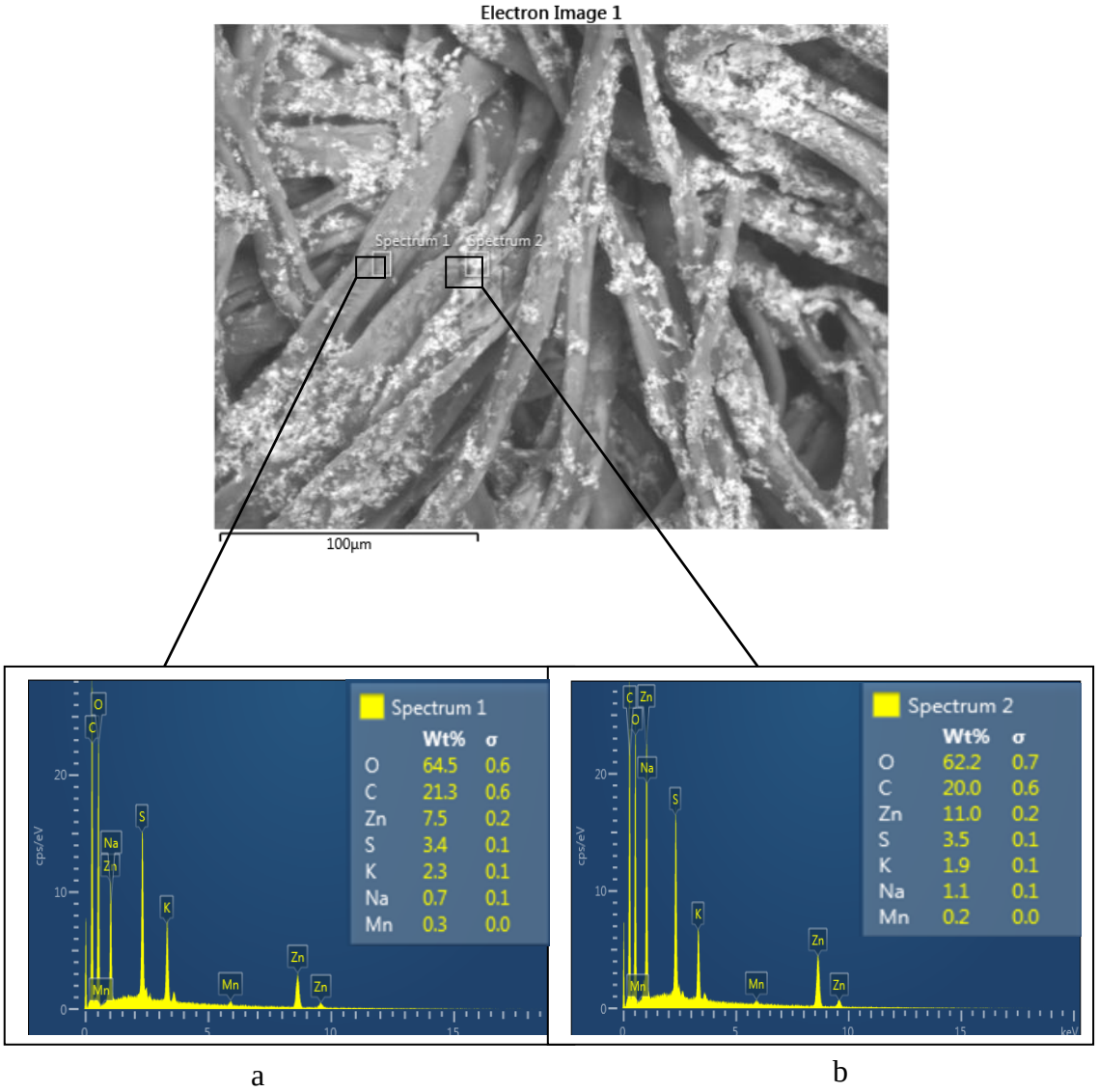

Figure 3.26. SEM image and EDX spectra of PVP-coated 5% Mn-doped ZnO nanoparticles on cotton textile (a) spectrum 1 and (b) spectrum 2.

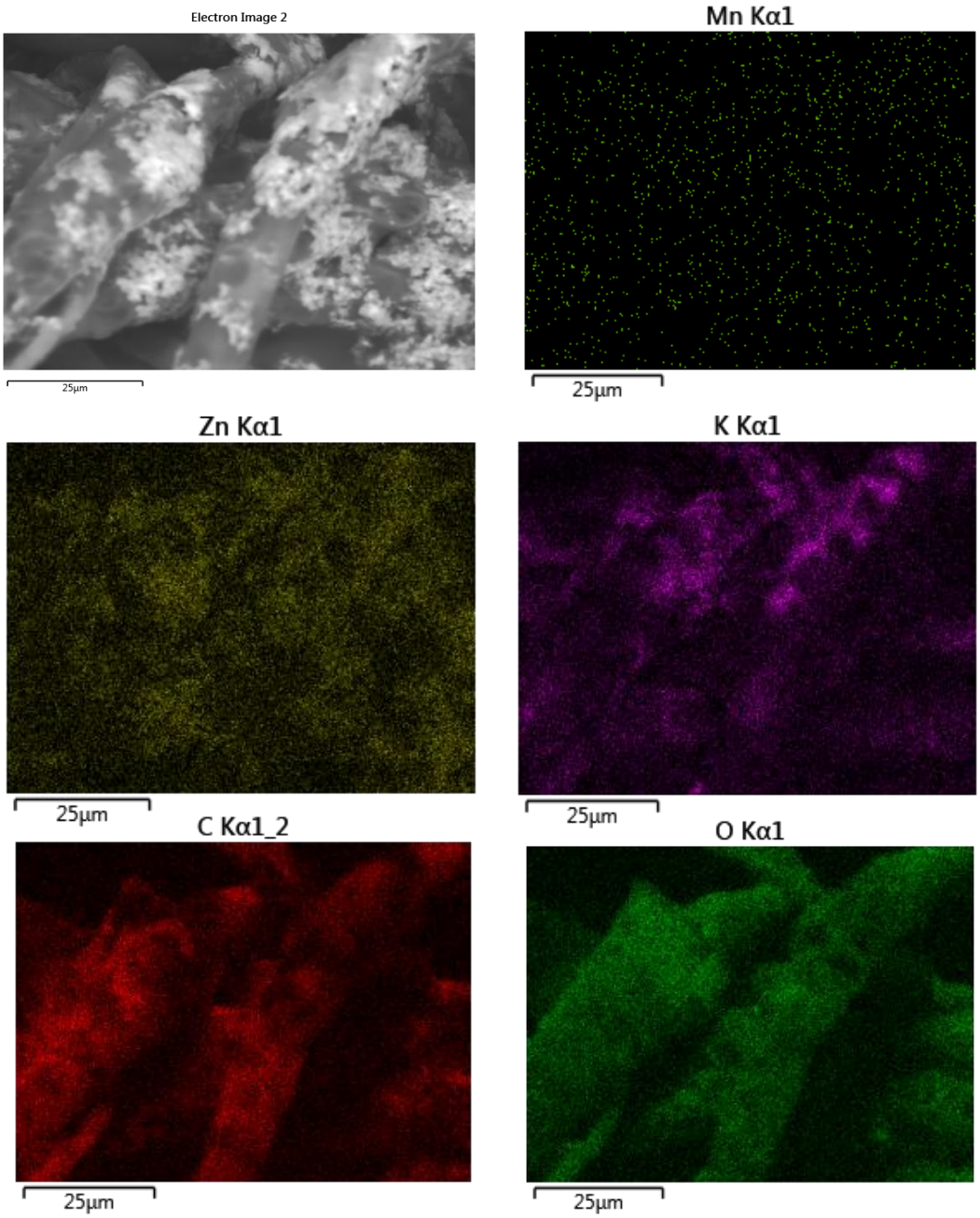

Figure 3.27. SEM image and EDX elemental maps of PVP-coated 5% Mn-doped ZnO nanoparticles attached cotton textile.

3.2.3 UV-Visible Absorption Studies

UV-visible absorption spectroscopy is a widely being used technique to examine the optical properties of nanosized particles. The UV-vis absorption spectra of the ZnO, 5% Mn doped ZnO, 7.5% Mn doped ZnO and 10% Mn doped ZnO nanoparticles are shown in Figure 3.28. All the samples were prepared at 55-65 °C and all samples have a strong absorption maximum below 400 nm. The absorption spectrum of ZnO nanopowder is shown in Figure 3.28 blue line. It exhibits a strong absorption band at around 378 nm. 5% Mn-doped ZnO, 7.5% Mn-doped ZnO, and 10% Mn-doped ZnO nanoparticles have an absorption band around 365 nm. The UV-vis absorption spectra of PVP-coated Mn-doped ZnO nanoparticles are shown in Figure 3.29.

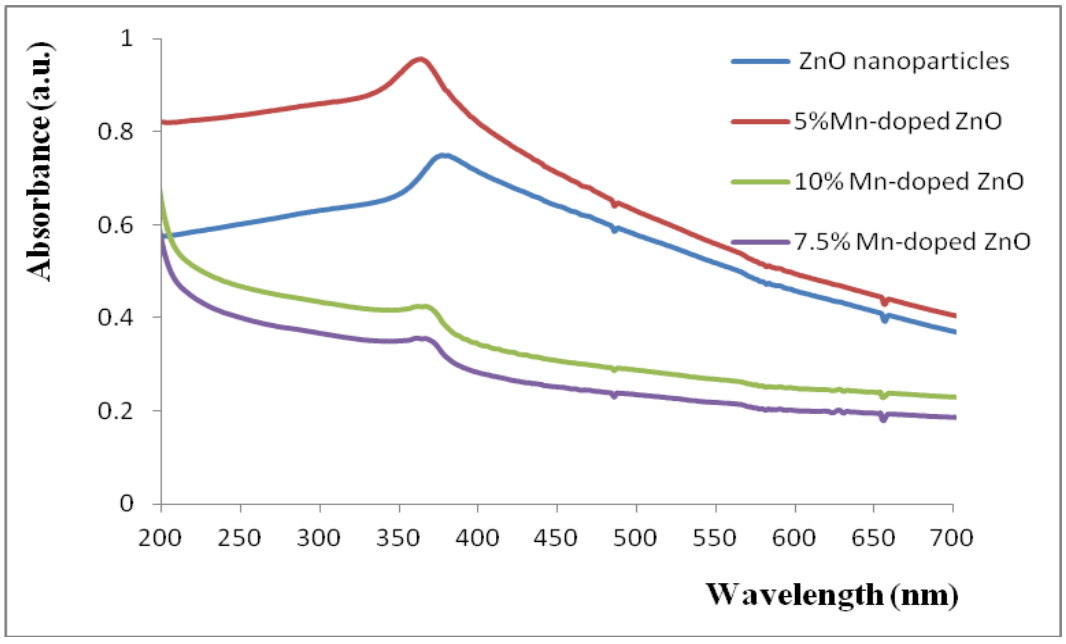

Figure 3.28. UV-visible absorption spectra of Mn-doped ZnO nanoparticles.

The doping of transition metal elements into ZnO offers a feasible means of fine tuning the band gap to make use as UV detector and light emitters. According to UV-vis absorption spectra, the absorption peak of ZnO nanoparticles shifted to the lower wavelength reagent upon Mn(III) doping. Other research groups have observed the same behavior for higher doping levels (5 % and up). On the other hand, Mn doping in ZnO resulted in the reduction of the band gap when very low concentration of Mn doping (less than 5% of Mn) was carried out according to the literature.[35-36] However our data are consistent with the changes in band gap observed with other synthetic methods when higher Mn doping levels are maintained. The UV-vis absorption spectra of PEG-coated Mn-doped ZnO nanoparticles are shown in Figure 3.30.

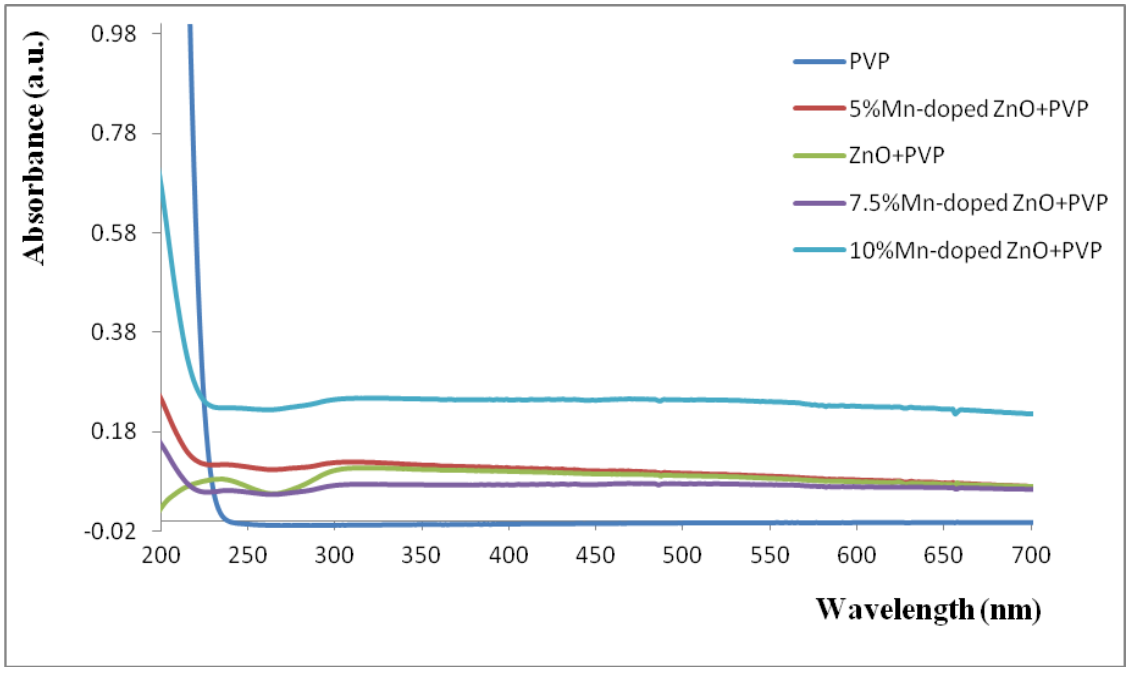

Figure 3.29. UV-visible spectra of surface functionalized Mn-doped ZnO nanoparticles with PVP (dispersed in water).

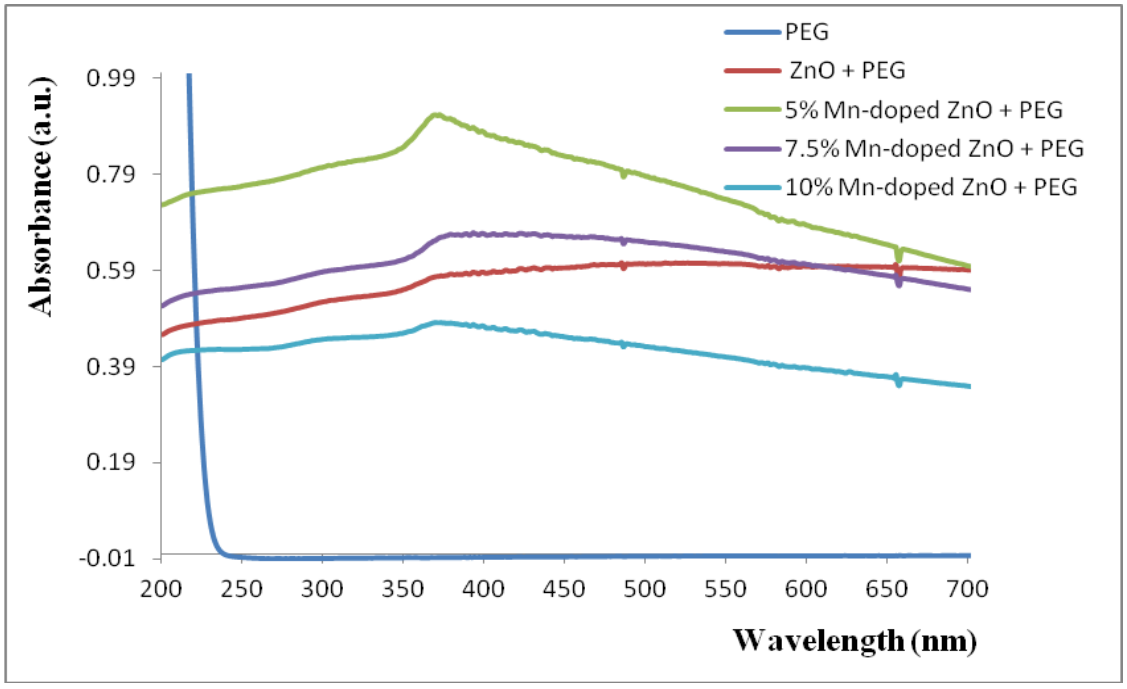

Figure 3.30. UV-visible spectra of surface functionalized Mn-doped ZnO nanoparticles with PEG.

The capping behavior between PEG and PVP could be attributed to the difference in adhesion strength. Because PVP has been widely known as a capping reagent for nanoparticles, adhesion of PVP was stronger than that of PEG. During the synthesis of ZnO nanoparticles, pH value of the solution was 6 at the beginning of synthesis and it was approximately 8 at the end of synthesis because of dropping KOH solution. Both PEG and PVP are non-ionic surfactants; they would be partially-charged. Especially oxygen in PVP would be charged more strongly than oxygen in PEG because of positively-charged nitrogen in PVP. Therefore, PVP would electrostatically adhere to the surface of ZnO nanoparticle more strongly than PEG.

3.2.4. Fourier Transform Infrared Studies

FTIR measurements of all the samples were performed in the wavenumber range from 400 to 4,000 cm^{-1}. Figure 3.31 shows the FT-IR spectra of the dried powder of ZnO and Mn-doped ZnO nanoparticles. The peaks at 670 and 555 cm^{-1} are related to the stretching vibrations of Zn-O bonds. [37] The peak at 3405 cm^{-1} indicates the presence of –OH residues, probably due to atmospheric moisture. [37] According to Figure 3.31, It was only observed a very strong band below 520 cm-^{1} due to the Zn-O and (Zn,Mn)-O stretching modes.

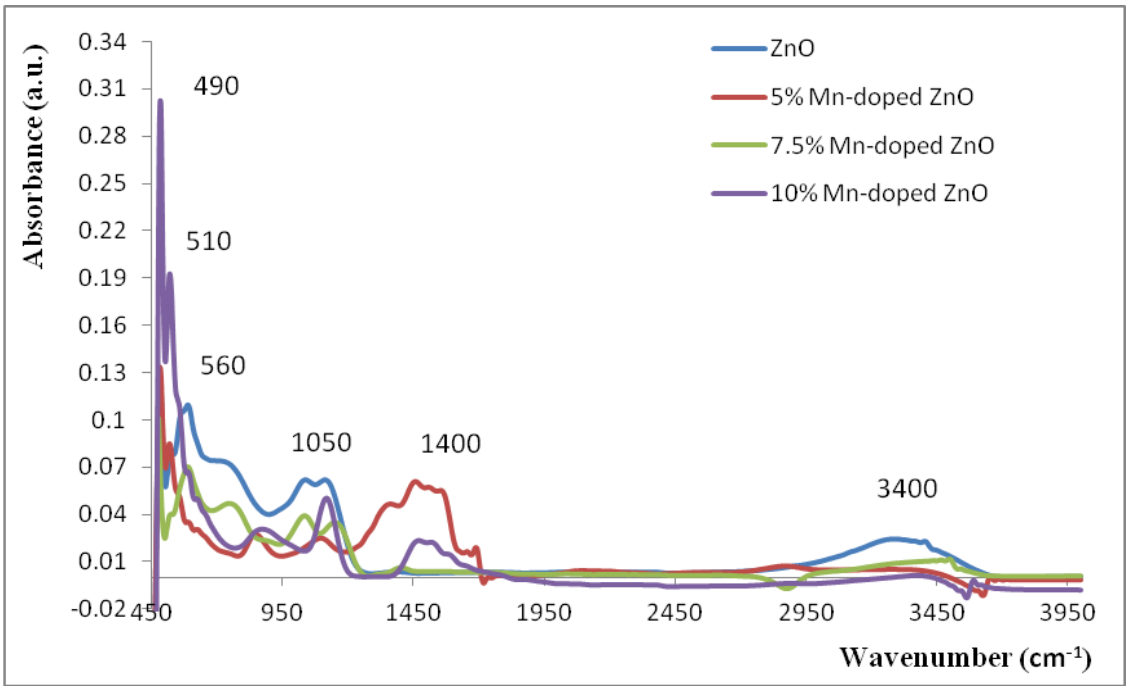

Figure 3.31. FT-IR spectra of ZnO, 5% Mn-doped ZnO, 7.5% Mn-doped ZnO, 10% Mn-doped ZnO nanoparticles.

FT-IR spectra of the PEG-coated ZnO and PEG-coated Mn-doped ZnO nanoparticles were obtained for the dried powders as shown in Figure 3.32. FT-IR spectroscopy gives qualitative information about the way in which the PEG molecules are bound to the surface of the ZnO nanoparticles. Figure 3.32 compares the FT-IR spectra of PEG, PEG-coated ZnO and PEG-coated 5% Mn-doped ZnO nanoparticles. According to Figure 3.32, the peak seen at 3450 cm^{-1} indicates the presence of hydroxyl groups. The absorption peak at 2850 cm^{-1} in the spectrum of Figure 3.32 corresponds to the CH group stretching vibration of PEG. It proves that the molecules of PEG were coated with ZnO nanoparticles Mn-doped ZnO nanoparticles. The connection between ZnO with PEG has been studied by the FTIR measurement. [38] The stretching mode of vibration corresponding to C=C originates at 1501 cm^{-1} and the alkyl group obtains in the range between 2847 to 2930 cm^{-1}. [38] The bands at 2871 cm^{-1} and 2926 cm^{-1} corresponds asymmetric and symmetric stretching vibration of the CH_2 group, respectively. [39] The bands at 3399 cm^{-1} and 3407 cm^{-1} attribute to the O–H mode of vibrations, due to the hydroxyl group originates from PEG. [39]

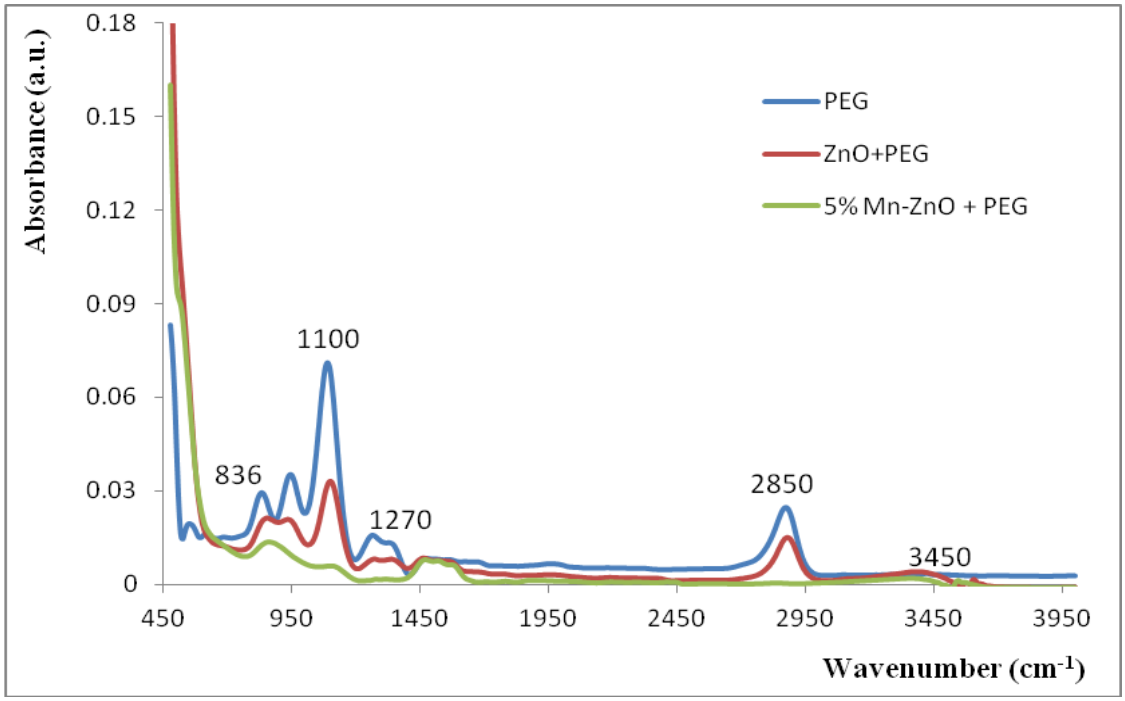

Figure 3.32 . FT-IR spectra of PEG, PEG-coated ZnO and Mn-doped ZnO nanoparticles.

In the FT-IR spectrum of PVP-coated ZnO and PVP-coated Mn-doped ZnO nanoparticles (Figure 3.33), several peaks are shown at 3300, 1600 and 1280, 1100, 560 and 480 cm^{-1}. The observed peak at 1600 cm^{-1} is a distinct stretching mode of carbonyl group on the PVP molecule and the peak at 1200 cm^{-1} is due to the bending mode of CH_2 while the peak at 1100 cm^{-1} results from the stretching mode of C-N in PVP molecule. [40] The PVP-coated of ZnO and Mn-doped ZnO nanoparticles is confirmed through FT-IR spectroscopy, which suggests that a PVP molecular layer on ZnO and Mn-doped ZnO nanoparticles surface be formed.

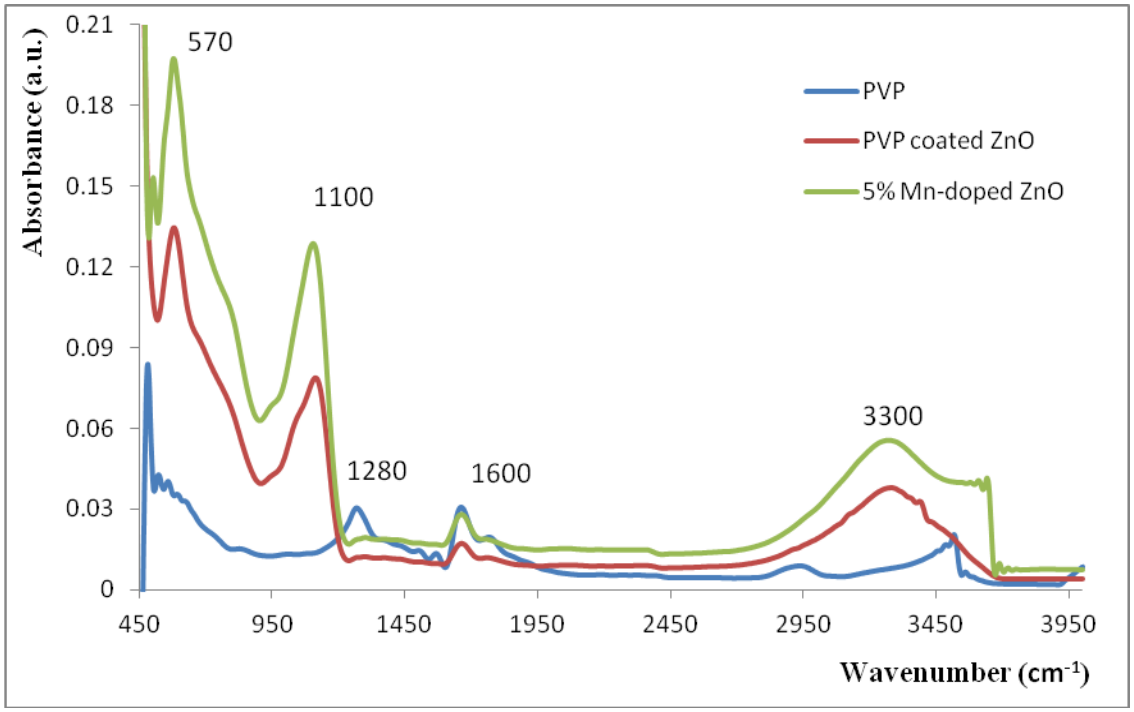

Figure 3.33. FT-IR spectra of PVP, PVP-coated ZnO and PVP-coated 5% Mn-doped ZnO nanoparticles.

3.2.5 Antibacterial activity of polymer-coated Mn-doped ZnO nanoparticles.

The antibacterial activity of polymer-coated Mn-doped ZnO nanoparticles was assessed using the Almar blue assay (AB), agar diffusion test and shake flask test method.

3.2.5.1. Minimum inhibitory concentration (MIC)

Alamar blue assay is a well known method to determine minimum inhibitory concentration of antibiotics.[41] The AB assay is used to assess cell viability based on the reduction potential of metabolically active cells. Bacteria cells were seeded in transparent 96 well plates and exposed to the polymer-coated Mn-doped ZnO nanoparticle

dispersions at concentrations ranging from 20 to 1 mg/mL with Alamar blue dye for 24 h at 37 ^{0}C. The experiments were performed at three times in the 96 wells for each time point and nanoparticle dose.

The mechanism of Alamar blue dye has been discussed in section 3.1.3.2. AB test of undoped ZnO nanoparticles are depicted in Figures 3.34–3.36 against three bacteria species used in this project. Similar experiments have been carried out for the Mn-doped ZnO nanoparticles as shown in Figures 3.37–3.39. Evaluated minimum inhibitory concentrations (MICs) of the nanoparticles are summarized in Table 3.4. According to Table 3.4, MIC value of polymer coated and uncoated ZnO nanioparticles have a slightly higher MIC value than Mn-doped ZnO nanoparticles. It suggested that Mn-doped ZnO nanoparticles have a slightly higher bacterial killing activity than ZnO nanoparticles for all doping levels. The MIC value of polymer-uncoated ZnO nanoparticles was 4 mg/mL and polymer-coated ZnO nanoparticles was 4 mg/mL against *S.aureus*. It suggested that polymer-coated and uncoated ZnO nanoparticles have same antimicrobial activity. According to MIC results, the MIC value of Mn-doped ZnO nanoparticles was 2.5, 2.25, 2.25 mg/mL for *E.coli, S.aureus* and *S.epidermidis* respectively. The MIC value is changed with Gram-positive bacteria and Gram-negative bacteria species. AB test has not been previously utilized for evaluating MIC values of Mn-doped ZnO nanoparticles. However, MIC values for ZnO nanoparticles have been determined by using agar dilution test method where the viable bacterial count was manually determined. The minimum inhibition concentration of ZnO nanoparticles were calculated to be 3.1 mg/mL for *E. coli* and 1.5 mg/mL for *S.aureus*.[42]

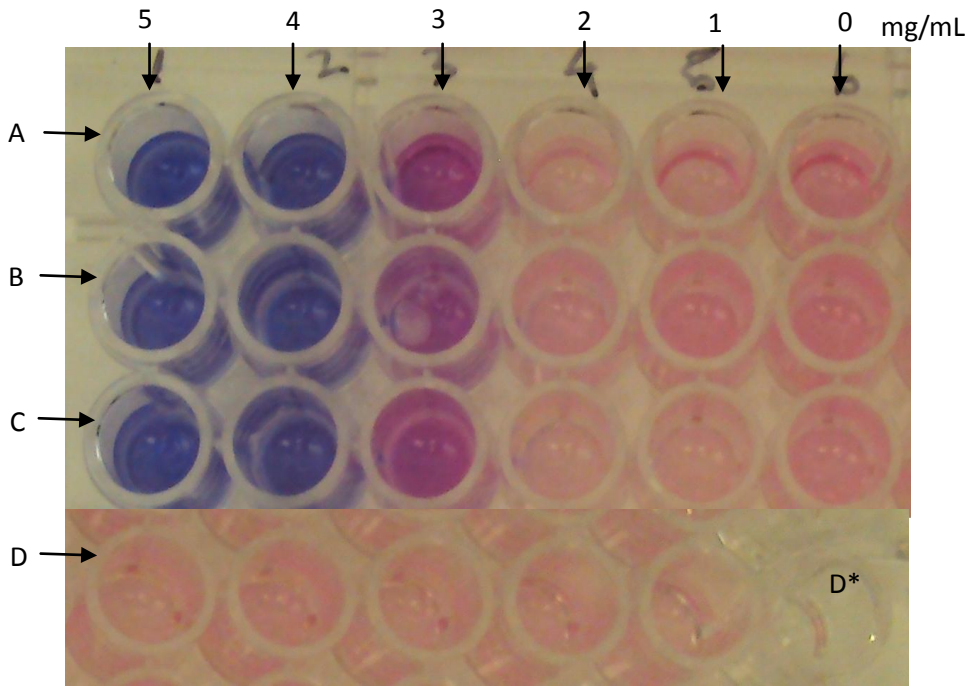

Figure 3.34. Alamar Blue assay using surface functionalized ZnO nanoparticles against *S.epidermidis* (A=ZnO, B=PEG coated ZnO, C=PVP coated ZnO nanoparticles and D = control, D*= negative control).

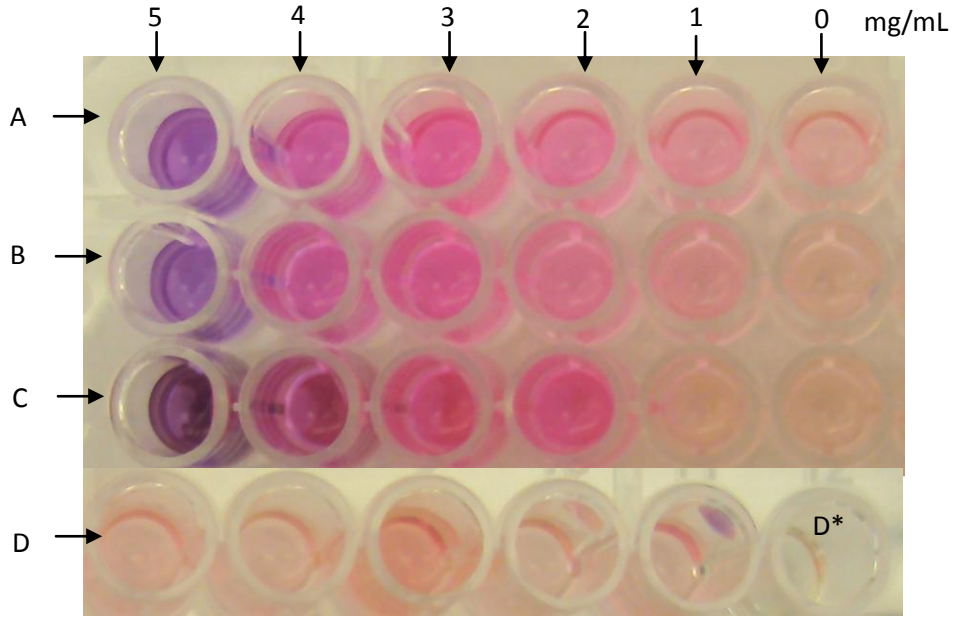

Figure 3.35. Alamar Blue assay using surface functionalized ZnO nanoparticles against *E.coli* (A=ZnO, B=PEG-coated ZnO, C=PVP-coated ZnO nanoparticles and D=control, D*= negative control).

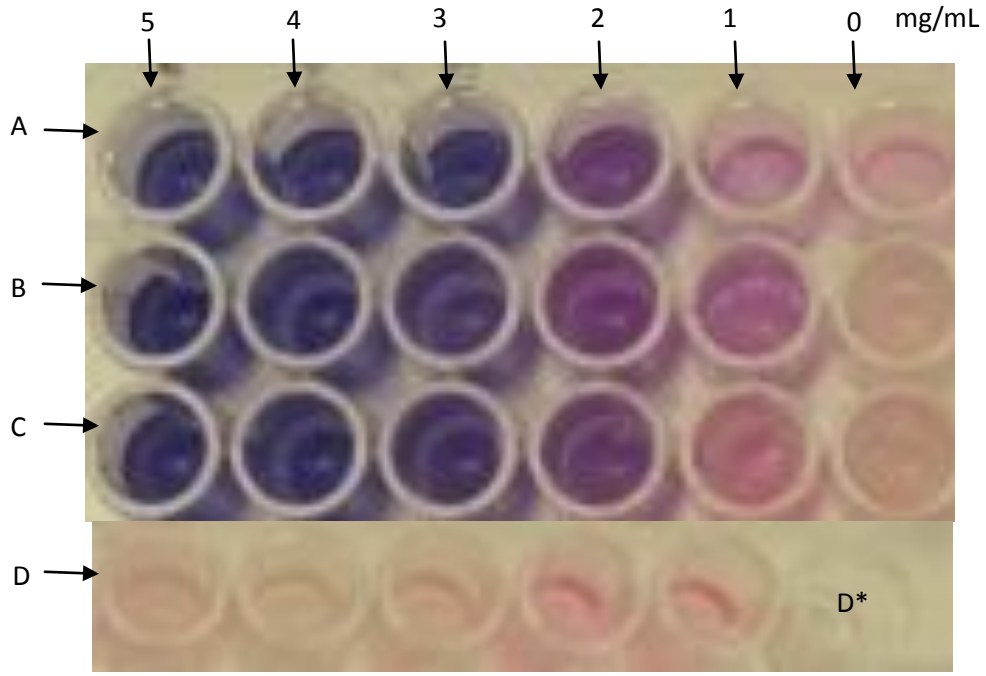

Figure 3.36. Alamar Blue assay using surface functionalized ZnO nanoparticles against *S.aureus* (A=ZnO, B=PEG-coated ZnO, C=PVP-coated ZnO nanoparticles and D=control, D*= negative control).

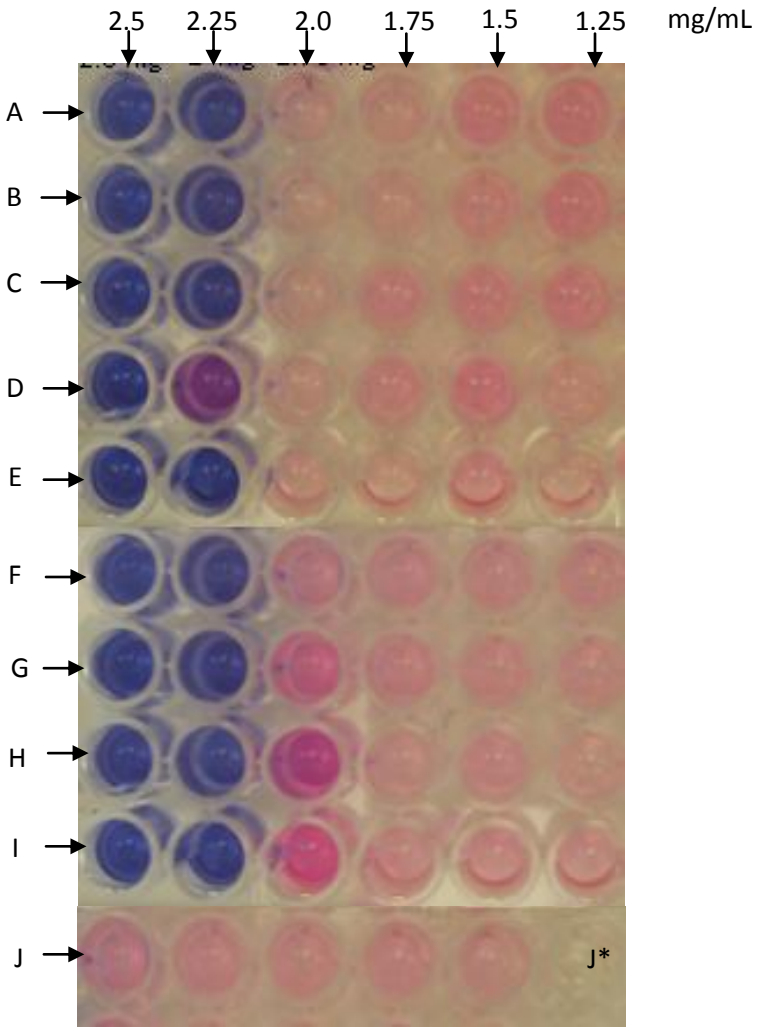

Figure 3.37. Alamar Blue assay using surface functionalized Mn-doped ZnO nanoparticles against *S.epidermidis* (A=Mn-doped ZnO, B=PEG-coated 5% Mn-doped ZnO, C=PVP-coated 5% Mn-doped ZnO nanoparticles, D=7.5% Mn-doped ZnO, E=PEG-coated 7.5% Mn-doped ZnO, F=PVP-coated 7.5% Mn-doped ZnO, G=10% Mn-doped ZnO, H=PEG-coated 10 % Mn-doped ZnO, I=PVP-coated 10 % Mn-doped ZnO nanoparticles and J= control, J*= negative control).

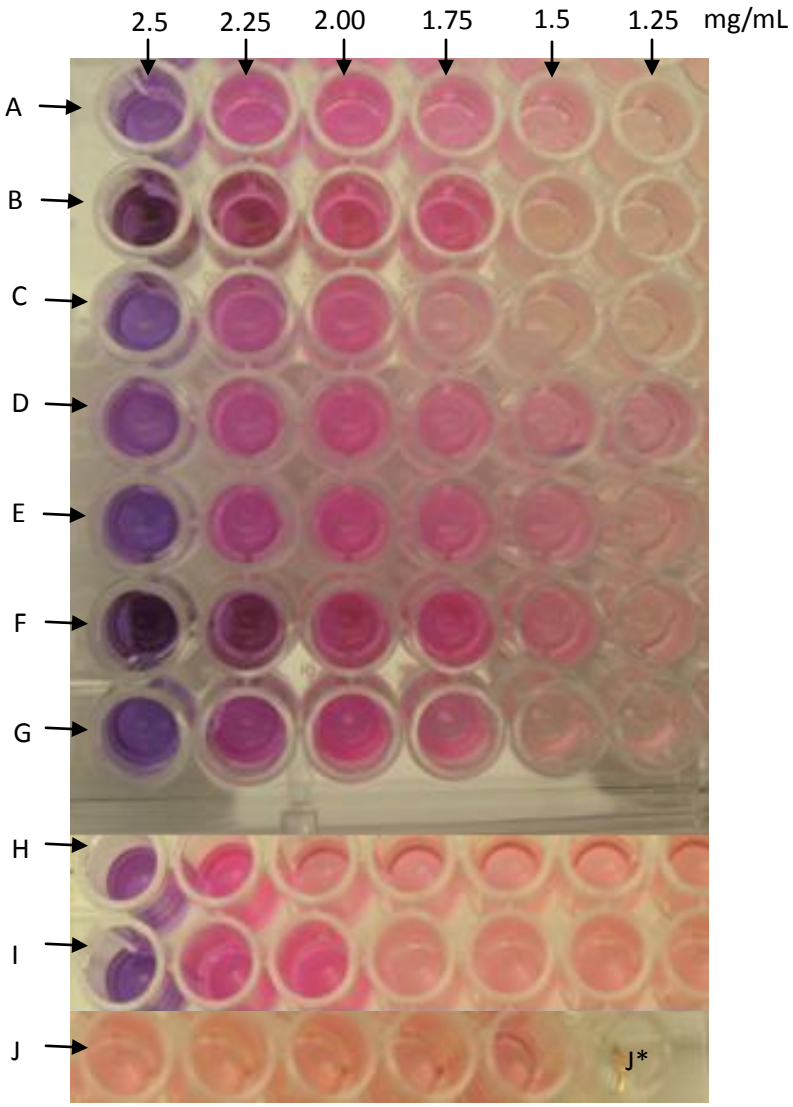

Figure 3.38. Alamar Blue assay using surface functionalized Mn-doped ZnO nanoparticles against *E.coli* (A=Mn-doped ZnO, B=PEG-coated 5% Mn-doped ZnO, C=PVP-coated 5% Mn-doped ZnO nanoparticles, D=7.5% Mn-doped ZnO, E=PEG-coated 7.5% Mn-doped ZnO, F=PVP-coated 7.5% Mn-doped ZnO, G=10% Mn-doped ZnO, H=PEG-coated 10 % Mn-doped ZnO, I=PVP-coated 10 % Mn-doped ZnO nanoparticles and J=control, J*= negative control).

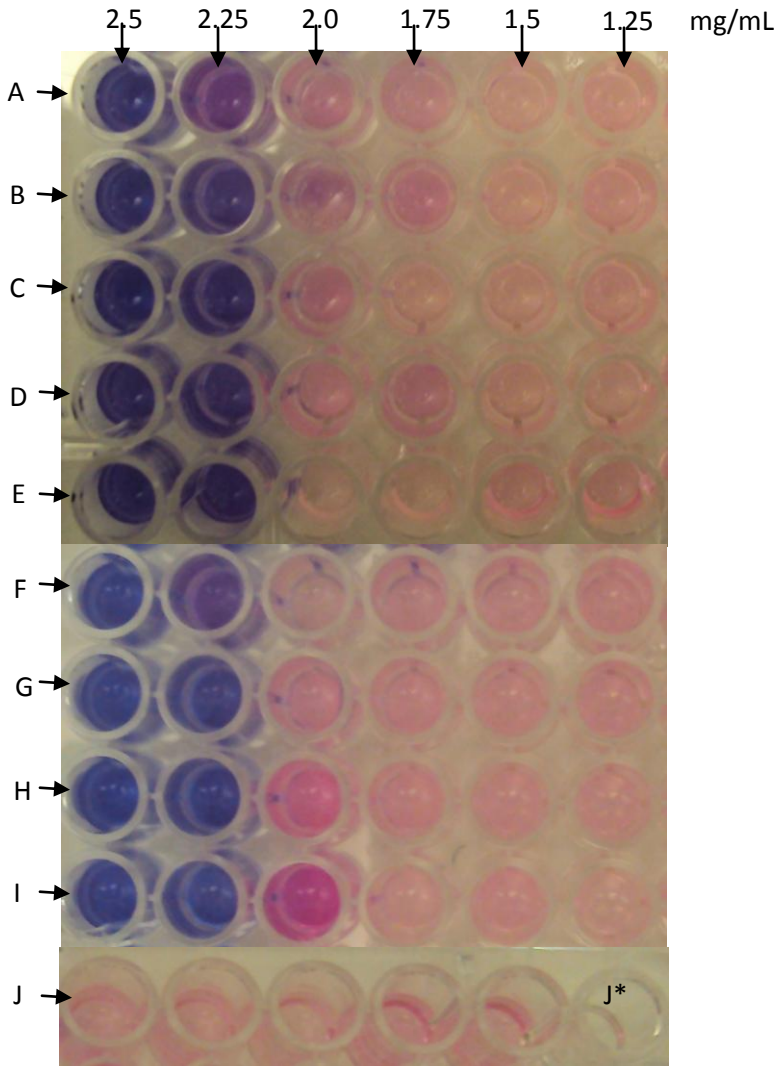

Figure 3.39. Alamar Blue assay using surface functionalized Mn-doped ZnO nanoparticles against *S.aureus* (A=Mn-doped ZnO, B=PEG-coated 5% Mn-doped ZnO, C=PVP-coated 5% Mn-doped ZnO nanoparticles, D=7.5% Mn-doped ZnO, E=PEG-coated 7.5% Mn-doped ZnO, F=PVP-coated 7.5% Mn-doped ZnO, G=10% Mn-doped ZnO, H=PEG-coated 10 % Mn-doped ZnO, I=PVP-coated 10 % Mn-doped ZnO nanoparticles and J=control, J*= negative control).

Table 3.4. Minimum inhibitory concentration of Mn-doped ZnO nanoparticles

Samples (Nanoparticles)	Minimum inhibitory concentration (mg/mL)		
	S.epidermidis	*S.aureus*	*E.coli*
ZnO	4	3	5
PEG-coated ZnO	4	3	5
PVP-coated ZnO	4	3	5
5% Mn-doped ZnO	2.25	2.25	2.5
PEG-coated 5% Mn-doped ZnO	2.25	2.25	2.5
PVP-coated 5% Mn-doped ZnO	2.25	2.25	2.5
7.5% Mn-doped ZnO	2.25	2.25	2.5
PEG-coated 7.5% Mn-doped ZnO	2.25	2.25	2.5
PVP-coated 7.5% Mn-doped ZnO	2.25	2.25	2.5
10% Mn-doped ZnO	2.25	2.25	2.5
PEG-coated 10% Mn-doped ZnO	2.25	2.25	2.5
PVP-coated 10% Mn-doped ZnO	2.25	2.25	2.5

3.2.5.2 Agar diffusion test for PVP and PEG-coated Mn-doped ZnO nanoparticles

The polymer-coated Mn doped ZnO nanoparticles were exposed to three different light conditions (a = UV light, b = normal light and c = dark condition) for 30 min. After that, the antibacterial activity was evaluated for light shined polymer-coated Mn-doped ZnO nanoparticles against *S.aureus, S.epidermidis* and *E.coil*. The antimicrobial result is shown in Figure 3.40 with three different light conditions. According to Figure 3.40, inhibition zone value of polymer-coated Mn-doped ZnO nanoparticles (a = nanoparticles exposed to UV light) was 12 mm. Inhibition zone value of polymer-coated Mn-doped ZnO nanoparticles (b = nanoparticles exposed to normal light) and (c = exposed to dark conditions) was 9 mm and 7 mm, respectively. Highest antimicrobial activity was observed for polymer-coated Mn-doped ZnO (exposed to UV light) condition. Lowest antimicrobial activity was observed for polymer-coated Mn-doped ZnO nanoparticles (c = nanoparticles exposed to dark condition) inhibition zone with 7 mm.

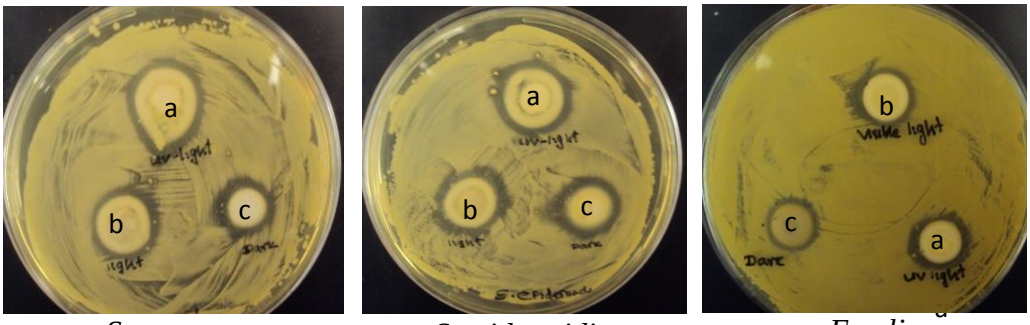

S.aureua *S.epidermidis* *E.coli*

Figure 3.40. Antimicrobial activity of 5% Mn-doped ZnO nanoparticle exposed to (a) UV light, (b) visible light and (c) dark conditions against *S.aureua, S.epidermidis* and *E.coli.*

Above experiments demonstrate the various light conditions affect the antimicrobial activity of polymer-coated Mn-doped ZnO nanoparticles. The antimicrobial activity of polymer-coated Mn-doped ZnO was enhanced due to the increased production of the reactive oxygen species (ROS) in the presence of UV light (a = exposed to UV light).

The mechanism of photocatalytic activity should be similar to the photocatalytic activity observed for semiconductor nanomaterials as TiO_2 nanoparticles.[43] An electron (e^-) in the valence band (VB) can be excited to the conduction band (CB) with the simultaneous generation of a hole (h+) in the VB so that electron–hole pairs (e^-h^+) exist. The holes and electrons might create $OH^{\bullet}$ and ($O^{2-\bullet}$) radicals.[44] These radicals have very high oxidative properties that might easily degrade organic molecules in microorganisms such as DNA, lipids and proteins.

The antibacterial activity of polymer coated Mn-doped ZnO nanomaterials and polymer-uncoated Mn-doped ZnO nanoparticles were carried out for both Gram positive and Gram negative bacteria. The antibacterial effect was analyzed by the study of inhibition zone in agar plates. The experimental result reveals the antibacterial effect on the basis of inhibition zone due to the presence of polymer uncoated and polymer coated Mn-doped ZnO nanoparticles. The average inhibition zone diameter is given in Table 3.5. As seen in Table 3.5, it confirms that inhibition zone does not decrease for polymer coated Mn-doped ZnO nanoparticles. Agar diffusion tests were repeated three times for all Mn-doped ZnO nanoparticles.

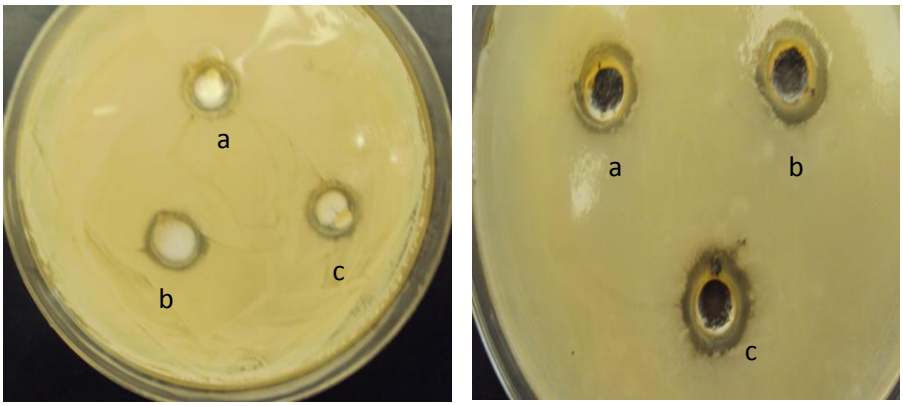

Plate 1 Plate 2

Figure 3.41. Antimicrobial activity of plate 1(a) ZnO nanoparticles, (b) PEG-coated ZnO nanoparticle, (c) PVP-coated ZnO nanoparticles, plate 2(a) 5% Mn-doped ZnO nanoparticle (b) PVP-coated 5% Mn-doped ZnO nanoparticles (c) PEG-coated 5% Mn-doped ZnO nanoparticles against *S.aureus* on tryptic soy agar.

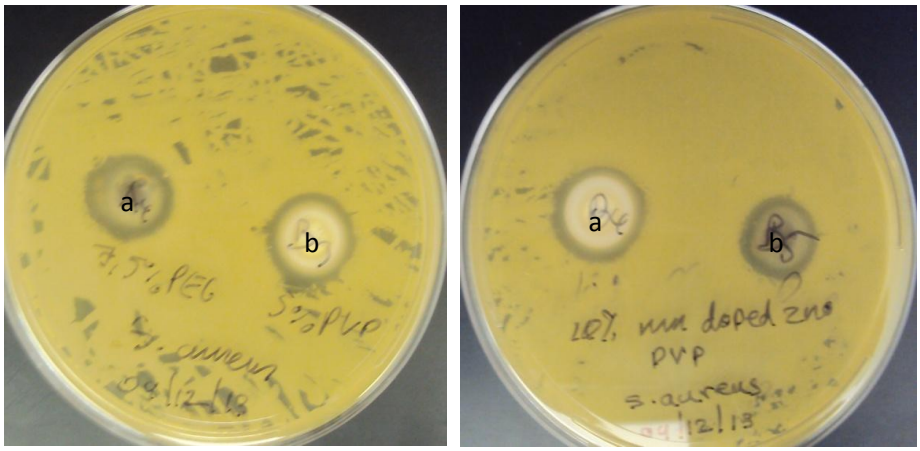

Plate 1 Plate 2

Figure 3.42. Antimicrobial activity of plate 1(a) PEG-coated 7.5% Mn-doped ZnO nanoparticle, (b) PVP-coated 7.5% Mn-doped ZnO nanoparticles, plate 2(a) PEG-coated 10% Mn-doped ZnO nanoparticle, (b) PVP-coated 10% Mn-doped ZnO nanoparticles against *S.aureus* on tryptic soy agar.

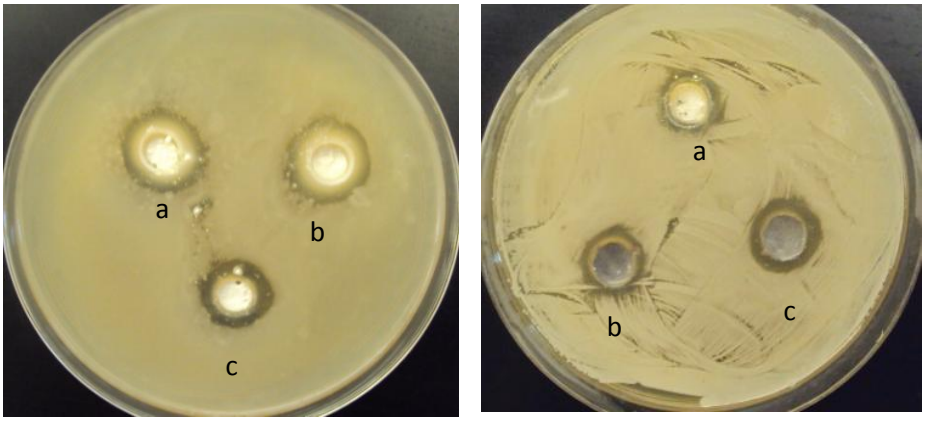

Plate 1 Plate 2

Figure 3.43. Antimicrobial activity of plate 1 (a) ZnO nanoparticles, (b) PEG-coated ZnO nanoparticle, (c) PVP-coated ZnO nanoparticles, plate 2 (a) 5% Mn-doped ZnO nanoparticle (b) PVP-coated 5% Mn-doped ZnO nanoparticles (c) PEG-coated 5% Mn-doped ZnO nanoparticles against *S. epidermidis* on tryptic soy agar.

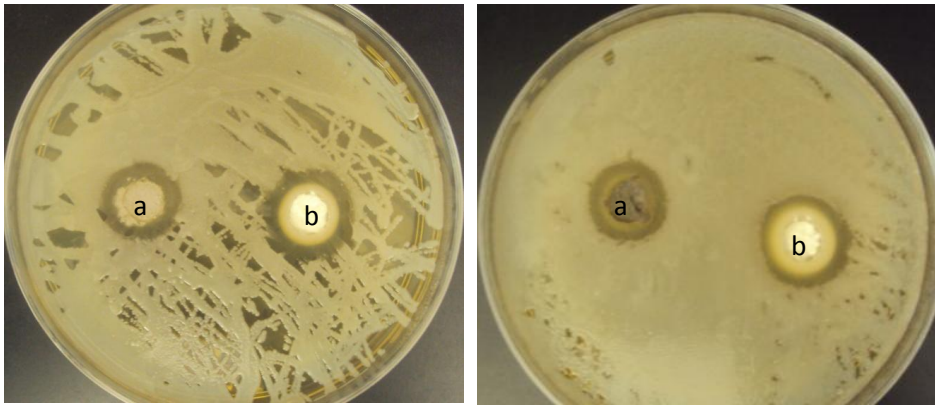

Plate 1 Plate 2

Figure 3.44. Antimicrobial activity of plate 1(a) PEG-coated 7.5% Mn-doped ZnO nanoparticle, (b) PVP-coated 7.5% Mn-doped ZnO nanoparticles, plate 2(a) PEG-coated 10% Mn-doped ZnO nanoparticle, (b) PVP-coated 10% Mn-doped ZnO nanoparticles against *S.epidermidis* on tryptic soy agar.

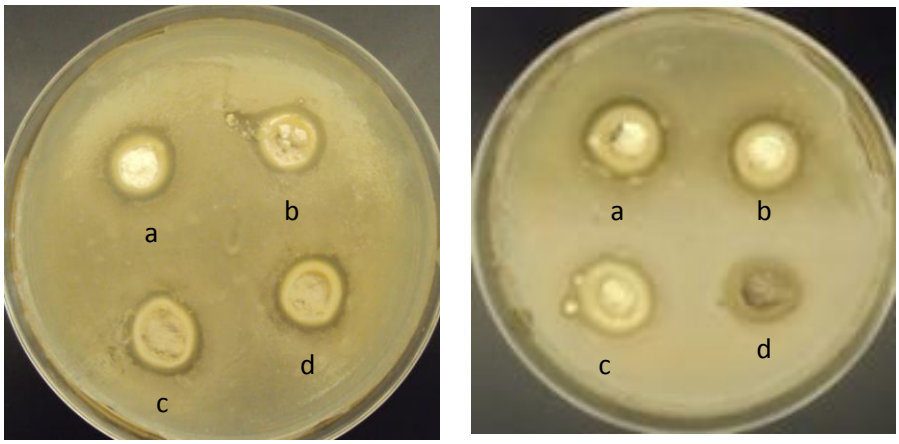

Plate 1 Plate 2

Figure 3.45. Antimicrobial activity of plate 1 (a) ZnO nanoparticles, (b) PEG-coated ZnO nanoparticle, (c) PVP-coated ZnO nanoparticles, (d) 5% Mn-doped ZnO nanoparticle, plate 2 (a) PVP-coated 5% Mn-doped ZnO nanoparticles (b) PEG-coated 5% Mn-doped ZnO nanoparticles, (c) PEG-coated 7.5% Mn-doped ZnO nanoparticle, (d) PVP-coated 7.5% Mn-doped ZnO nanoparticles against *E.coli* on tryptic soy agar.

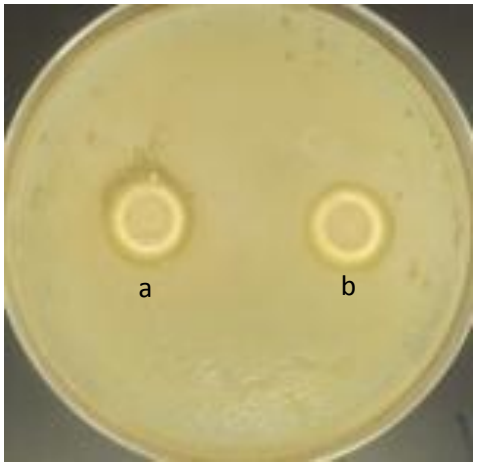

Figure 3.46. Antimicrobial activity of (a) PEG-coated 10% Mn-doped ZnO nanoparticle, (b) PVP-coated 10% Mn-doped ZnO nanoparticles against *E.coli* on tryptic soy agar.

Table 3.5. The inhibition zone diameter of Mn-doped ZnO nanoparticles

Samples (Nanoparticles)	The average inhibition zone diameter (mm)		
	S.epidermidis	*S.aureus*	*E.coli*
ZnO	9.0 ± 0.5	10 ± 0.5	8.0 ± 0.0
PEG-coated ZnO	9.0 ± 0.5	10 ± 0.5	8.0 ± 0.5
PVP-coated ZnO	9.0 ± 0.5	9.0 ± 0.5	8.0 ± 0.0
5% Mn-doped ZnO	10 ± 1.0	9.0 ± 0.5	8.0 ± 1.0
PEG-coated 5% Mn-doped ZnO	9.0 ± 0.5	9.0 ± 0.5	7.0 ± 0.5
PVP-coated 5% Mn-doped ZnO	10 ± 0.5	9.0 ± 0.5	7.0 ± 0.5
7.5% Mn-doped ZnO	9.0 ± 0.0	8.0 ± 0.5	7.0 ± 0.5
PEG-coated 7.5% Mn-doped ZnO	9.0 ± 0.5	8.0 ± 0.5	7.0 ± 1.0
PVP-coated 7.5% Mn-doped ZnO	10 ± 0.5	9.0 ± 0.5	7.0 ± 0.5
10% Mn-doped ZnO	9.0 ± 0.5	8.0 ± 0.5	7.0 ± 0.5
PEG-coated 10% Mn-doped ZnO	8.0 ± 0.0	9.0 ± 1.0	7.0 ± 0.5
PVP-coated 10% Mn-doped ZnO	8.0 ± 0.5	9.0 ± 0.5	6.0 ± 0.5
PEG	0	0	0
PVP	0	0	0

3.2.5.3. Agar diffusion test for PVP and PEG-coated Mn-doped ZnO nanoparticles incorporated cotton textile.

Antibacterial activity of unmodified and modified cotton textile samples (2 x 2 cm) was tested by agar diffusion method. The results are shown from Figure 3.47 to Figure 3.49. A clear inhibition zone is shown around polymer-coated Mn-doped ZnO treated cotton fabric, where as the unmodified cotton fabric has not clear inhibition zone. The modified cotton textile has excellent antibacterial activity against three representative bacteria, *Staphylococcus aureus*, *Staphylococcus epidermidis* (Gram-positive) and *Escherichia coli* (Gram-negative). The antibacterial activity of modified cotton textile samples was decreased with number of washing time. According to Figure 3.47 (plate 1) and 3.49 (plate 1), the greatest inhibitory effect of unwashed cotton was observed against *S. aureus* and *S.epidermidis* with a zone of inhibition 15 mm. Figure 3.48 (plate 1) is shown very low antibacterial activity against *E.coli*. The difference in susceptibility between Gram-positive and Gram-negative bacteria may be due to the changes in the interaction mechanisms of ZnO nanoparticles with the bacterial membrane. Gram-negative bacteria have much thicker peptidoglycan cell walls compared with Gram-positive bacteria, which results in a decreased susceptibility to membrane damage induced by ZnO nanoparticles.[45] Also *E.coli* has developed efficient pathways to defend against oxidative stresses by increasing expression of oxidative stress-responsive gene products such as superoxide dismutase, catalase, thioredoxin. Some genes are directly involved in the ROS neutralization in the *E.coli* cells. [46] However, the mechanism of action of ZnO nanoparticles has been discussed in section 3.2.5.2.

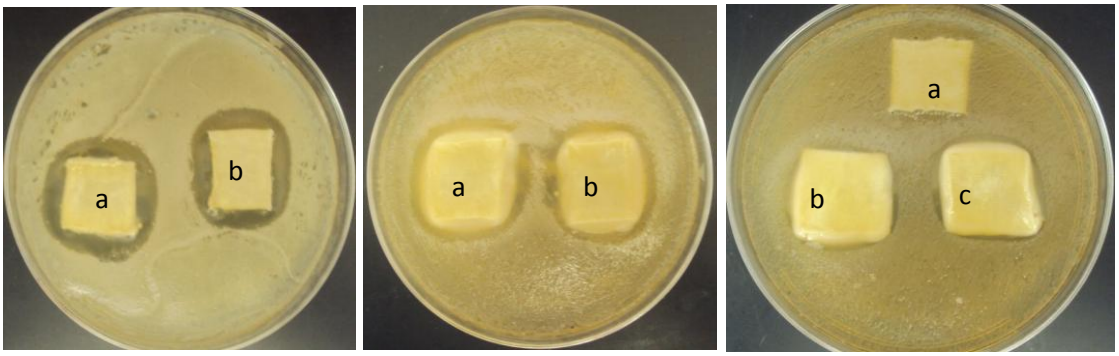

Plate 1 Plate 2 Plate 3

Figure 3.47. Agar diffusion test against *S.aureus* plate 1-(a) ZnO nanoparticles attached cotton textile, (b) PVP-coated Mn-doped ZnO nanoparticles attached cotton textile, plate 2- (a) PEG-coated 5% Mn-doped ZnO nanoparticles with cotton (b) PVP-coated 5% Mn-doped ZnO with cotton , plate 3- (Raw cotton), (b) PEG-coated 5% Mn-doped ZnO nanoparticles with cotton washing 1 time (c) PVP-coated 5% Mn-doped ZnO with cotton washing 1 time.

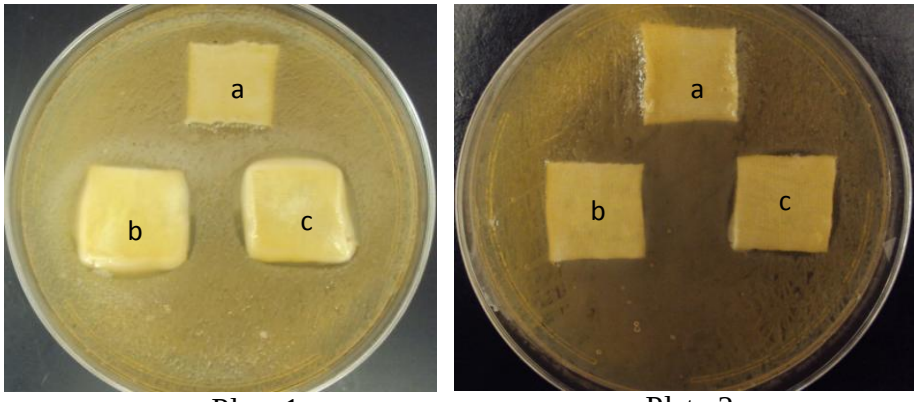

Plate 1 Plate 2

Figure 3.48. Agar diffusion test against *E.coli,* plate 1- (a) PEG-coated 5% Mn-doped ZnO nanoparticles with cotton (b) PVP-coated 5% Mn-doped ZnO with cotton , plate 2- (Raw cotton), (b) PEG-coated 5% Mn-doped ZnO nanoparticles with cotton washing 1 time (c) PVP-coated 5% Mn-doped ZnO with cotton washing 1 time.

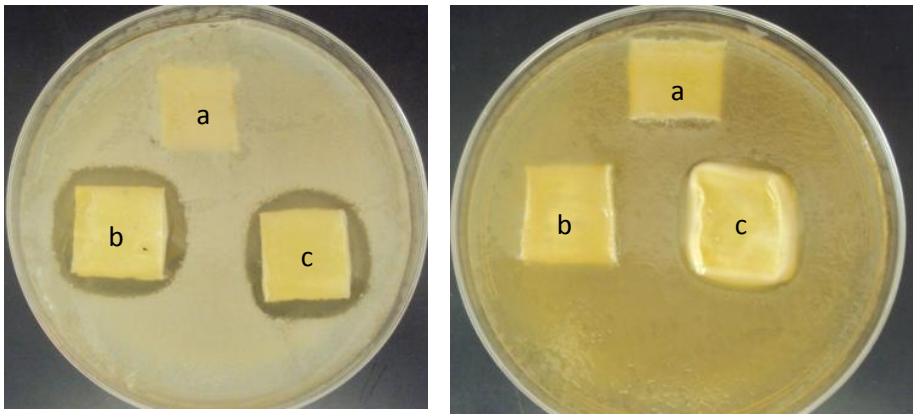

Plate 1 Plate 2

Figure 3.49 . Agar diffusion test against *S.epidermidis,* plate 1-(a) Raw cotton (b) PEG-coated 5% Mn-doped ZnO nanoparticles with cotton (c) PVP-coated 5% Mn-doped ZnO with cotton , plate 2- (a) Raw cotton, (b) PEG-coated 5% Mn-doped ZnO nanoparticles with cotton washing 1 time (c) PVP-coated 5% Mn-doped ZnO with cotton washing 1 time.

3.2.5.4. Shake flask test

The antibacterial efficiancy of the PVP-coated Mn-doped ZnO nanoparticles attached cotton textile were determined using the shake flask test method. Tryptic soya broth was used as the medium. In the case of the Tryptic soya broth test, bacteria growth was monitored by measuring the optical density of the medium over time. The shake flask test was evaluated against *E.coli, S.aureus* and *S.epidermidis.* Control flasks were used with all the initial reaction components with unmodified cotton textile. The control sample (cotton) is shown no antibacterial activity against three different bacteria. According to the Figures 3.50, 3.51, and 3.52, PVP-coated Mn-doped ZnO nanoparticle incorpareted cotton textile samples control the bacterial density with time. For example, the optical density value reached 0.7 after incubating control cotton samples with *E. coli*

for 7 hours (Figure 3.50). The optical density of 5% Mn-doped ZnO nanoparticle-coated cotton samples were about 0.2 after 7 hours. Thus, the cotton fabric exhibited great antimicrobial activity after doping with the nanoparticles. After completing the first wash cycle of the nanoparticle-incoorperated cotton samples, the optical density remianed the same as before washing. After the 2nd wash cycle, the optical density of the cotton samples only increased to about 0.25 at the 7th hour of incubation with *E. coli.* This value is slightly higher than the optical density observed for the nanoparticle-doped cotton samples but is not significant compared to the optical density value of the control sample (0.7). Results show that the cotton frabric retained its antimicrobial activity to a comparable level even after the second wash cycle. However, the optical density greatly increased after the 3rd wash cycle where the value reached 0.62 after 7 hours of incubation with bacteria. Result show that the antibacterial activity was dicreased after three washing cycles. Similar trends of antimicrobial activity was observed for the other two bacteria species studied in this work (Figures 3.51 and 3.52).

When Mn-doped ZnO nanoparticles and PEG-coated Mn-doped ZnO nanoparticles attached cotton textile were shaken in liquid culture tubes, more nanoparticles came out from textile to liquid medium. Therefore, opticle density of ZnO nanaparticles and PEG-coated Mn-doped ZnO nanoparticles attached cotton textile cannot be measered with time. Result show that Mn-doped ZnO nanoparticles and PEG-coated Mn-doped nanoparticles were not tightly bound to the cotton textile. However, PVP-coated Mn-doped ZnO nanoparticles were tightly bound into cotton textile. The coloni forming unit (CFU) has to be measered by using shake flask test.[43] This will be a scope of a future work.

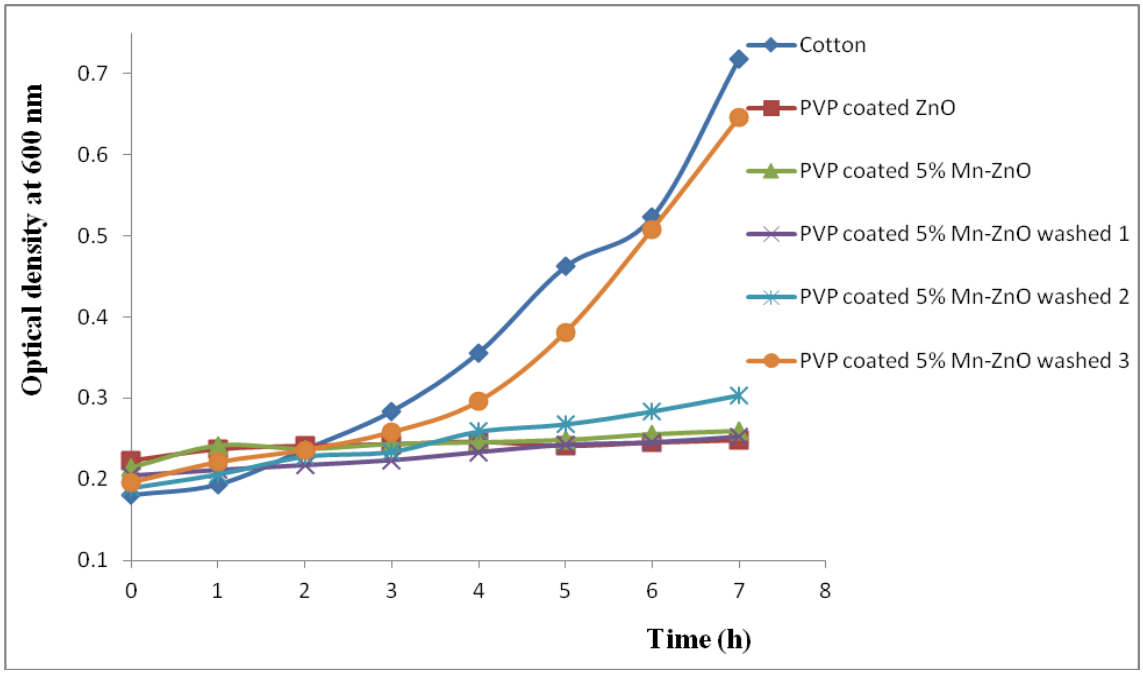

Figure 3.50. Showing change of optical density over time (7 h) for tryptic soy broth shake flask test against *E.coli.*

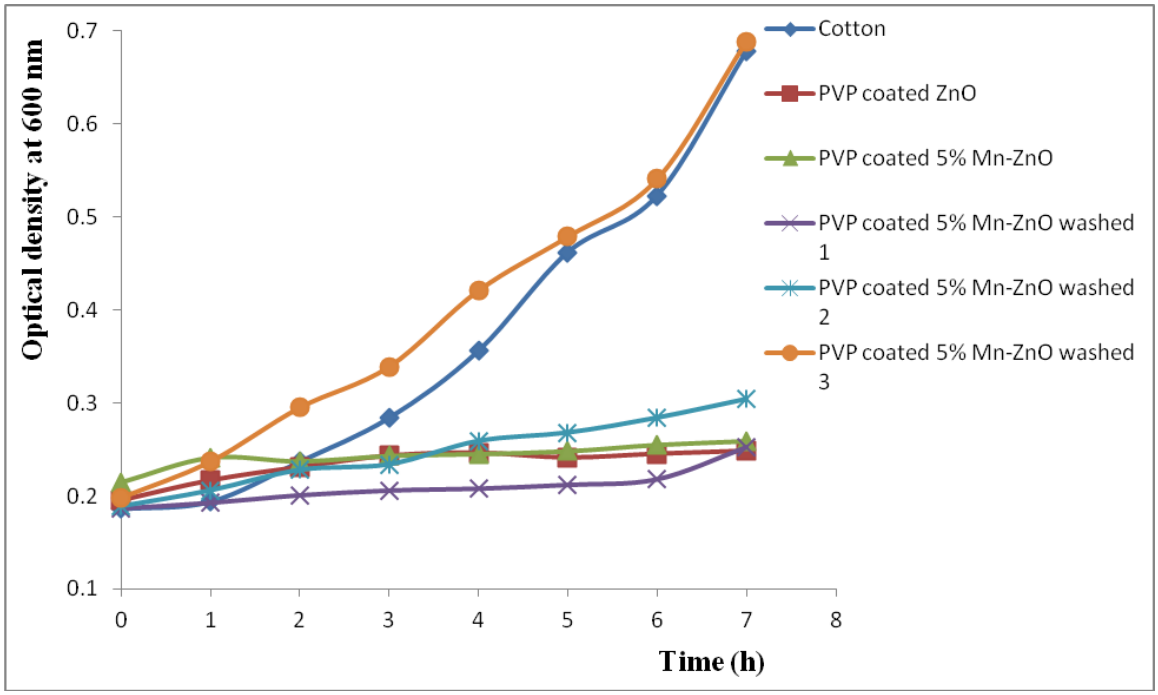

Figure 3.51. Showing change of optical density over time (7 h) for tryptic soy broth shake flask test against *S.aures.*

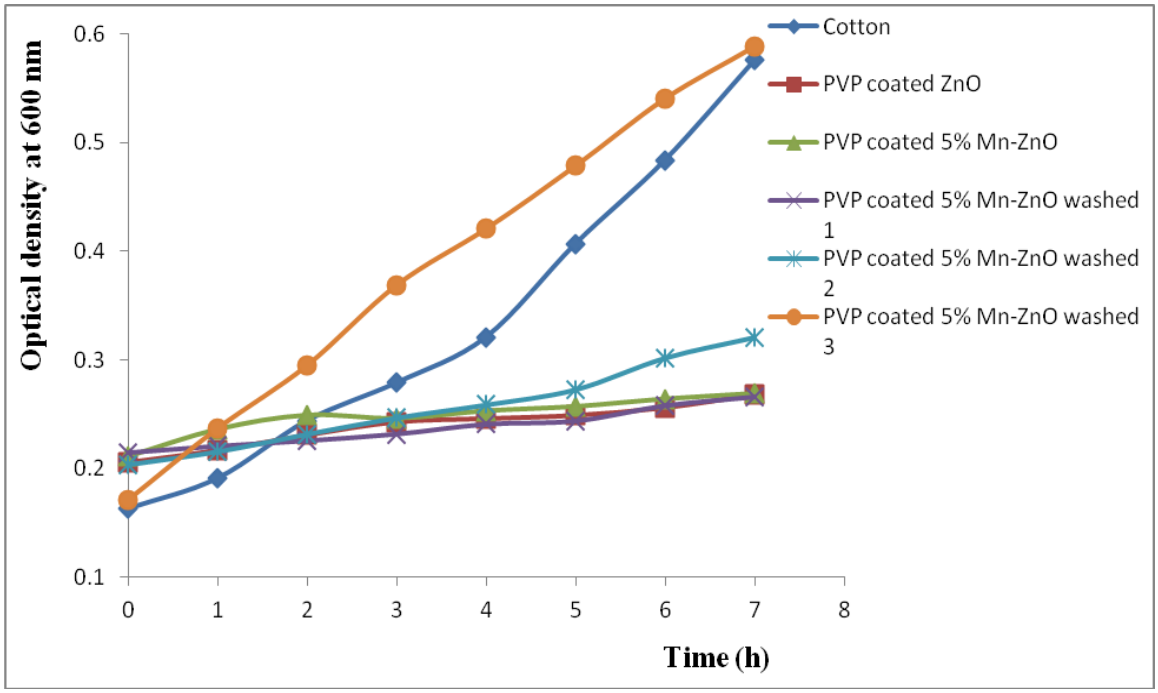

Figure 3.52. Showing change of optical density over time (7 h) for tryptic soy broth shake flask test against *S.epidermidis.*

3.2.6. Antifungal activity of Mn-doped ZnO nanoparticles.

The antifungal activity of the PVP-coated Mn-doped ZnO nanoparticles attached cotton textile were determined using parallel streak method. The AATCC 147 test method (parallel streak method) is a carrier-based, presumptive test method designed to quickly determine antibacterial and antifungal activity of diffusible antimicrobial agents on treated textile materials.[47] Antifungal activity of PEG-coated Mn-doped ZnO nanoparticles and PVP-coated Mn-doped ZnO nanoparticles is shown in Figure 3.52 and 3.53.

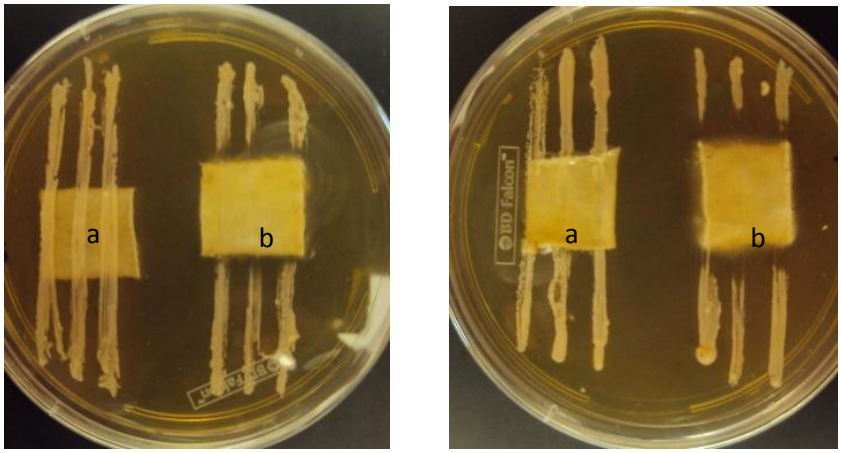

Plate 1 Plate 2

Figure 3.53. Parallel streak method against *Cryptococcus sp.* plate 1- (a) Raw cotton, (b) PEG-coated 5% Mn-doped ZnO nanoparticles with cotton, plate 2-(a) Raw cotton, (b) PVP-coated 5% Mn-doped ZnO nanoparticles with cotton.

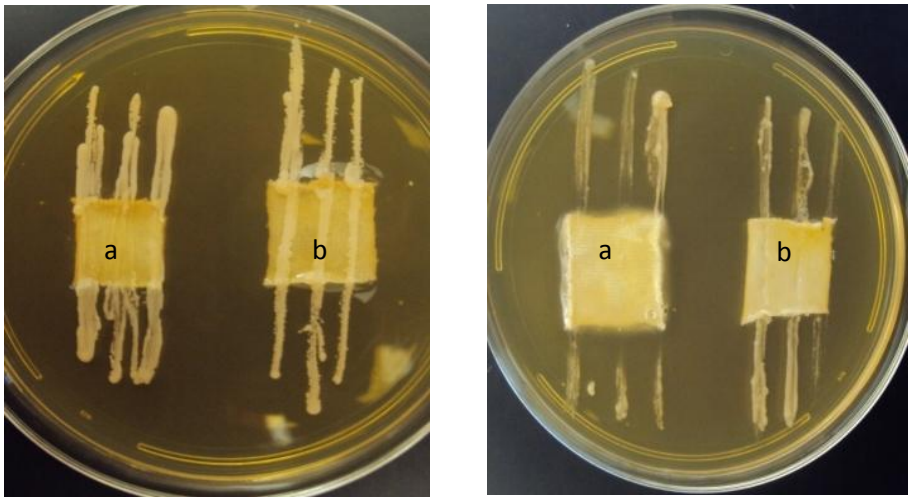

`

Plate 1 Plate 2

Figure 3.54. Parallel streak method against *Cryptococcus sp.* plate 1- (a) PEG-coated 5% Mn-doped ZnO nanoparticles with cotton washed 1 time and (b) PEG-coated 5% Mn-doped ZnO nanoparticles with cotton washed 2 time, plate (a) PVP-coated 5% Mn-doped ZnO nanoparticles with cotton washed 1 time and (b) PVP-coated 5% Mn-doped ZnO nanoparticles with cotton washed 2 time.

CHAPTER 4

CONCLUSIONS

In the first part of this project, the luminescent europium complex [$Eu(btfa)_3dmph$] was synthesized using btfa and dmph ligand combination. The europium complexes, $Eu(btfa)_3dmph$ and $Eu(btfa)_3(H_2O)_2$ are not water soluble due to their hydrophobic nature. The simple synthetic method was developed to prepare biocompatible and highly luminescent $Eu(btfa)_3dmph$ and $Eu(btfa)_3(H_2O)_2$ complex-incorporated silica nanomaterials using modified Stöber method. The nanoparticles were characterized by using various analytical methods. The luminescent studies show that $Eu(btfa)_3dmph$ incorporated silica nanoparticles have intense luminescence at 614 nm. The higher quantum yield value was observed for the 40 mg $Eu(btfa)_3dmph$ incorporated silica nanoparticles (11.58%) compared to 20 mg and 30 mg $Eu(btfa)_3dmph$ incorporated silica nanoparticles (3.1%). The diameter of the nanoparticles was found to be in the range from 30 to 50 nm using SEM imaging. The $Eu(btfa)_3dmph$ incorporated silica nanomaterial is highly dispersible in water with potential biomedical imaging applications. Additionally, the antimicrobial activity of the complexes was carried out using clinically important *S.aureus, S.epidermidis* and *E.coli* bacteria species. $Eu(btfa)_3dmph$ complex was found to exhibit higher antimicrobial activity than $Eu(btfa)_3(H_2O)_2$ complex. This may be due to the synergistic effect that increases the lipophilicity of the complexes and possible DNA intercalating ability of dmph ligand.

In the second part of this work, polymer-coated and uncoated Mn-doped ZnO nanoparticles were synthesized by using a modified co-precipitation method. All the

nanoparticle samples show Wurtzite crystal structure. Results obtained by XRD analysis show that the coating process and Mn-doping does not change the crystalline structure of the ZnO nanoparticles. The average particle sizes were estimated using SEM and TEM micrographs. The diameter of Mn-doped ZnO, PEG-coated Mn-doped ZnO, and PVP-coated Mn-doped ZnO nanoparticles are 36, 16, and 8 nm, respectively. Mn doped ZnO nanoparticles exhibit slightly higher antibacterial activity (2.5 mg/mL) than that of ZnO nanoparticles (4 mg/mL) against clinically important bacteria. However, agar diffusion results not showed any difference of antimicrobial property of ZnO nanoparticles and Mn-doped ZnO nanoparticles. The PEG and PVP-coated Mn-doped ZnO nanomaterials have been successfully investigated by FTIR analysis. It reveals the bonding between Mn-doped ZnO and polymer network. This PEG and PVP-coated nanoparticles helps the attachment to the cotton textile. Results show that, PVP-coated Mn-doped ZnO nanoparticles were tightly bound to cotton textile surface than PEG-coated Mn-doped ZnO nanoparticles. PVP-coated Mn-doped ZnO nanoparticles attached cotton textile exhibit antibacterial and antifungal activity with 3 washing cycles. From the above studies, it can be concluded that polymer-coated Mn-doped ZnO nanoparticles prepared by the co-precipitation method may be used as promising textile material in clinical settings.

REFERENCES

1. Weissman, S. I. Intramolecular Energy Transfer The Fluorescence of Complexes of Europium .*J. Chem. Phys*. **1942**, 10, 214.

2. Lal, M.; Levy, L.; Kim, K. S.; He, G. S.; Wang, X.; Min, Y. H.; Pakatchi, S.; Prasad, P. N. Silica nanobubbles containing an organic dye in a multilayered organic/inorganic heterostructure with enhance luminescence. *Chem. Mater*. **2000**, 12, 2632-2639.

3. Diamente, P. R.; Veggel, F.C.J.M.V. Water-Soluble Ln^{3+} Doped LaF_3 Nanoparticles: Retention of Strong Luminescence and Potentials as Biolabels. *J. Fluor*. **2005,** 15, 350.

4. Wang, H.; Wang, L. Synthesis and sensing application of highly luminescent and water stable polyaspartate functionalized LaF_3 nanocrystals *J. Mater. Chem. C*, **2013**, 1, 1105-1110.

5. Coll, J. L. Cancer optical imaging using fluorescent nanoparticles. *J. Nanomedicin*e **2012**, *6*, 7.

6. De Silva, C. R.; Vagner, J.; Lynch, R.; Gillies, R. J.; Hruby, V. J. Optimization of time-resolved fluorescence assay for detection of europium-tetraazacyclododecyltertraacetic acid- labeled ligand-receptor interactions. *Anal. Biochem.* **2010,** *398*, 15-23.

7. Galaup, C.; Azéma, J.; Tisnès, P.; Picard, C.; Ramos, P.; Juanes, O.; Brunet, E.; Rodríguez-Ubis, J. C. Luminescence of Eu^{+3} and Tb^{+3} Complexes of Two Macrobicyclic Ligands Derived from a Tetralactam Ring and a Chromophoric Antenna. *Helvetica chemical acta*, **2002**, 85, 1613-1625.

8. Tan, M.; Wang G.; Hai, X.; Ye, Z.; Yuan, J. Development of functionalized fluorescent europium nanoparticles for biolabeling and time-resolved fluorometric applications. *J. Mater Chem* , **2004**, 14: 2896-2901.

9. Handl, L.H.; Robert, J.; Gillies, R. J. Lanthanide-based luminescent assays for ligand-receptor interactions. *Life Sciences*, **2005**, 77 361 – 371.

10. Woods, M.; Donald, E.; Woessner, D. E.; Sherry, A. D. Paramagnetic lanthanide complexes as PARACEST agents for medical imaging. *Chem. Soc. Rev*, **2006**, 35, 500- 511.

11. Liu, Q.; Sun, Y.; Yang, T.; Feng, W.; Li, C.; Fuyou Li, F**.** Sub-10 nm Hexagonal

Lanthanide-Doped $NaLuF_4$ Upconversion Nanocrystals for Sensitive Bioimaging in Vivo. *J. Am. Chem. Soc*, **2011**, 133 (43), 17122–17125.

12. Escribano, P.; López, B. J.; Aragó, J. P.; Cordoncillo, E.; Viana, B.; Sanchez, C. Photonic and nanobiophotonic properties of luminescent lanthanide-doped hybrid organic–inorganic materials. *J. Mater. Chem.***, 2008**, 18, 23-40.

13. Philippot, C.; Bourdolle, A.; Maury, O.; Dubois, F.; Boury, B.; Brustlein, S.; Brasselet, S.; Andraud, C.; Ibanez, A. Doped silica nanoparticles containing two photon luminescent Eu(III)complexes for the development of water stable bio-labels. *J. Mater. Chem.***, 2011,** 21**,** 18613-18622.

14. Patil, S. K,; Naik, V. M.; Bilehal, D. C.; Mallur, N. D. Synthesis, Spectral and Antimicrobial Studies of Lanthanide (III) Nitrate Complexes with Terdentate ONO Donor Hydrazones. *J. Experimental Sciences* **2011**, 2(7), 15-20.

15. Rampersad, N. S. Multiple Applications of Alamar Blue as an Indicator of Metabolic Function and Cellular Health in Cell Viability Bioassays. *J. Sensors*. **2012**, 12, 12347-12360.

16. Gudasi, K. B.; Havanur, V. C.; Patil, S. A.; Patil, B. R. Antimicrobial Study of Newly Synthesized Lanthanide(III) Complexes of 2-[2-hydroxy-3-methoxyphenyl]-3-[2-hydroxy-3-methoxybenzylamino]-1,2-dihydroquinazolin-4(3H)-one.*Met Based Drugs*. **2007**, 37348.

17. Neely, A. N.; Maley, M. P. Survival of Enterococci and Staphylococci on Hospital Fabrics and Plastic. *J. Clin Microbiol*. **2000**, 38(2), 724–726.

18. Singh, G.; Joyce, E. M.; James Beddow, J.; Mason, T. J. Evaluation of antimicrobial activity of ZnO nanoparticles coated sonochemically onto textile fabrics. *J. Microbiology,Biotechnology.* **2012** , 2 (1), 106-120.

19. Peter, Y. Yu. Fundamentals of Semiconductors, Physics and Materials Properties, Fourth Edition.

20. Seow, Z. L. S.; Wong, A. S. W.; Thavasi, V.; Jose, R.; Ramakrishna, S.; Ho, G.W. Controlled synthesis and application of ZnO nanoparticles, nanorods and nanospheres in dye-sensitized solar cells. *Nanotechnology* 20, **2009**, 045604.

21. Cong, C. J.; Hong, J. H.; Liu, Q. Y.; Liao, L.; Zhang, K. L. Synthesis, structure and ferromagnetic properties of Ni-doped ZnO nanoparticles. *Solid State Communications*, **2006**, 138, 511.

22. Kaur, J.; Kumar, P.; Sathiaraj, T. S.; Thangaraj, R. Structural, optical and fluorescence properties of wet chemically synthesized ZnO:Pd^{2+} nanocrystals. *International Nano Letters*, **2013**, 3.

23. Singla, M. L.; Muhamed, S. M.; Kumar. M. Optical characterization of ZnO nanoparticles capped with various surfactants. *J. Luminescence*, **2009**, 129, 434-438.

24. Nabiyouni1, G.; Barati, A.; Saadat, M. Surface adsorption of polyethylene glycol and polyvinyl alcohol with variable molecular weights on zinc oxide nanoparticles. *Iranian Journal of Chemical Engineering*, **2011**, 8, 20-30.

25. Nihonyanagi, S.; Kanemitsu, Y. Enhanced luminescence from electron–hole droplets in silicon nanolayers. *Appl Phys. Lett*. **2004**, 85, 5721.

26. Ibrahim, I. A. M.; Zikry, A. A. F.; Sharaf, M. A. Preparation of spherical silica nanoparticles: Stober silica. *J. Amer Sci*, **2010**, 6(11), 985-989.

27. Lu, Z.; Rong, K.; Li, J.; Yang, H.; Chen, R. Size-dependent antibacterial activities of silver nanoparticles against oral anaerobic pathogenic bacteria. *J Mater Sci. Mater Med.* **2013**, 24(6), 1465-1471.

28. Baker, C. N.; Tenover, F. C. Evaluation of alamar colorimetric broth microdilution susceptibility testing method for staphylococci and enterococci. *J. Clin. Microbiol.* **1996**. 34**:**2654-2659.

29. Rekha, K.; Nirmala, M.; Manjula, G. N.; Anukaliani, A. Structural, optical, photocatalytic and antibacterial activity of zinc oxide and manganese doped zinc oxide nanoparticles. *Physics of Condensed Matter*, **2010**, 405, 3180–3185.

30. http://upload.wikimedia.org/wikipedia/commons/4/42/Polyethylene_glycol.png.

31. Sigel, A.; Sigel, H. Metal ions in biological system, the lanthanides and their interaction with biosystem. **2003**, Volume 40.

32. Rampersad, S. N. Multiple Applications of Alamar Blue as an Indicator of Metabolic Function and Cellular Health in Cell Viability Bioassays. *J. Sensors*. **2012**, 12347-12360.

33. Page, A. B.; Page, A. M.; Noel, C. A new fluorimetric assay for cytotoxicity measurements in vitro. *Int. J. Oncol*. **1993**, 3, 473–476.

34. http://en.wikipedia.org/wiki/File:ResazurinTOresorufin.png.

35. Omri, K.; Ghoul, J. E.; Lemine, O. M.; Bououdinac, M.; Zhang, B.; Mir, L. E. Magnetic and optical properties of manganese doped ZnO nanoparticles synthesized by sol–gel technique. *J. Superlattices and Microstructures*. **2013**, 60,139–147.

36. VidyaSagar, R.; Buddhudu, S. Structural and photoluminescence analysis of Zn1-xMnxO nanocrystalline powders. *J. Phys Lett.* **2009**, 373:3184-3189.

37. Venkataprasad B. S.; Deepak, F. L. Tuning the bandgap of ZnO by substitution with Mn^{2+}, Co^{2+} and $Ni^{2+.}$ Solid State Communications. **2005**, 135, 345-347.

38. Loria-Bastarrachea, M. I.; Carrillo-Escalante, H. J.; Aguilar-Vega, M. J. Grafting of poly(acrylic acid) onto cellulosic microfibers and continuous cellulose filaments and characterization. *J. Appl. Polym. Sci.* **2002**, 86, 386–393.

39. Viswanatha, R.; Sapra, S.; Gupta, S. S.; Satpati, B.; Satyam, P.V. Synthesis and Characterization of Mn-Doped ZnO Nanocrystals. *J.Phys. Chem. B*, **2004**, 108, 6303-6310.

40. Nejati, K.; Pakizevand, R. Synthesis of ZnO Nanoparticles and Investigation of the Ionic Template Effect on Their Size and Shape. *Int. Nano Lett*, **2011**, 1, 75-81.

41. Collins, L. A.; Franzblau, S. G. Microplate alamar blue assay versus BACTEC 460 system for high-throughput screening of compounds against *Mycobacterium tuberculosis* and *Mycobacterium avium*. Antimicrob. *J. Agents Chemother*. **1997**, 41, 1004-1009.

42. Baker, C. N.; Tenover, F. C. Evaluation of alamar colorimetric broth microdilution susceptibility testing method for staphylococci and enterococci. *J. Clin. Microbiol.* **1996**. 34**:**2654-2659.

43. Sawai, J. Quantitative evaluation of antibacterial activities of metallic oxide powders (ZnO, MgO and CaO) by conductimetric assay. *J. Microbiol. Methods.* **2003**, 54, 177–182.

44. Ameen, S.; Akhtar, M. S.; Kim, Y. S.; Yang, O. B.; Shin, H. S. Synthesis and characterization of novel poly(1-naphthylamine)/zinc oxide nanocomposites: application in catalytic degradation of methylene blue, *J. Colloid Polym. Sci*. **2010**, 288, 1633–1638.

45. Reddy, K. M.; Kevin, F.; Jason, B.; Denise, G. W.; Cory, H.; Alex, P. Selective toxicity of zinc oxide nanoparticles to prokaryotic and eukaryotic systems. *J. Appl. Phys. Lett.* **2007**, 90(21), 1-3.

46. Raghupathi, K. R.; Koodali, R. T.; Manna, A. C. Size-Dependent Bacterial Growth Inhibition and Mechanism of Antibacterial Activity of Zinc Oxide Nanoparticles. *Langmuir*. **2011**, 27, 4020–4028.

47. Rajendran, R.; Balakumar, C.; Ahammed, H. A. M.; Jayakumar, S.; Vaideki, K.; Rajesh, E. M. Use of zinc oxide nano particles for production of antimicrobial textiles. *Inter. J. Engineering, Science and Technology*. **2010**, 2(1), 202-208.